POLITECNICO DI TORINO
UNIVERSITÉ PARIS-SACLAY

International Master Course in Physics of Complex Systems

POLITECNICO
DI TORINO

Master Thesis

DESIGNING MODELS USING MACHINE LEARNING: ONE-BODY REDUCED DENSITY MATRICES AND SPECTRA

Thesis advisor:

Prof. Renato GONNELLI

Scientific Supervisors:

Dr. Jean-Pascal RUEFF

Dr. Jack WETHERELL

Scientific Co-Supervisors:

Dr. Lucia REINING

Dr. Matteo GATTI

Candidate

Andrea COSTAMAGNA

July 2020

Summary

This thesis project was born from the shared curiosity of Jean-Pascal Rueff, an experimentalist working at Synchrotron SOLEIL, and three theoreticians of the LSI laboratory at the École Polytechnique: Jack Wetherell, Lucia Reining and Matteo Gatti.
They shared a common desire to explore the growing interest of the scientific community in Machine Learning (ML) techniques and, particularly thanks to the presence at LSI of Jack Wetherell, who took part to the development of the `iDEA` code and who is also working in the context of Machine Learning for image recognition, it has been possible to design a Thesis project whose purpose was to explore ways in which ML techniques can be used both in theoretical and in experimental physics.

One of the biggest challenges in condensed matter physics is to calculate properties of materials taking into account the quantum many-body nature of matter. While the Coulomb interaction is universal, its effects cannot be separated from the specific material under consideration, which leads to a huge theoretical and computational effort. Recently, Machine Learning (ML) has raised new hopes as a tool that could be used to screen and predict properties of broad classes of materials. Indeed, the statistical structure of ML tools is particularly well suited to deal with quantum mechanics, thanks to the statistical information encoded in the state vector $|\Psi\rangle$, and in recent years ML has been used for addressing various classes of problems [1]. In quantum physics and chemistry, researchers mainly used ML to predict energies and forces starting from the atomic composition [2–17]. Another research line lies in the domain of Density Functional Theory (DFT) [18]: here the system is described by its electronic density, in other words, its properties are functionals of the density. These functionals are in general not known and must be approximated. So far, ML was mainly used with the aim to determine energies as density functionals [19–23]. The central topic of the present thesis was the design of a density functional. However, the strategy underlying the present work differs from the usual approach in two ways: first, instead of being *observable specific*, we concentrated on an important *building block*, the one body reduced density matrix (1-RDM) $\hat{\gamma}$. The knowledge of this quantity allows one to directly access much useful information, such as the kinetic and exchange energies, or the correlation strength of a material. We hence investigated the functional connecting the 1-RDM to the density: $\hat{\gamma}[n]$. Second, instead of using ML merely as a clever interpolation tool, we asked a methodological question, namely *Is it possible for the model maker to learn with the machine?* This would allow one to build functionals that could then be used *without* creating huge data-sets beforehand.
Many of the result obtained in this context were included in the paper "Insights into one-body density matrices using deep learning" [24].
The original thesis project was based on another methodological question: *How can we use ML to augment low resolution calculations and experiments?* This question could only be partially

addressed, since adverse conditions did not allow us to obtain the necessary experimental data.

What learning with the machine means and the object learned: The first methodological question, at the focus of the thesis, necessitates some clarification. It is important to note that we do not want the machine to learn blindly what output must be associated to any input, we want to use it for constructing models. Therefore, at first we tried to learn from the way the machine structures the data in order to create new theoretical models. In a second moment we inverted the roles and we investigated how we can inform the machine or use it for improving analytically derived theoretical models, with a focus on building density functionals.
DFT guarantees that the full information on the system is encoded in the electronic ground state density (n), an object that is much simpler than the state vector itself. This implies that $|\Psi\rangle$ as well as any observable must be writable as a functional of the density. To find these functionals is, however, difficult. It is therefore useful to introduce an intermediate step: all one body observables can be expressed in terms of the 1-RDM, as $O[\gamma] = \text{Trace}(\hat{O} \cdot \hat{\gamma})$. When the operator is non-local, like the kinetic energy, this cannot be transformed into a simple density functional. However, DFT guarantees the existence of the functional $\hat{\gamma}[n]$, and if we could find it, we would know O as functional of n. The functional $\hat{\gamma}[n]$ is particular; $\gamma(r,r';[n])$ is a matrix in real space, and its diagonal $r = r'$ is the density itself, $\gamma(r,r;[n]) = n(r)$. Therefore, this problem consists in finding the functional constraints that map the diagonal into the off-diagonals. Most importantly, DFT guarantees that the information contained in γ can be compressed. This creates an analogy to image processing: the functional constraints are not much different from the ones that map the picture of a flower to the word "flower" in our brain. Not all pictures are pictures of flowers, and similarly, not all matrices of two space arguments are 1-RDMs. This analogy suggests to use methods that are successful in image processing, such as ML in general, and in particular, artificial neural networks (ANNs). Our idea was therefore to apply the existing algorithms to increase our knowledge on $\hat{\gamma}[n]$.
In order to investigate the functional, in this work we focused on numerically solvable 1D systems of two electrons with opposite spin.

Using machine learning for human learning: Principal Component Analysis (PCA) played a central role while we were attempting to learn from the way the machine structures the data. PCA is a ML technique that, given a data-set of objects characterized by N_f features, is able to learn the linear constraints existing in between the features. We showed how PCA can learn all of the known linear constraints of the 1-RDM: normalization of the density, vanishing of the density at the boundaries and symmetry of the 1-RDM. Moreover, the PCA detected additional linear constraints, because the potential is not a completely arbitrary function. Finally, we found a one-to-one mapping in between the PCA on the 1-RDM and the density. The combination of these findings allowed us to build the first functional, named the *PCA-functional*. In the thesis the formal derivation I developed will be described and the resulting 1-RDM will be compared to the exact one. Moreover it will be demonstrated that the absence of non-linearity can be treated as noise, using ANNs. This finally makes our theoretical model numerically exact.

Using human learning for machine learning: Usually, one is not completely ignorant about a functional, but one knows, e.g. some limiting cases. Teaching the machine this knowledge might be of great benefit. We argued how this problem could be circumvented but, rather than exploring this approach, we decided to study the nature of the non-linearity. For this reason I focused on the Hubbard Dimer (HD), the simplest possible system since its 1-RDM is a 2×2

symmetric matrix. Being the desired functional already present in literature in the limiting cases of strongly interacting and non-interacting electrons, I performed the exact diagonalization of the Hamiltonian under specific conditions for the potential and I derived the two results following the prescription reported in [25]. I then focused on teaching these limiting cases to the machine using ANNs. Rather than brute force machine learning it, however, the insight gained from the theoretical derivation was used in a process known as *feature engineering*. The analytical knowledge has been used for shaping the architecture of the network and the minimization of the ignorance on the theoretical model has been shown to have a counterpart in the minimization of the complexity of the network. In fact I have shown how the simplest possible ANN can learn both the limiting cases when receiving engineered data.
Finally, I used the insight gained in the derivation of the limiting cases for designing a model able to determine $\hat{\gamma}[n]$ at intermediate values of the interaction in between the electrons. The analytical model was proposed together with the ANN optimization done to determine a good way to approximate the deviation from the exact result. In order to complete the characterization of the HD I also found the functional $|\Psi[n]\rangle$, in the two limiting cases, and I studied the way the non-interacting 1-RDM can be mapped into the strongly interacting one with the aid of ML.

The Hubbard Dimer as an auxiliary system for building the 1-RDM of an extended lattice: The study of small model systems allows one to understand some fundamental points. Moreover, often larger systems can be simulated by a small system embedded in an effective environment. Along this line, I finally focused on constructing the functional $\hat{\gamma}[n]$ for a lattice with a number of grid-points $N_g > 2$ using the HD as an auxiliary system for the construction of the N_g grid-points 1-RDM. I first tried to estimate the 1-RDM of the three site lattice using three HDs. This led me to propose two different approaches named the *forward* and *inverse* approaches. I then argued why the bad scaling with N_g of the first one makes the *inverse approach* preferable and, using it, I found an empirical functional. Finally I moved to applying the idea to a $N_g = 20$ lattice. I showed that, when using HDs having the density at the two sites equal to the corresponding density of the extended system, there is no difference in using strongly interacting HDs and non-interacting HDs and I proposed a qualitative explanation of the reason why this simple functional is extremely accurate in the estimation of some entries of the 1-RDM while overestimates dramatically others. Finally, the functional was corrected using an ANN analogous to the one used for the PCA-functional.

Using the machine to increase resolution: The original project aimed at using ML to reduce the computational and experimental burden to the absolute essential needed without loosing in accuracy. Since the experiments could not be carried out, the focus of the project shifted to the building of functionals, and the results presented in this last section are to be considered as a preliminary analysis to future studies.
The physical object chosen for addressing this question was the electronic spectrum of a material, measured via Inelastic X-ray Scattering experiments (IXS). The spectrum is a two variable function $S(q,\omega)$ corresponding to the count of photons emitted by the irradiated material at a certain energy and momentum. Once fixed the momentum, a scan in energy must be repeated several times for having a satisfactory accuracy due to the uncertainty in the measurement, resulting in an extremely time demanding process. Therefore, it would be desirable to use ML to reduce the number of measurements while guaranteeing the same final accuracy. Keeping this purpose in mind, Gaussian Process Regression (GPR) is a technique well suited for fitting functions with an intrinsic randomicity. For the preliminary analysis, I could use already available data measured

on titanium dioxide in the rutile and anatase phases. I first worked on the energy-dependence of the spectra at fixed momentum. I showed how using the GPR it could be possible to reduce the number of samplings in energy from 221 to 32 without loosing much information. This was not directly useful for the real task but was a good sign for the choice of the ML tool. Considering the 2D data I then compared different GPR models basing on their capability of reproducing portions of the spectra not used in the fitting. An essential moment of the experience would have been a more detailed experiment. Unfortunately, adverse conditions have hindered it and this preliminary analysis will find its application later in July.
Similar ML tools might also be useful to connect observables coming from cheap simulations to observables that would require expensive simulations. This is a key candidate for a follow up work and it may be used for connecting the 1-RDM of the simple models proposed to more complex 3D many body problems.

Acknowledgements

I would like to express my gratitude to all of my supervisors, without whom this project would not have been possible. Their constant kindness, availability and passion for learning were at the basis of the extremely stimulating environment in which I had the opportunity to spend the last months. I will never find the way to properly thank Jean-Pascal Rueff for his curiosity, Matteo Gatti for his thoughtful and unique approach to physics, Lucia Reining for her capability to make ideas bloom in the discussion and to Jack Wetherell for his limitless love for physics and for all of the nights spent working together. A big thank you goes also to Renato Gonnelli for all of the help he gave me both on the thesis and on the handling of any issue occurred in the last years.
I would like to express my thankfulness to Elena Ferro for being constantly on my side both in science and in life. To our aperitifs and to our scientific discussions I owe respectively the light-heartedness and the productivity of this parisian lock down.
I thank my family, my roots, for having made this work possible as a consequence of the two decades in which they shaped and supported me. I will forever be grateful to all of them for the unshakable ideals we share. I thank my father for the unmovable coherence between his life and his work. I thank my mother for her "Austro-Hungarian" sense of duty and for her unstoppable love for knowledge. I thank Cinzia for the eternal youth of her soul, I thank Marta for her precision and rigor and I thank the two of them for being ever present in my life.
In them I find my models, to them I owe everything.

Table of Contents

Acronyms

QM Quantum Mechanics

BOA Born Oppenheimer Approximation

CAR Canonical Anticommutation Relation

DFT Density Functional Theory

1-RDM One body Reduced Density Matrix

RDMFT Reduced Density Matrix Functional Theory

ML Machine Learning

PCA Principal Component Analysis

MLP Multi Layer Perceptron

FNN Fully connected Neural Network

NN Neural Network

AE Autoencoder

CNN Convolutional Neural Network

iDEA interacting Dynamic Electrons Approach

DAE Denoising Autoencoder

MAPE Mean Absolute Percentage Error

FE Feature Engineering

XOR Exclusive OR

FPGA Field Programmable Gate Array

HD Hubbard Dimer or two sites Fermi-Hubbard modle
HT Hubbard Trimer or three sites Fermi-Hubbard modle

GPR Gaussian Process Regression
GP Gaussian Process

IXS Inelastic X-ray Scattering

RBF Radial Basis Function

WN White Noise

Chapter 1

Introduction to Functional theories and Machine Learning

This chapter contains a mathematically oriented introduction to the two cornerstones of the thesis: Density Functional Theory (DFT) and Machine Learning (ML).
The starting point will be the introduction of the many-body electron problem. This problem might be completely solved by determining a function containing all of the information of the system, namely the state function. Nonetheless, the complexity of this function causes the problem to be theoretically and computationally intractable. This led to Density Functional Theory, a re-formulation of quantum mechanics that is based on the fact that the whole information on the system is encoded in the electronic density. This is to say that any observable is in principle writable as a functional of the density, shifting the problem to finding these functionals.
In this work we will focus on getting insight on one of these density functionals, trying to extract the one-body reduced density matrix (1-RDM) γ from the density. The reason is that knowing this functional would automatically yield other density functionals, such as the kinetic energy.
We will address the problem using machine learning (ML). ML is a term used for labelling a class of computational methods, specifically designed for extracting patterns from the observation of data. Of all the algorithmic manifestations of ML we will focus on principal component analysis (PCA) and neural networks (NN), that will be introduced in the present chapter. Since the 1-RDM contains the density, DFT guarantees the existence of strong correlations among the entries of this matrix, corresponding to the functional constraints defining the desired density functional. Therefore, we will motivate the choice of the ML techniques analyzed starting from our wish to exploit their capability of learning constraints among the features. This approach will need the disposal of large data-sets for informing the machine. We will therefore introduce the `iDEA` code, a software for finding the numerically exact state function in 1D few electron systems. Afterwards we will characterize the data-set we will use, corresponding to a set of randomly generated smooth potentials, each of which is populated by two electrons with opposite spin.

1.1 The purpose: Functional Theories and One Electron Reduced Density matrix

1.1.1 From the principles of quantum mechanics to Density Functional Theory

The principles of quantum mechanics (QM) state that the whole information needed for characterizing any pure state of a physical system can be encoded in a unit vector $|\Psi\rangle$, belonging to a Hilbert space $\mathscr{H}$. In this vector it is encoded the probabilistic information of the system that can be used to determine the outcome of a measurement. The way this is done is by introducing observables of interest, that in the QM theoretical framework correspond to hermitian operators $\hat{O} : \mathscr{H} \mapsto \mathscr{H}$. Then, the validation of any theoretical model comes from the comparison of the experiment with the following functional of the state vector:

$$O[|\Psi\rangle] = \langle\Psi|\hat{O}|\Psi\rangle \in \mathbb{R} \tag{1.1}$$

This functional corresponds to a statistical expectation value.
When working in the context of quantum chemistry and in condensed matter, a wide class of properties of a material can be determined considering the *ground state* of the system at the absolute zero $T = 0K$. In the most general formulation, this amounts to solve a many-body problem in which electrons, protons and neutrons coexist with phonons in a dynamical equilibrium. Let us fictitiously assemble this system. When an atom becomes part of a solid its electron cloud splits into two parts. The electrons populating the stablest states, named *core* electrons, remain attached to the nucleus forming the *ions*. Conversely, the wave-functions of the remaining electrons, named *valence* electrons, overlap with the ones of the valence electrons of the contiguous atoms. The overlap results in the formation of new available modes whose occupation induces an higher stability on the ionic subsystem. In this picture, the *Born-Oppenheimer Approximation*[26] (BOA) is a widely effective technique. According to it, the difference in weight between the valence electrons and the stable ion can be exploited. This is done by assuming that the changes of the electrons are so fast that the valence electrons subsystem quickly rearrange in response to any change in the ionic one. In this way, the two subsystems can be decoupled and the whole material can be regarded as a slowly varying ionic lattice in which the valence electrons live in a succession of ground states. Consequently, the electronic ground state will be parametrized by the ionic environment to which they are subjected. In this way, the main task becomes the characterization of this (parametric) electronic ground state.
Following the notation used in the lecture notes of Jan Philip Solovej on many-body quantum mechanics [27], the electronic subsystem is a many body system of identical particles, each of which can be described on its own Hilbert space $\mathfrak{h}$. Furthermore, the Hilbert space describing the system as a whole corresponds to the anti-symmetric orthogonal subspace of the tensor product of the single particle Hilbert spaces. In fact, when working with N_e bodies the full representation would be guaranteed by working on the tensor product of the single particle Hilbert spaces ($\bigotimes^{N_e}\mathfrak{h}$). The resulting space can always be divided into two orthogonal subspaces, the symmetric one ($\bigotimes^{N_e}_{sym}\mathfrak{h}$) and the anti-symmetric one ($\bigwedge^{N_e}\mathfrak{h}$), a sub-division that suits well the distinction in nature of two kinds of microscopic bodies: bosons and fermions. Hence,

the Hilbert space in which it is possible to work when considering an ensemble of electrons is

$$\mathscr{H}_{N_e} = \bigwedge^{N_e} \mathfrak{h} \subset \bigotimes^{N_e} \mathfrak{h},$$

where N_e is the number of identical particles. In order to determine the ground state of the system it is necessary to quantify the energy cost for an electron to be in any state. Let us reduce ourselves to processes involving up to two electrons. Each process can be associated to an operator acting on a state and modifying it with a certain amplitude. We will consider one body operators $\hat{h}_i \doteq \mathbb{1}^{\otimes^{i-1}} \otimes \hat{h}_i^{(1)} \otimes \mathbb{1}^{\otimes^{N_e-i}}$, acting on the i-th single particle hilbert space and two body operators $\hat{W}_{i,j}$, acting on the tensor product of two interacting particle Hilbert spaces $\mathfrak{h}_i \otimes \mathfrak{h}_j$. These last operators will be present only in case of interaction. This having been said, a generic Hamiltonian taking into account one and two bodies phenomena can be written as

$$\hat{H} = \sum_{i=1}^{N_e} \hat{h}_i + \Theta_{int} \sum_{1 \leq i < j \leq N_e} \hat{W}_{i,j} \qquad \Theta_{int} = \begin{cases} 1 & \text{if interacting} \\ 0 & \text{if non interacting} \end{cases} \tag{1.2}$$

This is the general form in which it is possible to write the electronic many-body Hamiltonian of a material under the BOA. More explicitly, by introducing the ions positions $\{\mathbf{R}_I\}_{I=1}^{N_I}$:

$$\hat{H}(\{\mathbf{R}_I\}_{I=1}^{N_I}) = \hat{T} + \hat{V}^{ext}(\{\mathbf{R}_I\}_{I=1}^{N_I}) + \hat{V}^{e-e} = \sum_{i=1}^{N_e} \hat{T}_i + \hat{V}_i^{ext} + \sum_{1 \leq i < j \leq N_e} \hat{V}_{i,j}^{e-e} \tag{1.3}$$

where $\hat{T}_i$ is the single particle kinetic energy, $\hat{V}_i^{ext}(\{\mathbf{R}_I\}_{I=1}^{N_I})$ is the external potential acting on the i-th electron and introducing the parametric dependence of the Hamiltonian on the ionic coordinates and $\hat{V}_{i,j}^{e-e}$ is the many-body term, accounting for the electron-electron interaction.

Before to proceed any further, it is important to remark that we will mainly work in the second quantization formalism. In this formalism, the indistinguishability is exploited to describe each state in terms of the number of particles living in each single particle state. In order to do that, let us introduce the fermionic Fock space ($\mathscr{F}^F$), allowing to describe processes in which the number of particles changes. This is done by means of a tensor sum ($\bigoplus$) of all of the fermionic spaces at fixed number of electrons

$$\mathscr{F}^F = \bigoplus_{N_e=0}^{\infty} \bigwedge^{N_e} \mathfrak{h} \tag{1.4}$$

In this space, each many-body state can be written in a basis formed by tensor products of single particle states $|\alpha_i\rangle \in \mathfrak{h}_i$. Notably, a generic basis vector reads

$$|\psi_{\alpha_1,\cdots,\alpha_{N_e}}\rangle \doteq |\alpha_1,\cdots,\alpha_{N_e}\rangle = \frac{1}{\sqrt{N_e!}} |\alpha_1\rangle \otimes |\alpha_2\rangle \otimes \cdots \otimes |\alpha_{N_e}\rangle \tag{1.5}$$

In order to operate in such formalism it is essential to introduce the vacuum vector $|0\rangle$ and the creation and the annihilation operators, i.e. the fermionic ladder operators. Doing this corresponds to describe each electron as a field perturbing the vacuum state.

$$\begin{cases} \hat{c}_\alpha^\dagger : \mathscr{H}_{N_e} \mapsto \mathscr{H}_{N_e+1} & \hat{c}_\alpha^\dagger |\alpha_1,\cdots,\alpha_{N_e}\rangle \doteq |\alpha,\alpha_1,\cdots,\alpha_{N_e}\rangle \\ \hat{c}_\alpha : \mathscr{H}_{N_e} \mapsto \mathscr{H}_{N_e-1} & \hat{c}_\alpha |\alpha_1,\cdots,\alpha_{N_e}\rangle \doteq \sum_{k=1}^{N_e} (-1)^k \langle \alpha|\alpha_i\rangle |\alpha_1,\cdots,\alpha_{k-1},\alpha_{k+1},\alpha_{N_e}\rangle \end{cases} \tag{1.6}$$

In order to satisfy the statistics of fermionic identical particles, these ladder operators need to satisfy the Canonical Anti-Commutation Relations (CAR)

$$\{\hat{c}_i, \hat{c}_j^\dagger\} = \delta_{i,j} \qquad \{\hat{c}_i, \hat{c}_j\} = \{\hat{c}_i^\dagger, \hat{c}_j^\dagger\} = 0 \tag{1.7}$$

The formalism having been introduced, it is in principle possible to use this theoretical framework to make predictions of physical observables. The resulting theoretical expectations obtained using Eq. 1.1 need then to be validated, and this is done by comparing them with the experiments. In order to do that, however, one should determine the state $|\Psi\rangle$ of the system that, according to the variational principle [28], is the state minimizing the energy functional.

$$E_{GS} = min_\Psi\{E[\Psi](\{\mathbf{R}_I\}_{I=1}^{N_I})\} = min_\Psi\{\langle\Psi|\hat{H}(\{\mathbf{R}_I\}_{I=1}^{N_I})|\Psi\rangle\} \tag{1.8}$$

or, equivalently [29], solving the eigen-equation

$$\hat{H}(\{\mathbf{R}_I\}_{I=1}^{N_I})|\Psi(\{\mathbf{R}_I\}_{I=1}^{N_I})\rangle = E|\Psi(\{\mathbf{R}_I\}_{I=1}^{N_I})\rangle \tag{1.9}$$

However, as argued by Kohn in his nobel lecture [18], the knowledge of the state vector is of arguable feasibility. The state vector, that should contain all of the information of the system, turns out to be far too unwieldy to be extracted exactly or to be stored in any modern computer as a consequence of the so called *exponential wall* [18] and to the fact that the number of degrees of freedom is proportional to the number of electrons N_e. This observation led Kohn to the formulation of a new computational quantum mechanical modeling approach called Density Functional Theory (DFT). The key observation at the basis of this theory was the fact that, in the computation of the integrals of the kind presented in equation 1.1, many degrees of freedom are integrated out. This led to the Hohenberg-Kohn theorem [18, 30], which states that the whole information content of a physical system is completely encoded in the one body density

$$n(r) = N_e \cdot \langle r|\mathrm{Tr}_{2,\cdots,N_e}\{|\Psi\rangle\langle\Psi|\}|r\rangle = N_e \cdot \int\left(\prod_{j=2}^{N_e} dr_j\right)|\Psi(r, r_2, \cdots, r_{N_e})|^2 \tag{1.10}$$

The Hohenberg Kohn theorem shows, in an exact way, that the ground state of the system and, consequently, the expectation value of any observable should in principle be writable as a functionals of the density

$$O[|\Psi\rangle] = \langle\Psi[n]|\hat{O}|\Psi[n]\rangle = O[n] \in \mathbb{R}.$$

The determination of these density functionals is at the heart of theoretical DFT.
The fact that the whole information of the system is compressed in the electronic density is essential due to the much higher simplicity of this object when compared to the state vector. This also results in a simplification in the constrained functional minimization problem, that now reads

$$E_{GS} = min_{n(r)}\{E[n]\} = min_{n\leftarrow\Psi}\{E[\Psi]\} \tag{1.11}$$

and the constraint is on the number of particles in the system. This minimization problem, in comparison to the one defined in equation 1.8, is a functional minimization of a three variable function, that is much simpler than the N_e-proportional multivariate function of the previous method and, most importantly, it is also possible to store the result.

1.1.2 Kohn-Sham auxiliary system contrasted with orbital free Density Functional Theory

DFT is a formally exact reformulation of quantum mechanics that has had predominant importance in the last fifty years, both in theoretical calculations and in computational modelling. Its success is largely owed to the ideation of the Kohn-Sham auxiliary system [31]. This is a fictitious system of non-interacting electrons moving in an effective external potential. Specifically, the new external potential is chosen in such a way that the *charge density* is the same as the one of the real system. Without considering the Kohn-Sham auxiliary system, only the external potential energy E^{ext} can be obtained analytically as a functional of the density thanks to its *locality*:

$$E^{ext}[n] = -e\langle\Psi[n]|\hat{V}^{ext}|\Psi[n]\rangle = -e\int dr\, V^{ext}(r)n(r). \tag{1.12}$$

Whereas both the kinetic energy and the electron-electron interaction energy cannot. In fact, their density functionals, $T[n]$ and $E^{e-e}[n]$, whose existence is guaranteed by DFT, remain to date unknown. This is particular dramatic for what concerns the kinetic term since it corresponds to a large contribution to the total energy. The electron-electron interaction, on the other hand, can be split into two terms: the electrostatic contribution to the energy $E_{Hartree}$ and the exchange-correlation energy E_{xc}. Of the two, the Hartree part can be written as a functional of the density and is often the dominant contribution, leaving only the exchange correlation functional to be approximated. This is remarkable since, for many systems, E_{xc} turns out to be small and to admit a reasonable approximation. It is also worth mentioning that, even if it is small, this "Nature's glue", as E_{xc} is called by Stefan Kurth and John Perdew [32], contains lots of important physics. On account of this, when E_{xc} is badly approximated, key phenomena are missed in the description.

The problem of the kinetic energy is avoided by using a fictitious system of non-interacting electrons, as the kinetic energy can be written exactly as functional of the single particle wavefunctions, namely the orbitals. As said before, this is the Kohn-Sham system and the electrons are assumed to be non-interacting. Once introduced the single particle orbitals $\{\phi_i\}_{i=1}^{N_e}$, it is then possible to construct the ground state by forcing the Pauli exclusion principle via a Slater determinant:

$$\Psi_{ks}(x_1,\cdots,x_{N_e}) = \frac{1}{\sqrt{N_e!}}\det\left(\begin{bmatrix} \phi_1(x_1) & \cdots & \phi_1(x_{N_e}) \\ \vdots & \ddots & \vdots \\ \phi_{N_e}(x_1) & \cdots & \phi_{N_e}(x_{N_e}) \end{bmatrix}\right) \tag{1.13}$$

The introduction of these orbitals, subject to the constraint $n(r) = \sum_{i=1}^{N_e}|\phi_i(r)|^2$, allows to write the Kohn-Sham kinetic functional

$$T_{ks}[\{\phi_i\}_{i=1}^{N_e}] = \sum_{i=1}^{N_e}\int dr\, \phi_i(r)^*\left(-\frac{\hbar^2}{2m}\nabla^2\right)\phi_i(r) \tag{1.14}$$

while the Hartree term has already been argued to be writable as a density functional

$$E_{Hartree}[n] = \frac{e^2}{2}\int dr\, \int dr'\, \frac{n(r)n(r')}{|r-r'|} \tag{1.15}$$

A weakness of the state-of-the-art in DFT is that even the functional associated to a one-body operator as the kinetic energy, despite its important role in the total energy, needs to be

approximated. This dictates the substitution of *orbitals* to the density in the description of the system.
In order to overcome this limitation and to move to orbital-free DFT while confining the estimation to only the many-body effects, a different approach can be considered. In this alternative modus operandi, the functionals are not directly expressed in terms of the density but in terms of an intermediate and more complicated object. This object is the one-body reduced density matrix (1-RDM) and contains not only the density but also some additional non-local information [33–36]. In the next section it will be shown how, thanks to the additional non-local information, any one-body operator can be expressed in terms of the 1-RDM. This approach was mainly introduced for describing systems characterized by strong correlations, in which Kohn-Sham DFT fails due to the importance of the exact kinetic information.

1.1.3 One body reduced Density matrix as the key ingredient for orbital free Density Functional Theory: Finding the density functional of the one-body reduced density matrix

In order to go beyond Kohn-Sham (orbital dependent) DFT it is necessary to determine a systematic theoretical approach to be used for checking the theory against the experiment. In particular it ought to be independent from the introduction of orbitals. Starting from equation 1.1 for a one-body operator $\hat{O} = \sum_{i=1}^{N_e} \hat{O}_i$ and considering the 4-dimensional variable $x_i = (r_i, \sigma_i)$, containing all of the degrees of freedom of the single electron, it is possible to show that the desired observable can be written in the form of a trace:

$$\begin{aligned} O[\Psi] &= N_e \int dx_1 \cdots dx_{N_e} \Psi^*(x_1, \cdots, x_{N_e}) \hat{O}(x_1') \delta(x_1' - x_1) \Psi(x_1', \cdots, x_{N_e}) = \\ &= \int dx_1 \hat{O}(x_1, x_1') \delta(x_1' - x_1) \left[N_e \int \left(\prod_{i=2}^{N_e} dx_i \right) \Psi(x_1', \cdots, x_{N_e}) \Psi^*(x_1, \cdots, x_{N_e}) \right] = \\ &\doteq \int dx_1 \hat{O}(x_1, x_1') \gamma(x_1', x_1) \delta(x_1' - x_1) = \\ &= \mathrm{Tr}(\hat{O}\hat{\gamma}) \rightarrow O[\gamma] = \mathrm{Tr}(\hat{O}\hat{\gamma}) \in \mathbb{R} \end{aligned}$$

Where the one electron (or body) reduced density matrix (1-RDM) $\gamma(x_1', x_1)$ has been introduced. In particular, processes involving spin changes will be neglected. This introduces a subspace Ω of possible spin configurations and we will refer to the 1-RDM as the one in which also the spin degrees of freedom are integrated out in the Ω-subspace:

$$\hat{\gamma}(r', r) \doteq \sum_{(\sigma, \sigma') \in \Omega} \hat{\gamma}(x', x) = \sum_{\sigma = \uparrow, \downarrow} \hat{\gamma}(r', \sigma, r, \sigma) \tag{1.16}$$

By comparing equations 1.16 and 1.10 it is possible to evince that the diagonal of the 1-RDM is the density of the system. Consequently, the 1-RDM contains both local information and the information regarding the self-dependency of the electron at a point of the space with itself at another point of the space. In rough terms, it tells how dependent is the cloud of probability of the single particle at two different points of space. Thanks to the representation independence of the trace operator, this result is extremely general and makes it possible to write all of the one-body operators as explicit functionals of the 1-RDM, together with all of the many-body operators for which there exist approximation schemes mapping them into effective one-body

operators.
If one notices that the 1-RDM is directly constructed from the state vector $|\Psi\rangle$ and that DFT guarantees that this object must be writable as a functional of the density[1], there must necessarily exist a density functional of the 1-RDM. Moreover, its knowledge would yield directly the knowledge of many density functionals, including the kinetic energy:

$$\boxed{\gamma[n] \Rightarrow O[n] = O[\gamma[n]]} \tag{1.17}$$

Therefore, the purpose of the work done has been to get some insight on the structure of the 1-RDM in order to write it as a functional of the density: $\hat{\gamma}[n]$. In a more pictorial way, considering a 1D system in which a domain has been sampled at N_g grid-points in order to treat the problem from a numerical point of view, the problem corresponds to expressing the matrix as

$$\hat{\gamma}[n] = \begin{bmatrix} n(r_1) & \gamma[n](r_1,r_2) & \dots & \gamma[n](r_1,r_{N_g}) \\ \gamma[n](r_2,r_1) & n(r_2) & \dots & \gamma[n](r_2,r_{N_g}) \\ \vdots & & \ddots & \vdots \\ \gamma[n](r_{N_g},r_1) & \gamma[n](r_{N_g},r_2) & \dots & n(r_{N_g}) \end{bmatrix}$$

and the real unknown is what are the functional constraints mapping the diagonal to the off-diagonals.

It is also worth mentioning that these same observations led the condensed matter community to a functional theory called Reduced Density Matrix Functional Theory (RDMFT), in which the minimization problem reads

$$E_{GS} = min_{\gamma}\{E[\gamma]\} = min_{\gamma \leftarrow \Psi}\{E[\Psi]\} \tag{1.18}$$

and the 1-RDM takes the role of the density as the quantity encoding the system. However, this functional theory has the disadvantage that the dimensionality of the object with which the functionals are to be constructed, and with respect to which the energy needs to be minimized, is much more complex than the density, even if it is far simpler than the wavefunction. It is essential to remark that our aim *is not* to work in the field of RDMFT. Some tools from this theory will be used but our purpose is to express the 1-RDM as a functional of the density, namely to understand and make explicit the functional constraints existing between the off-diagonal entries of the 1-RDM and the diagonal. This amounts to perform the compression in the information guaranteed by DFT.
Before to proceed, it is worth describing the meaning of the object we are willing to determine. In order to do that, let us introduce the field operator $\hat{\psi}^{\dagger}_{\sigma}(\mathbf{r})$, that is an operator creating a localized electron with a certain spin at the spatial position r: $|x\rangle = \hat{\psi}^{\dagger}_{\sigma}(r)|\rangle$. Starting from this,

[1] In the density is compressed all of the information on the system

the 1-RDM becomes:

$$\gamma(r,r') = N_e \int \left(\prod_{i=2}^{N_e} dx_i\right) \sum_{\sigma,\sigma',\sigma_2,\cdots,\sigma_{N_e}} \Psi(x',\cdots,x_{N_e})\Psi^*(x,\cdots,x_{N_e}) =$$
$$= \langle\Psi| \left[N_e \int \left(\prod_{i=2}^{N_e} dx_i\right) \sum_{\sigma,\sigma',\sigma_2,\cdots,\sigma_{N_e}} \frac{1}{\sqrt{N_e!}} (|x\rangle \otimes \cdots \otimes |x_{N_e}\rangle)(\langle x'| \otimes \cdots \otimes \langle x_{N_e}|) \frac{1}{\sqrt{N_e!}} \right] |\Psi\rangle =$$
$$= \langle\Psi| \left(\sum_{\sigma,\sigma'} |r,\sigma\rangle\langle r',\sigma'| \right) |\Psi\rangle = \langle\Psi| \left(\sum_{\sigma,\sigma'} \hat{\psi}^\dagger_\sigma(r)\hat{\psi}_\sigma(r') \right) |\Psi\rangle$$

In the case in which only one orbital was considered for each state, as happens when considering simple lattices, the field operator becomes a simple ladder operator $\hat{\psi}^\dagger_\sigma(r) = \hat{c}^\dagger_{r,\sigma}$ the formula becomes

$$\gamma(r,r') = \langle\Psi| \left(\sum_{\sigma,\sigma'} \hat{c}^\dagger_{r,\sigma}\hat{c}_{r',\sigma'} \right) |\Psi\rangle \tag{1.19}$$

In these terms the 1-RDM can be defined as the limit of the one-body reduced Green function, in which the two instants of time coincide: $\gamma(r,r') = \lim_{t'\to t^+} G(r,t;r',t')$. Alternatively, in a less rigorous way, it is possible to think that the many body ground state is made by indicating the number of electrons living in each single particle state. However, since the particles are indistinguishable, you can never say which particle is in which state. Therefore, it is useful to consider the *ground-state* of a *interacting* system of electrons as an *excited-state* of a system of *non-interacting* electrons, driven to higher energies to to the repulsive interaction with the other electrons. From this perspective, the element $\gamma_{\alpha,\beta}$ expresses the likelihood that when an electron leaves the state β, an electron appears in the state α. So $\gamma_{\alpha,\beta}$ indicates the degree of self-dependency of the probability cloud of an electron at two different positions of the space, i.e. it carries an information on the reciprocal subsequent exploration of the states α and β, dictated by the easiness with which it is possible to go from one to the other in this fictitious quantum stochastic process occurring at the microscopic scale.

1.2 Using machine learning as a tool: the role of constraints

The working table we have chosen for investigating the applicability of ML in designing models is finding the functional $\gamma[n]$. Since the diagonal of the 1-RDM is the density, this problem corresponds to find the functional constraints mapping the diagonal into the off-diagonals, exploiting the compression guaranteed by DFT. The functional constraints appearing are not much different from the ones that map the picture of a flower to the word "flower" and to its name in our brain. This analogy is particularly pertinent if we consider that, for a 1D system, any 1-RDM can be thought of as an image. In fact it can be pictorially represented by associating to the value of each entry a color in a colormap as can be observed in Fig. 1.1

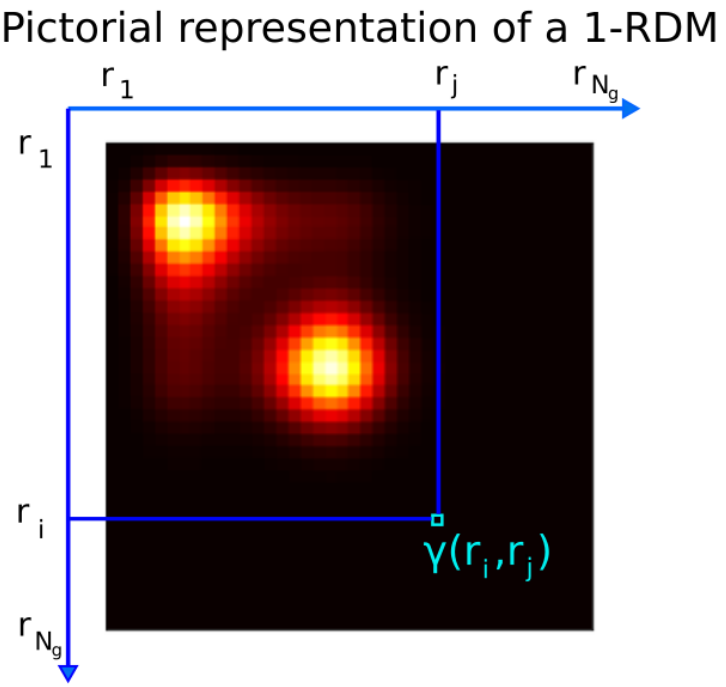

Figure 1.1: Pictorial representation of a 1-RDM for a 1D system in which the space has been quantized at N_g points, consequently solving the Schödinger equation and finding the associated 1-RDM. The pixel associated to the element $\gamma(r_i, r_j)$ has been highlighted in order to show how the numerical value of an entry of the matrix is associated to a color. Dark colors correspond to low values of the entries while the lighter the colors are the higher will be the associated entries.

As well as not all the pictures are pictures of flowers, not all the matrices are 1-RDMs or pictures of human faces. What identifies a matrix as belonging to a certain class is the presence of certain constraints between its entries. Details vary when considering objects belonging to sub-classes (a rose and a daisy, different density profiles or different people) but the distinctive constraints will be constantly present and they will differ in nature from class to class.
Let us focus on an hypothetical data-set of pictures of human faces. All of them share some constraints among the entries since there exist some anatomical elements that repeat in all of the figures. A pixel is generally non independent on the others and any two points of the whole matrix are generally strongly correlated as a consequence of the information contained in the matrix, i.e. the structure of the human faces. The intuition that under the nose there must be a mouth corresponds to conditions on the 1-RDM like the symmetry or the fact that the diagonal must be normalized to the number of electrons. This identifies a first kind of constraints, corresponding to the conditions that characterize the object as belonging to the class under analysis. The knowledge of these constraints, called *validity constraints*, is essential and must be included in any functional we will construct. There is then a different kind of constraints and an intuition on them can be found on the fact that our brain associates different names of individuals to different anatomical details, while respecting the validity constraints. This corresponds to the fact that different density profiles will be associated to different numerical values of the off-diagonals, while respecting the validity constraints. These are called *universal constraints* and are the complicated and unknown general functional relations mapping the object on which the functional is built (the name or the density) to the corresponding manifestation (the anatomical part or a certain off-diagonal entry). Finally, we can introduce a third kind of

constraints that comes from the sub-class of problems contained in the data-set. These are called *characterization constraints* and are strictly related to the particularization of the system. They force the 1-RDM to have features that are like this just because of the nature of the system under analysis. These constraints are the most useful ones in the construction of the functionals since their exploitation is what allows to build functionals for the class of potentials considered. Therefore it is of fundamental importance to keep in mind their existence since they will define the domain of applicability of the results found.
Starting from this analogy we moved to considering ML due to its success in image analysis tasks. In fact, in the course of the last year several ML tools have been proved to be effective in extracting this kind of spacial information from images, and to use it in classification tasks (e.g. determining if a picture is a picture of a flower or of a dove) and in image processing (e.g. compressing images). We hence tried to apply the existing algorithms to increase our knowledge on $\gamma[n]$.

1.3 The tools: fully connected neural networks, principal component analysis and autoencoders

As mentioned in the previous section, the main goal of the analysis is to get some insight on the quantum object 1-RDM and to use this information to design analytical models for the functional $\gamma[n]$. The way this will be done is by using Machine Learning (ML) techniques. It is worth being noticed that our aim is not to brute force machine learn the functional. On the contrary, the purpose is to start from the awareness that, given a sufficiently large data-set, Machine Learning tools can learn existing patterns. Then, the way the different tools structure the information is studied to determine how the acquired insight can be exploited for building density functionals. The way the tools will be presented is non-conventional but hopefully useful for the understanding of what are the key properties of the ML techniques employed for the specific task under analysis.

In this work we used the Python programming language [37]. The machine learning algorithms used were not implemented from scratch. We used pre-existing libraries named Keras [38] and Scikit-learn [39]. Moreover, for all the neural network drawings we used the software developed by Alexander LeNail [40].

1.3.1 Principal Component Analysis

Principal Component Analysis (PCA) is an unsupervised[2] ML technique that, given a large data-set of T objects, each of them characterized by a number of features N_f, is able to determine the most informative new set of features in which to describe the given data-set [41]. In the following, PCA will be introduced in an Hilbert-Space oriented formalism that allows to present it as a decomposition technique.
Let us consider a generic object $v^{(t)}$, that we know admits a representation in terms of N_f features. Given this information, it is possible to associate to that object a vector $|v^{(t)}\rangle$ and to define an

[2]Unsupervised learning is a subclass of ML in which only the input data is considered and the purpose is to extract information on the structure of the data.

orthonormal basis

$$\mathscr{B}_f = \{|f_s\rangle\}_{s=1}^{N_f}$$

and the corresponding identity operator

$$\mathbb{I} \doteq \sum_{s=1}^{N_f} |f_s\rangle\langle f_s|$$

The object can then be represented as

$$|v^{(t)}\rangle = \sum_{s=1}^{N_f} \langle f_s|v^{(t)}\rangle \cdot |f_s\rangle = \sum_{s=1}^{N_f} v_s^{(t)} \cdot |f_s\rangle \tag{1.20}$$

where the projection $v_s^{(t)} = \langle f_s|v^{(t)}\rangle \in \mathbb{R}$ corresponds to the numerical value of the s-th feature. Analogously, by implicitly referring to the basis of the representation, the same object can be written as

$$\underline{v}^{(t)} = \begin{bmatrix} v_1^{(t)} & v_2^{(t)} & \cdots & v_{N_f}^{(t)} \end{bmatrix} \in \mathbb{R}^{N_f}$$

As said before, the interest is in considering a large number of such objects since we are willing to discover the existence of correlations among the features. To this end, the data-set can be thought of as a matrix $V \in \mathbb{R}^{T\times N_f}$:

$$V = \begin{bmatrix} \underline{v}^{(1)} \\ \vdots \\ \underline{v}^{(T)} \end{bmatrix} \in \mathbb{R}^{T\times N_f}$$

The disposal of this data-set allows us to define a new basis with which it is possible to describe the v-vectors. PCA is considered a linear numerical method to determine the following two sets of quantities:

- $|v_0\rangle$: The mean vector. Its knowledge allows to write each vector belonging to the same class as those in the data-set in terms of its variations from the mean $|v\rangle = |v_0\rangle + |\tilde{v}\rangle$. $|\tilde{v}\rangle$ is termed the mean-adjusted vector. The mean vector components in the previously defined basis read

$$(v_0)_i = \frac{1}{T}\sum_{t=1}^{T} v_i^{(t)}.$$

- $\mathscr{B}_{pca} = \{|p_l\rangle\}_{l=1}^{N_f}$: A new orthonormal basis, corresponding to the principal components (or principal directions). They are the normalized eigenvectors of the covariance matrix

$$C = \frac{1}{T-1}V^\dagger V = \sum_{s,s'=1}^{N_f} c_{s,s'}|f_s\rangle\langle f_{s'}|$$

$$c_{s,s'} = \frac{1}{T-1}\sum_{t=1}^{T}(v_s^{(t)} - (v_0)_s)(v_{s'}^{(t)} - (v_0)_{s'}).$$

  The eigenvalues of such a matrix are termed the variances $\{\sigma_i^2\}_{i=1}^{N_f}$. The principal components are the directions along which, in the data-points, there are the most informative variations with respect to the average vector. They are sorted by importance depending on the value of the associated eigenvalue.

A widespread approach for intuitively introducing these concepts is to consider a 2D example (see [42]). In Fig. 1.2 it is possible to find a data-set of points randomly distributed along a line. In order to have a visual understanding of the quantities introduced so far a PCA has been performed on this data-set and the quantities have been drawn.

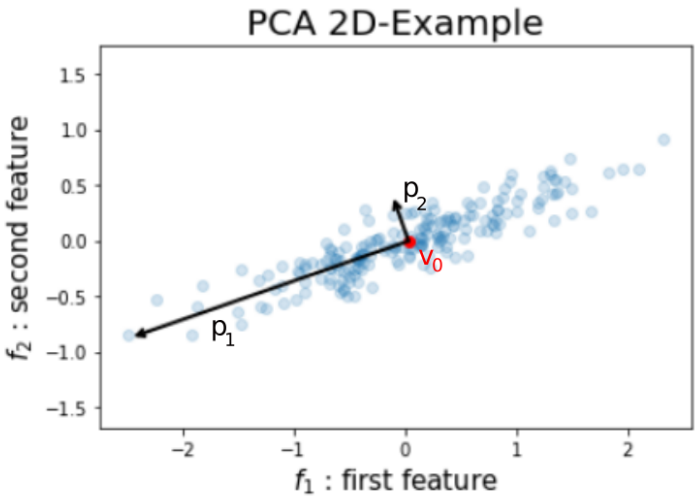

Figure 1.2: 2D example of PCA. The data-points are in light blue, the mean data-point is in red and the principal components are multiplied by a scaling factor proportional to the associated eigen-value.

The mean vector $\underline{v}_0 = [(v_0)_1, (v_0)_2]$ is represented in red and any point in the data-set can be represented starting from this point. The maximally informative direction is the eigen-vector of the correlation matrix associated to the biggest eigenvalue, namely $\underline{p}_1$. The principal components have been re-scaled proportionally to the associated eigen-values to take into account the different importance in describing the data. PCA has been able to understand that the most striking feature of the data-set under analysis is the distribution of the points along the line. Therefore, the first principal component ($\underline{p}_1$) identifies that line. Finally, the second eigen-vector, necessarily orthogonal to the first one, takes into considerations the remaining information.

At this point we have discussed how the knowledge of the data-set implies that, by solving the eigen-equation

$$C|p_l\rangle = \sigma_l^2 |p_l\rangle$$

one can determine the coefficients $\langle f_r|p_l\rangle$ in the expansion

$$|p_l\rangle = \sum_{s=1}^{N_f} \langle f_s|p_l\rangle |f_s\rangle. \tag{1.21}$$

Each object can then be expressed in this new basis in an expansion called *principal components decomposition*:

$$|v^{(t)}\rangle = |v_0\rangle + \sum_{l=1}^{N_f} \langle p_l|\tilde{v}\rangle \cdot |p_l\rangle. \tag{1.22}$$

The main property of PCA is that the existence of linear constraints between the features of the object under analysis (entries of the vector) leads to vanishing eigenvalues, associated to non-informative principal components. For instance, in the 2D example, if the randomness was further reduced, PCA would find a value even smaller for the second eigen-value. In the limit in which we remove completely the randomness, sampling the points on the line, the first principal component would suffice in locating uniquely any data point. This amounts to a compression of the information by using a reduced number $\eta < N_f$ of components, that means that the decomposition

$$|v\rangle = |v_0\rangle + \sum_{l=1}^{\eta} \langle p_l|\tilde{v}\rangle \cdot |p_l\rangle. \tag{1.23}$$

is lossless, thanks to the compression.

The very same concept can be applied to the analysis of matrices after a flattening procedure. Starting from the general object[3]

$$\gamma^{(t)} = \begin{bmatrix} \gamma_{11}^{(t)} & \cdots & \gamma_{1N_g}^{(t)} \\ \vdots & \ddots & \vdots \\ \gamma_{N_g1}^{(t)} & \cdots & \gamma_{N_gN_g}^{(t)} \end{bmatrix} \in \mathbb{R}^{N_g \times N_g}. \tag{1.24}$$

In order to represent this matrix, it is possible to define a N_g^2-dimensional basis, each component of which points to a different entry of the matrix

$$\mathscr{B}_e = \{|e_s\rangle\}_{s=1}^{N_g^2} = \{|e_{s[i,j]}\rangle\}_{i,j=1}^{N_g}$$

This basis leads to the 'flattened' version of the original matrix, represented as the following vector:

$$|\gamma^{(t)}\rangle = \sum_{i,j=1}^{N_g} \langle e_{s[i,j]}|\gamma^{(t)}\rangle \cdot |e_{s[i,j]}\rangle = \sum_{i,j=1}^{N_g} \gamma_{i,j}^{(t)} |e_{s[i,j]}\rangle \tag{1.25}$$

or, also

$$\underline{\gamma}^{(t)} = \begin{bmatrix} \gamma_{1,1}^{(t)} & \gamma_{1,2}^{(t)} & \cdots & \gamma_{N_g,N_g}^{(t)} \end{bmatrix} \in \mathbb{R}^{N_g^2}. \tag{1.26}$$

The data-set of T such vectors is then introduced:

$$\Gamma = \begin{bmatrix} \underline{\gamma}^{(1)} \\ \vdots \\ \underline{\gamma}^{(T)} \end{bmatrix} \in \mathbb{R}^{T \times N_g^2} \tag{1.27}$$

The disposal of the data-set allows for the definition of the PCA basis $\mathscr{B}_{pca} = \{p_l\}_{l=1}^{N_g^2}$ and each matrix can then be expressed as its principal components decomposition:

$$|\gamma^{(t)}\rangle = |\gamma_0\rangle + \sum_{l=1}^{N_g^2} \langle p_l|\tilde{\gamma}^{(t)}\rangle \cdot |p_l\rangle. \tag{1.28}$$

[3]The choice of the notation will be cleared in the following.

For what concerns the possibility of the existence of linear constraints, for instance, if the matrix is symmetric $\gamma^{(t)}_{i,j} = \gamma^{(t)}_{j,i}\ \forall t$, the data can be compressed to $\eta \leq N_g + \binom{N_g}{2} = \frac{N_g(N_g+1)}{2}$, and the matrix can be losslessly represented using a reduced number of principal components

$$|\gamma^{(t)}\rangle = |\gamma_0\rangle + \sum_{l=1}^{\eta} \langle p_l|\tilde{\gamma}^{(t)}\rangle \cdot |p_l\rangle. \tag{1.29}$$

By contrast, even if the constraints among the features are not exactly linear but approximately, this implies that the variances may be safely neglected above a fixed value of η. Among the different possible criteria for choosing when to consider the reconstruction to be optimal, the one we will often use is the determination of the component above which the cumulative sum of the explained variance ratio is above a certain threshold R^{σ}_{th}, i.e.

$$|\gamma^{(t)}\rangle \equiv |\gamma_0\rangle + \sum_{l=1}^{\eta} \langle p_l|\tilde{\gamma}^{(t)}\rangle \cdot |p_l\rangle \Leftrightarrow R^{\sigma}_{\eta} = \sum_{l=1}^{\eta} \frac{\sigma_l^2}{\sum_{m=1}^{N_g^2} \sigma_m^2} < R^{\sigma}_{th}$$

Eigen-faces and PCA-functional

A widespread example of the potential use of the principal component decomposition is the one of *eigen-faces*, a practical explanation of which can be found at [43]. The data-set considered is a collection of flattened matrices, each of which corresponds to a human face. As a first thing PCA finds $|\gamma_0\rangle$, corresponding to the average face. $|\gamma_0\rangle$ contains the common structure and will reasonably be an ovaloid with two depressions for the eyes etcetera. This average matrix partially contains the *validity constraints* since it is a strong starting point from which details can only deviate. Then, the deviations from the average face will be considered by looking at the biggest variations of the anatomical details, in order of importance. Simplistically, depending on the faces present in the data-set, it may be that the first principal component is totally dedicated to the shape of the eyes or that the first principal component treats simultaneously the color of the eyes and of the hair. Each principal component is dedicated to increase the resolution of the face adding anatomical details, possibly linearly related to each-others and sharing the degree of variability in the data-set. In order to go in more detail let us consider the principal components associated to the Olivetti faces data-set [39]. The details can be observed in figure 1.3. As it is possible to evince, the principal components are not dedicated to a single anatomical parts, as they were simplistically introduced before. This would probably be the case if we had a data-set of caricatures. By contrast, when normotypes are concerned, there exist many constraints between the different anatomical part that result in a merging of the information throughout the list of the principal components, manifesting the presence of constraints among the entries.

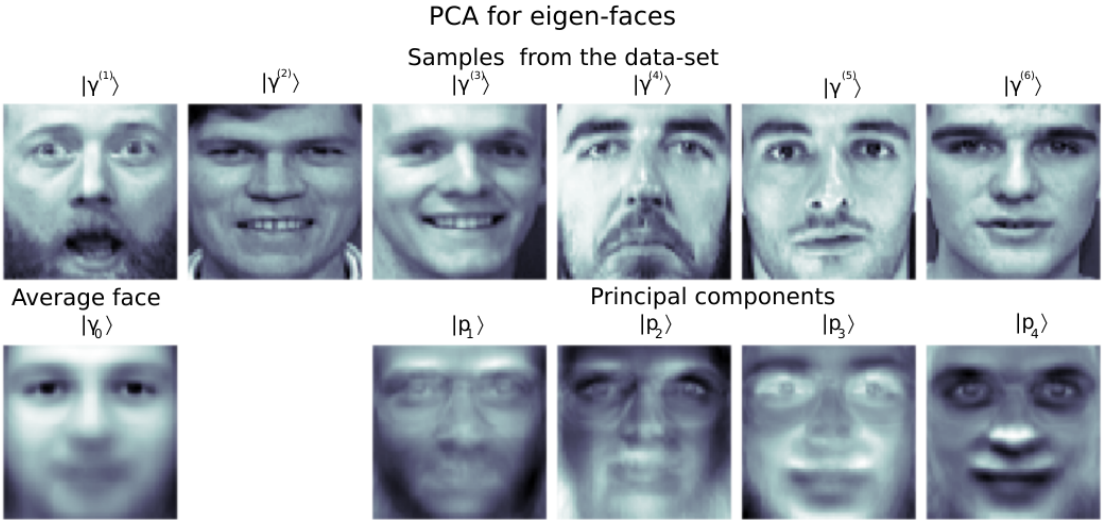

Figure 1.3: PCA on the Olivetti faces data-set. On the top row six examples are presented, followed by the average face on the bottom left and by the first four principal components on the right. In this picture the vectors on which the PCA has been performed have been reshaped to be represented as matrices.

Therefore, once having associated to each principal component a linear combination of features, sorted by importance, the face of any individual $|\gamma^{(name)}\rangle$ can be written by specifying the intensity of variation along the principal components for the specific individual:

$$|\gamma^{(name)}\rangle = |\gamma_0\rangle + \sum_{l=1}^{N_g^2} \langle p_l|\tilde{\gamma}^{(name)}\rangle \cdot |p_l\rangle = \\ = |\gamma_0\rangle + \sum_{l=1}^{N_g^2} \omega_l[name] \cdot |p_l\rangle$$

So if you want to estimate the face of a new individual, not present in the original data-set, and you know only what are his/her anatomical details, the only thing you need to do is to know the average face from which you start for doing the identikit and the information contained in the principal components. Then, in order of importance of the new features, by properly adjusting the correct coefficient ω_l for a certain person it is possible to construct his/her face. In these terms, *the face of a person is a non trivial functional of his/her name* as well as the 1-RDM is a functional of its density. This idea led to the construction of the first functional. The hearth of the functional is the fact that the "name" of the 1-RDM is the density, contained in the object itself. Knowing everything about the density, the purpose is thus to extract the full matrix. As it is possible to evince from the principal components in Fig. 1.3, all the entries of each component must be strongly related. Consequently, the idea at the basis of the PCA-functional will be to reconstruct the density with the stored principal components and, thanks to the presence of the constraints, this information will be propagated to the off-diagonal entries.

1.3.2 Principal component analysis for data compression: a linear Neural network

Let us go back to considering a general input vector $\underline{v}^{(t)}$. In this section a graphical representation of the PCA will be introduced. As told in the previous section, PCA can be used for compressing data. Starting from the V data-set, after having determined the principal directions $\{|p_l\rangle\}_{l=1}^{N_f}$, it is possible to exploit the existence of linear constraints between them by determining the number of principal components $\eta < N_f$ for which the reconstruction is lossless (or acceptable) $\{p_l\}_{l=1}^{\eta}$. Once chosen this number and the corresponding principal components, each data can be compressed from N_f to η. Let us represent this process graphically. Stored the principal components, one needs to determine the weights $\langle p_l|v^{(t)}\rangle$. From a practical point of view, what is needed is a way to represent the scalar product

$$\langle p_l|v^{(t)}\rangle = \sum_{s=1}^{N_f} \langle p_l|f_s\rangle\langle f_s|v^{(t)}\rangle = \\ = \sum_{s=1}^{N_f} \omega_{l,s} v_s^{(t)} \in \mathbb{R}$$

Where the coefficients $\omega_{l,s} = \langle p_l|f_s\rangle$ are known, since they are the numerical components of the eigen-vectors of the correlation matrix. Whatever input vector is considered, each of its entries needs to be multiplied by the corresponding entry of the principal component. Finally, all of the coefficients thereby found need to be summed, resulting in a scalar that is the new feature, i.e. the projection of the vector onto the l-th principal component. In Fig. 1.4 the scheme on the left describes this process. The s-th node corresponds to the s-th entry of the input vector, the value $\langle f_s|v\rangle$. The colors correspond to different values of the projection of the principal component, i.e. to the so called *weights* $\omega_{l,s}$

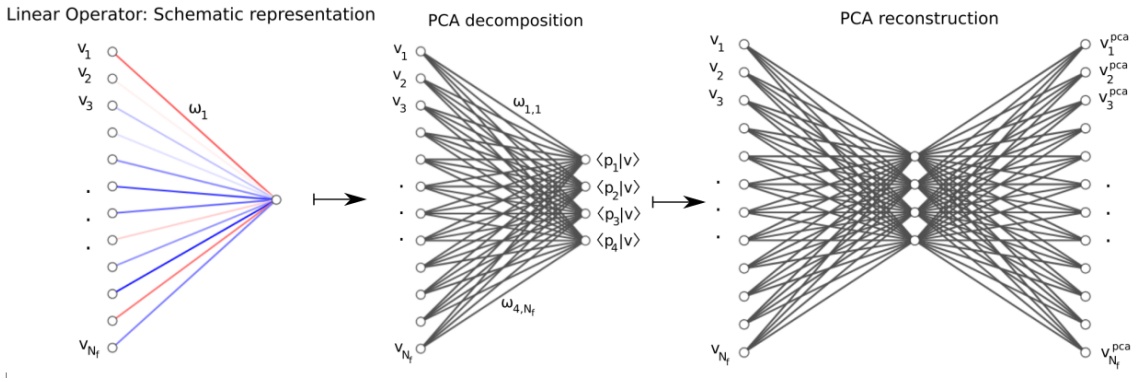

Figure 1.4: Schematic representation of the concepts entering in PCA, used for introducing NN-architectures. On the left a generic operator is represented. The nodes on the left correspond to the input values, the colors correspond to the coefficient to be multiplied to each entry of the input vector and the right node corresponds to the resulting weighted sum of the input entries, later including a constant term. The scheme in the center represents the calculation of the projections onto the first 4 principal directions while the scheme on the right corresponds to the reconstruction of the input vector by using only the first 4 principal directions. In the last two schemes the colors have been omitted.

Finally, the output node corresponds to the result of the scalar product and it is the projection of the input data onto the l-th principal component, the new feature. This can be repeated for all of the η principal components under analysis, leading to the scheme in the center of Fig. 1.4, schematically representing the mapping

$$\{v_s^{(t)}\}_{s=1}^{N_f} \longmapsto \{\langle p_l | v^{(t)} \rangle\}_{l=1}^{\eta}.$$

Finally, by inverting the network while preserving the weights, it is possible to graphically exploit the content of equation 1.23, as it can be seen on the left of Fig. 1.4.
More in general, this scheme represents a process of linear compression of the information for then restoring it, with the purpose of giving as an output the exact input, in case of presence of linear constraints between the features or, otherwise, the closest approximation obtainable by exploiting the linear constraints. The exactness is quatified by the distance of R_η^σ from the optimal value, namely $R_{\eta^*}^\sigma = 1$.

1.3.3 Neural Network architectures and Autoencoders

Let us go back to the scheme on the left of Fig. 1.4. In it it is represented an architecture that receives N_f inputs and converts them to a scalar value. Now the weights and the parameters of the model introduced so far were optimized for the linear compression task described before. However, the first scheme in Fig. 1.4 can be associated to a more general class of objects. In particular, let us substitute the vector $|p_l\rangle$ with another generic vector $|\theta_l\rangle$. By assuming that a constant term is implicitly added to the output, this architecture can equally represent the generic linear operator

$$\hat{F}^L = \langle \cdot | \theta_l \rangle + b : \mathbb{R}^{N_f} \to \mathbb{R} \qquad \hat{F}^L | v^{(t)} \rangle = \langle v^{(t)} | \theta_l \rangle + b.$$

This is a linear parametric method that, given a data-set $V = \{\underline{v}^{(t)}\}_{t=1}^T$ and the corresponding values of a function of these variables $Y = \{y^{(t)}\}_{t=1}^T$ can be fit to linearly approximate the desired function. The first scheme in Fig. 1.4 can thus be used for graphically represent a linear model for regression, whose weights need to be determined and carrying an implicit additive factor b, named *bias*, in the output. This is nothing else than the building block used in PCA for extracting the new features[4] but under this perspective and with this notation it is clearer the way to go beyond that linear technique. Let us assume that we want to use this model to learn a non-linear function of the input variables. The way this can be done is by introducing an appropriate non-linearity in the mapping $\mathbb{R}^{N_f} \to \mathbb{R}$:

$$\hat{F}^{NL} = f^\sigma(\langle \cdot | \theta_l \rangle + b) : \mathbb{R}^{N_f} \to \mathbb{R} \qquad \hat{F}^{NL} | v^{(t)} \rangle = f^\sigma(\langle v^{(t)} | \theta_l \rangle + b)$$

[4]Being PCA linear the building block is necessarily just the scalar product.

Where $f^{\sigma}(\cdot)$ is an appropriate function, to be chosen depending on the task to be accomplished. By explicitly writing the scalar product, it is possible to obtain

$$\begin{aligned} F^{NL}(v^{(t)}) &= f^{\sigma}(\langle v^{(t)}|\theta_l\rangle + b) = \\ &= f^{\sigma}\left(\sum_{s=1}^{N_f}\langle v^{(t)}|f_s\rangle\langle f_s|\theta_l\rangle + b\right) = \\ &= f^{\sigma}\left(\sum_{s=1}^{N_f} v_s^{(t)}\theta_{l,s} + b_l\right) \rightarrow \boxed{F^{NL}(v^{(t)}) = f^{\sigma}\left(\sum_{s=1}^{N_f} v_s^{(t)}\theta_{l,s} + b_l\right)} \end{aligned}$$

This equation corresponds to a non-linear parametric model to be fitted and is generally called *perceptron*. Its weights can be determined by means of an algorithm called back-propagation [44] that is based on the idea of showing to the network several examples of the functional relation to be determined and by adjusting the parameters of the model in order to minimize a function called *loss function*;

$$Loss = Loss(\{\omega_s\}_{s=1}^{N_f}, b) = Loss(\{||F^{NL}(v^{(t)}) - y^{(t)}||_m\}_{t=1}^{T}) : \mathbb{R}^{N_f+1} \rightarrow \mathbb{R}.$$

This function is a multivariate function defined on the hyperspace of the parameters and it is a scalar accounting for the distance, in some chosen metrics m, between the target value of the function and the predicted value of the architecture. The back-propagation algorithm is an algorithm allowing to determine the minimum of this function, i.e. exploiting the following equation

$$(\{\omega_s^*\}_{s=1}^{N_f}, b^*) = argmin\{Loss(\{\omega_s\}_{s=1}^{N_f}, b)\} \tag{1.30}$$

In general, when there is a data-set at disposal for this task it is divided into two parts, a training part and a test part. The training part is used for solving the minimization problem while the test part is used for checking the generality of the model and to make sure that no overfitting has occurred, that is to say that allows to check that the machine is not learning by heart.
Moving to the second scheme in Fig. 1.4, it is directly possible to generalize the method to non-scalar fields mapping $\mathbb{R}^{N_f}$ to an arbitrary dimension $\mathbb{R}^{N_1}$. As the figure suggests, this can be done by stacking N_1 perceptrons one on top of the others. Each of them needs to be fitted in order to properly estimate the corresponding component of the vectorial function. In formulas, the output of the l-th perceptron reads

$$F_l^{NL}(v^{(t)}) = f^{\sigma}\left(\sum_{s=1}^{N_f}\omega_{l,s}v_s^{(t)} + b\right) \qquad \text{for } l = 1, \cdots, N_1$$

As the task to be accomplished is a regression task, it is worth mentioning the fact that the perceptron introduces the non-linearity but it cannot approximate every function due to its simplicity. By contrast, just adding an additional layer is sufficient for solving any regression problem. The universal approximation theorem [45], in fact, states that for any real function there exists a *Multi Layer Perceptron* (MLP), also known as *Fully connected Neural Network* (FNN), with one hidden layer of appropriate dimension, able to approximate it. In formulas, the model

$$F^{NL}(v^{(t)}) = f^{\sigma_o}\left(\sum_{s=1}^{N_1}\omega_{l,s}^o \cdot f^{\sigma_h}\left(\sum_{l=1}^{N_f}\omega_{l,s}^h v_s^{(t)} + b_l^h\right) + b^o\right) \tag{1.31}$$

is an universal approximator[5] given an appropriate choice of N_1, of the non-linearities f^{σ_o} and f^{σ_h} and the use of the back-propagagion algorithm .
The MLP is one of many architectures in the family of the *Neural Network* (NN) architectures. In the previous section PCA has been introduced. At this point it can be thought of as a linear data compression technique, that exploits the existence of linear constraints between the features for generating new ones. It is linear since each new feature is a weighted sum of the old ones, with appropriate weights. The only limitation of PCA compression is that it is effective only in the extremely limiting case of linear constraints among the features. At this point it is straightforward that PCA is a special form of neural network specialized in the task of reconstructing the input after having compressed it into what is generally called its *latent space* representation. This NN works in linearity and the weights vectors are orthogonal. By imposing all of these constraints and by training the neural network to reconstruct the mean adjusted input vector while working in linearity, the back-propagation algorithm must learn that the biases are negligible and that the weights vectors $|\theta\rangle$ correspond to the principal components. By removing the orthogonality condition and by introducing the non-linearity it is then possible to take into account the existence of non linear dependencies between the features and to explicit them in order to give rise to the best possible compression. These architectures are named *autoencoders* (AE) and are data-set specific information compressors[6]. In figure 1.5 a schematic representation of the way an AE works is presented. It is important to stress that, in order to perform an effective compression, the machine needs to learn how to encode the data and, as a consequence, it has to learn the underlying structure of the data. This is particularly interesting in our case since, accordingly to DFT, the 1-RDM should be completely encoded in its diagonal, the density. This amounts to say that DFT guarantees the existence of an AE characterized by a latent space having the same dimensionality as the density. Finding this AE and being able to interpret the architecture would amount to find the connection between the 1-RDM and the density, corresponding to the desired functional.

[5]The label o stays for output while the label h stays for the hidden layer

[6]Data specific shall mean that, in contrast with other classical compression techniques, if this machine is trained to optimally compress images of a certain class, say pictures of daisies, it will not be able to compress images of a different class, say pictures of foxes.

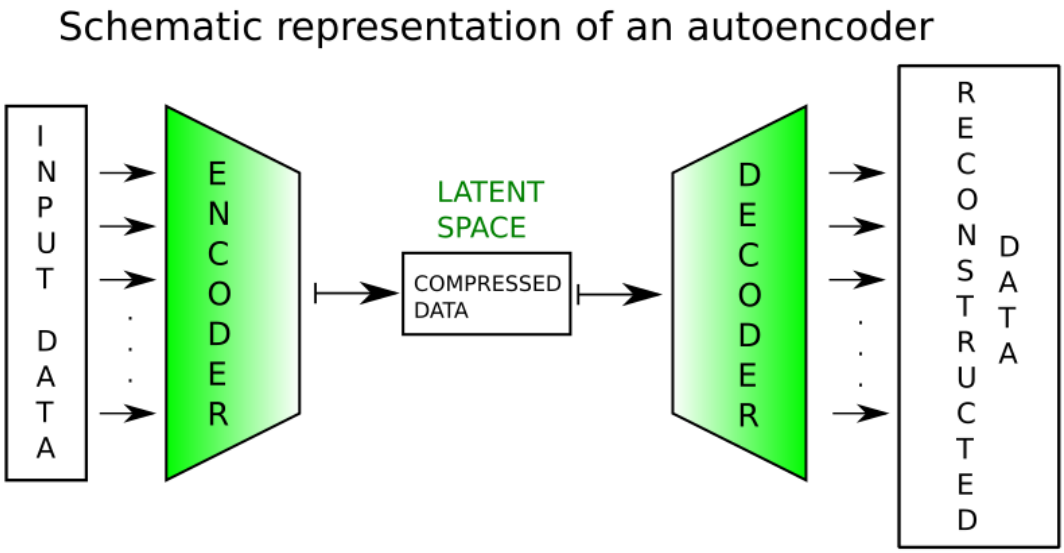

Figure 1.5: Schematic representation of an autoencoder. The input data enters into the encoder part that performs the compression, transforming the input into its compressed version, represented into the *latent space*. Then, the decoder has to restore the input data by using the compressed version alone.

1.3.4 Convolutional Neural Network

So far only one subclass of NN has been considered, the FNN. As mentioned before, this architecture can in principle approximate any function. However, it may be not the optimal architecture for all the tasks. Let us consider an image represented as a $N_g \times N_g$ array of pixel values. Any image can be flattened,i.e. reduced to a vector, and the correlations between the entries can be studied. However, when performing the flattening, an essential spacial information is thrown away. When an image is represented as a matrix, in fact, the value stored in an entry is indicative of the surrounding values. When an image is representing a pattern, the pattern is much clearer when represented in its matrix form. Convolutional Neural Networks (CNN) are a specific class of NN-architectures able to work with images and to extract this kind of information via an operation called *convolution*. In order to understand this kind of architecture, let us consider a generic matrix $\gamma \in \mathbb{R}^{N_g \times N_g}$ and a 3 by 3 kernel

$$K = \begin{bmatrix} k_{-1,-1} & k_{-1,0} & k_{-1,1} \\ k_{0,-1} & k_{0,0} & k_{0,1} \\ k_{1,-1} & k_{1,0} & k_{1,1} \end{bmatrix}$$

The convolution operation is then an operation performing a mapping $\mathbb{R}^{N_g \times N_g} \to \mathbb{R}^{(N_g-2)\times(N_g-2)}$ where the (r,c) entry of the new matrix is defined as

$$F_{r,c} = (\gamma \circledast K)_{r,c} \doteq \sum_{i\in\{-1,0,1\}} \sum_{j\in\{-1,0,1\}} k_{i,j} \cdot \gamma_{r+i,c+j} \tag{1.32}$$

Just as before the Back-propagation algorithm was meant to learn the weights of the architecture, in this case what is to be learned are the entries of the kernel matrix, meaning that the machine is able to learn non-local features. Let us assume, for instance, that the CNN has learned the following kernel, also known as North Kirsch Mask[46]

$$K = \begin{bmatrix} 5 & 5 & 5 \\ -3 & 0 & -3 \\ -3 & -3 & -3 \end{bmatrix}$$

This would mean that the network, for the task at hand, has learned that an important feature to be learned is the detection of an horizontal edge of growing intensity from the bottom to the top. The resulting image is usually called *filter*, and it can be used for feeding another convolutional layer or it can be flattened and used for feeding a Dense layer.

By combining the building blocks presented so far it is possible to create arbitrarily complex architecture, to be fitted.

1.4 The dataset

In order to use ML tools it is essential to construct a large data-set of external potentials, charge densities and 1-RDMs. Moreover, if the goal was to extract general information on the 1-RDM, it would be necessary to have an extremely variegated data-set, comprising different interaction physics. Due to the unfeasibility of handling a general data-set, further restrictions need to be done on the systems under analysis. This is the origin of the previously discussed *characterization constraints*.
To generate the data-sets the `iDEA` code [47–49] has been used. Ideated by Piers Lillyston [47] and developed by researchers at the university of York, among which Jack Wetherell, this software allows to numerically solve the many-body Schrödinger equation for finite systems of up to four electrons interacting via a softened Coulomb interaction on a one-dimensional real-space grid, given any arbitrary local external potential. In addition, it provides implementations of many widely-used approximate methods. After computing the exact many-body wavefunction, any required observables can be directly obtained via expectation values. The model systems solved by the `iDEA` code have been used in the past to develop improved approximations to DFT [50], many-body perturbation theory [51], as well as investigating the nature of exact potentials [49], where the model systems have been shown to well describe crucial features as that of real three-dimensional molecules [52].
In this work the system under analysis will be a 1-dimensional system in which two electrons oppositely spin resolved are forced to live, interacting or not in the presence of a randomly generated, smooth and confining external potential. Despite the constraints imposed, it is worth mentioning that this model can be thought of as a potential model for a two-electron molecules, such as the Hydrogen molecule, in the singlet ground state. For each system a random smooth potential $V(x)$ is generated and the exact ground-state many-body wavefunction is computed. From this the charge density $n(x)$ and the 1-RDM $\gamma(x,x')$ are directly obtained. For the same potential, the same quantities are computed also in the case of non-interacting electrons (NON). As these are bounded systems, the ground-state wave-function can always be chosen to be real. Any complex multiplicative factor, if present, must be independent on the positional argument since, if this were not so, the application of the current operator would yield a result different

from zero, that is in contradiction with the concept of stable ground states orbitals. The external potential is generated as a sum of randomly distributed Fourier components within a large confining potential[53]:

$$V(x) = Dx^{10} + T\sum_{n=1}^{N}\left(a_n\cos\left(\frac{n\pi x}{L}\right) + b_n\sin\left(\frac{n\pi x}{L}\right)\right), \tag{1.33}$$

where $L = 15(\text{a.u.})$[7] is the width of system, $N = 3$ is the number of Fourier terms, $D = 10^{-11}$ is the damping factor of the confining term and $T = 0.1$ is the damping factor of the Fourier terms. a_n and b_n are generated randomly with a uniform distribution from $-\frac{2L}{3}$ to $\frac{2L}{3}$. In this work will be mainly considered the data-sets of 50,000 systems obtained for 2, 3, 8, 20 and 42 grid points. The number of grid-points will be generally denoted as N_g.

Fig.1.7 shows the first five elements of the 50,000 test systems in the data-set with 42 grid points. It is worth remarking that, in this work, a more pythonic-oriented representation of the 1-RDMs has been chosen and a generic 1-RDM , *redefined by introducing the increment* Δr, reads

$$\gamma^{(t)} = \begin{bmatrix} \gamma^{(t)}(r_1,r_1)\Delta r & \cdots & \gamma^{(t)}(r_1,r_{N_g})\Delta r \\ \vdots & \ddots & \vdots \\ \gamma^{(t)}(r_{N_g},r_1)\Delta r & \cdots & \gamma^{(t)}(r_{N_g},r_{N_g})\Delta r \end{bmatrix} = \begin{bmatrix} \gamma^{(t)}_{1,1} & \cdots & \gamma^{(t)}_{1,N_g} \\ \vdots & \ddots & \vdots \\ \gamma^{(t)}_{N_g,1} & \cdots & \gamma^{(t)}_{N_g,N_g} \end{bmatrix} \in \mathbb{R}^{N_g\times N_g}. \tag{1.34}$$

Contrary to a more widespread representation in physics, in which the diagonal goes from bottom left to top right.
The presence of the element $\Delta r = 2L/N_g$ implies that

$$\sum_{i=1}^{N_g}\gamma_{i,i} = \sum_{i=1}^{N_g}\gamma(r_i,r_i)\Delta r = 2.$$

These data-sets have been used to train and test the different machine learning models.
The non-interacting system of two electrons in the singlet state is a very special condition. In fact, the spacial part of the two body state in the position representation is nothing else than the product of the single particle states. Moreover, due to the fact that the ground state must be real, that the modulus square of the single particle state must sum to one and that the two electrons must share the lowest energy mode, the state vector in the position basis reads

$$\begin{aligned} |\Psi\rangle &= \int dr_1 dr_2 \Psi(r_1,r_2)|r_1,r_2\rangle = \\ &= \int dr_1 dr_2 \psi(r_1)\psi(r_2)|r_1,r_2\rangle = \\ &= \int dr_1 dr_2 \sqrt{\rho(r_1)\rho(r_2)}|r_1,r_2\rangle \end{aligned}$$

where $\rho(r)$ is the single particle density function. This having been said, the 1-RDM of the non-interacting case is known to be

$$\begin{aligned} \gamma(r,r') &= N_e\sqrt{\rho(r')\rho(r)}\int dr_2\rho(r_2) = \\ &= \sqrt{n(r)n(r')} \end{aligned}$$

[7]Hartree atomic units: $m_e = \hbar = e = 4\pi\varepsilon_0 = 1$.

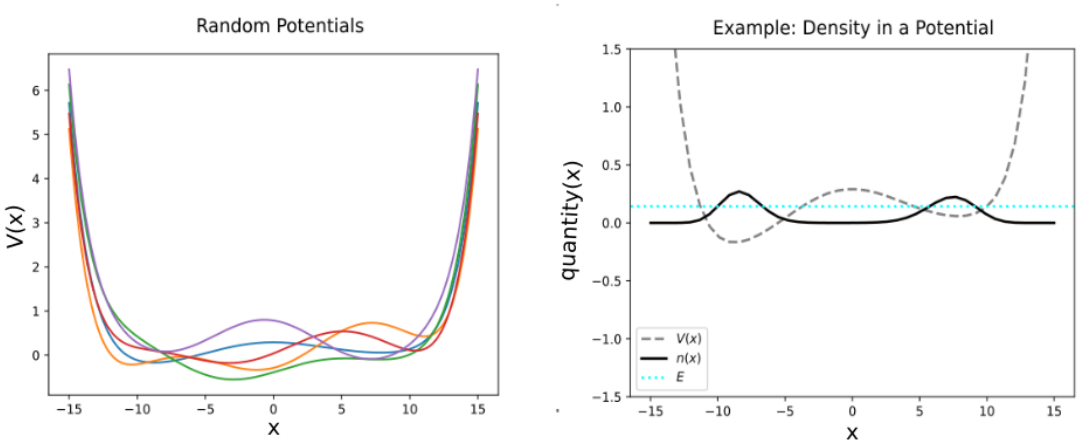

Figure 1.6: On the left Random Potential examples are represented while on the right a specific potential has been selected and the corresponding 1-electron density and energy have been plotted.

This corresponds exactly to the desired functional. The purpose is to find a way to estimate the analogous functional in the interacting case.

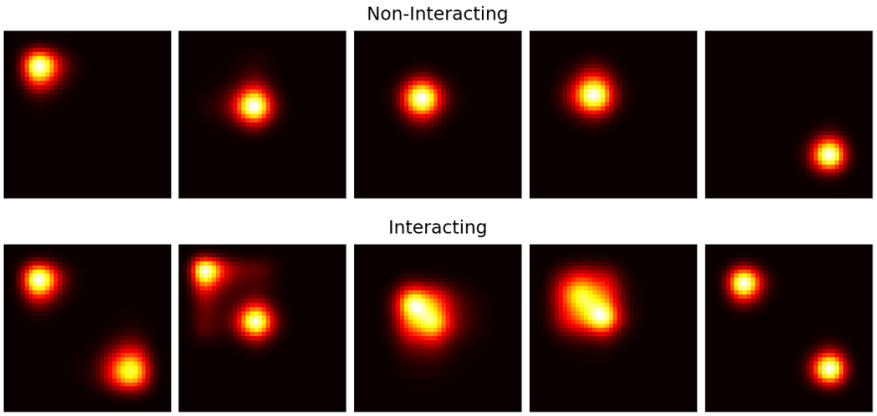

Figure 1.7: First five 1-RDMs in the data-set. For the same potential landscape the one on the top is the non-interacting 1-RDM while the one in the bottom is the interacting one.

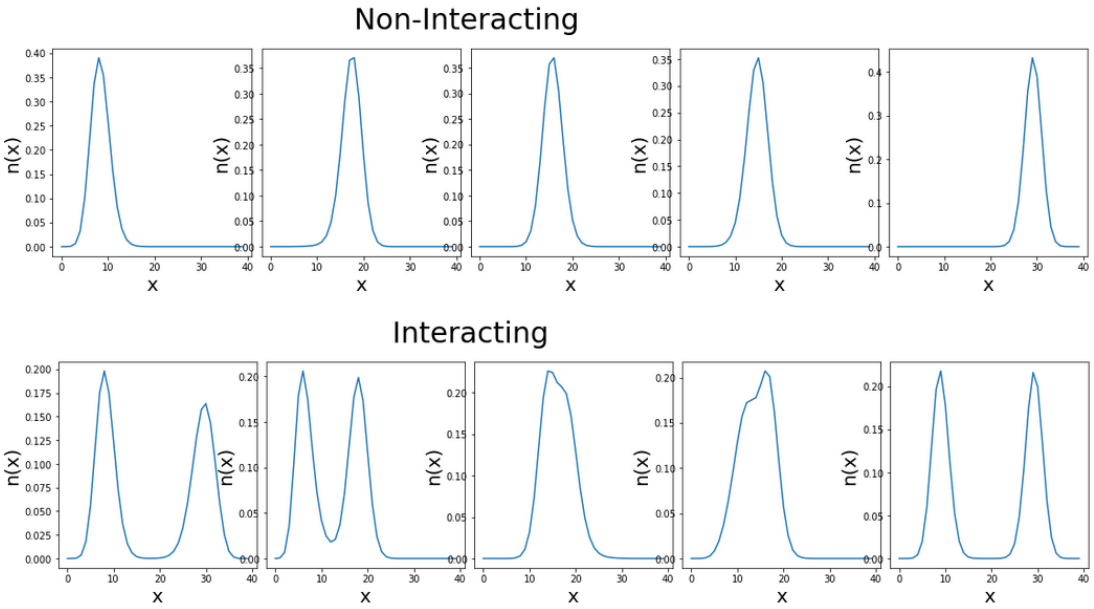

Figure 1.8: Density examples for five potential landscapes. While the densities on the top rows come from the solution of the Schrödinger equation in absence of interaction, the ones on the bottom rows are derived after the solution of the Schrödinger equation in the same potential but with the softened coulomb interaction between the electrons switched on.

1.4.1 Characterization constraints and validity of the results: the importance of auxiliary systems

It is now possible to discuss the validity domain and the potential applicability of the results that have been found during the thesis and that will be presented starting from the next chapter. When working with ML, while some of the *validity constraints* are known and their role in the compression can be taken for granted, the remaining *validity constraints* are merged with the *universal constraints* and with the *characterization constraints* (see Sec. 1.2). The biggest limitation induced by them on the applicability is the one coming from the *characterization constraints* since, due to their data-set dependency, they bind the description to two electrons systems that can be described via potential sharing features with the ones appearing in the data-set. However, the reader must not be misled by the common belief that once the machine is trained it can only give information on the kind of examples it is shown in the training. The data-set is always divided into two parts: the *training set* and the *validation set*. This is done so that, after the machine has been trained, the generality of the result can be tested against inputs belonging to the same class but never seen before by the machine. Some features must be in common, and they will be learned by the machine, but no two densities should be equal to each-others due to the randomness in the definition of the potentials. The results obtained are therefore general for all of the systems that can be mapped to the class we are considering. The functionals we have found can be used for any system that can be mapped into the kind of system present in the data-set, including two electron molecules and many body system admitting a description in terms of two effective electrons. This introduces the essential concept of *auxiliary system* since the generality of the result is extended to the capability of approximately describe a real system via one of the model systems described in the thesis. The concept of *auxiliary system*

also implies that the result is not only the functional, but also the method for deriving it. As soon as the real system problem has been mapped to a reasonable numerically exactly solvable system, it is possible to generate the associated data-set by randomly varying the environment. This induces a generation of many example systems that could describe the physics considered and, the characterization of the functional starting from this data-set, can later be used for mapping the real system density to the associated 1-RDM.

Chapter 2

Principal component Analysis and the linear functional

Starting from the knowledge of the existence of linear constraints, in this chapter PCA will be applied to determine the number of principal components needed to fully characterize a 1-RDM. The resulting compression of the information will show that, as expected from DFT, the correlation of the entries goes beyond the few linear constraints of which we are aware of. Instead, for what concerns the remaining constraints, it is not guaranteed that they are actually linear in nature but PCA will be able to find the best linear way to describe them. A PCA will be performed both on the data-set of 1-RDMs and on the corresponding subset of densities. Then, it will be shown that the first few principal components of the two data-sets, containing the largest part of the information, can be mapped to each other. On the basis of this observation, I will suggest a linear approximation to the density functional for the density matrix. Finally, the details missed by this functional will be treated as noise to be corrected using a neural network (NN) named denoising autoencoder (DAE).

2.1 Learning Linear Constraints

We begin with the known linear constraints. The most general linear constraint, to which a matrix is subject to, can be expressed as the following condition

$$g(\gamma) = \sum_{i,j=1}^{N_g} \beta^g_{i,j}\gamma_{i,j} + \beta^g_0 = 0 \tag{2.1}$$

Starting from this, the diagonal of the 1-RDM corresponds to the density and, hence, it must necessarily sum to the number of electrons present in the system. Accordingly to the re-normalization performed on the 1-RDM,

$$\sum_{i=1}^{N_g} \gamma_{i,i} = \sum_{i=1}^{N_g} \gamma(r_i, r_i)\Delta r = N_e. \tag{2.2}$$

This corresponds to a linear constraint in which $\beta^g_{i,j} = \delta_{i,j}$ and $\beta^g_0 = -N_e$.
Secondly, due to the confining nature of the potential, at the boundaries the state vector is

constrained to vanish. As a direct consequence, also the 1-RDM must vanish when at least one of its arguments corresponds to a boundary point.

$$\gamma_{i,j} = 0 \qquad \text{if } i = 1, N_g \vee j = 1, N_g \tag{2.3}$$

This is an ensemble of $4(N_g - 1)$ linear constraints having all of them $\beta_0^g = 0$ and only one of the $\beta_{i,j}^g = 1$, with at least one between i and j at the boundary.
Finally, the 1-RDM is Hermitian. For this reason, in general $\gamma_{i,j} = \gamma_{j,i}^*$ or, in our particular case,

$$\gamma_{i,j} = \gamma_{j,i}. \tag{2.4}$$

Corresponding to $\binom{N_g}{2}$ linear constraints, one per each ordered pair of indices (i, j), each of which is characterized by $\beta_0^g = 0$ and $\beta_{i,j}^g = 1$ while $\beta_{j,i}^g = -1$.

2.1.1 Principal component analysis on the density and on the density matrix

In this sub-section I will introduce some of the main results obtained when performing PCA on our data-set. The 8 grid-points system and the 20 grid-points system will be put in comparison in order to discuss the one-to-one mapping between the 1-RDM and the density, induced by the strong linearity of the constraints in the considered data-set.
Let us start from the density of the 8 grid-points system. Considering the constraint 2.3, the confining nature of the potential forces the system to be an effective 6 grid-points system. Moreover, as a consequence of the constraint 2.2 on the normalization of the density the number of principal components needed for fully describing the density is reduced to

$$\eta^{(n)} \leq N_g - 3 = 5$$

This can be observed in Fig. 2.1. After having checked that PCA has been able to learn all of the linear constraints to which the density is subject to, let us focus on the 1-RDM. When flattened, the 1-RDM is a N_g^2-dimensional vector containing among its entries the density components. In Fig. 2.2 it is possible to observe that there exist linear constraints reducing the dimension from $N_g^2 = 64$ to 10. However, not all of them can be explained with the three known constraints previously introduced. In fact, according to equation 2.3, the first and the last row and the first and the last column must vanish, leading to $(N_g - 2)^2 = 36$ needed components. In addition to this, according to 2.4 the matrix is symmetric and, for this reason, half of the diagonal entries must be subtracted $\binom{N_g-2}{2} = 15$. Finally, one entry of the diagonal is for free if we take into account 2.2. This leads to understand that $\eta^{(\gamma)} = (N_g - 2)^2 - \binom{N_g-2}{2} - 1 = 20$ principal components are needed, in principle, for a complete reconstruction. The reason for which this is not the case is the existence of both data-set dependent and general additional constraints between the off-diagonals and the diagonal. The three constraints are certainly not sufficient for obtaining a 1-RDM since almost no information on the way the diagonal relates to the off-diagonals has been inserted. Other covariations must necessarily exist since, if it was not the case, any symmetric matrix with a normalized diagonal would be a 1-RDM and, most importantly, the same density could be erroneously associated to different 1-RDMs. Therefore, the important information is that PCA has managed to confirm the presence of a compression, theoretically guaranteed by DFT. In addition it has been able to linearly encode the covariations in the most efficient possible way. The way the correlations have been encoded could be interpreted as a data-set

dependent existence of additional constraints that are approximately linear. The smoothness of the potential and the consequent smoothness of the density leads to the existence of such (almost) linear constraints, increasing the potential of PCA in the compression, despite its limitation of working in linearity.

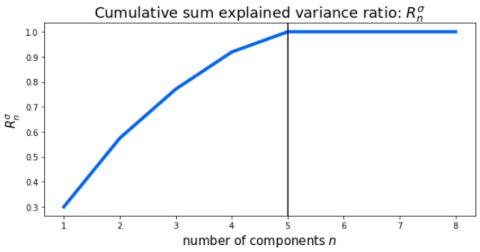

Figure 2.1: PCA on the Density: Cumulative sum of the explained variance ratio.

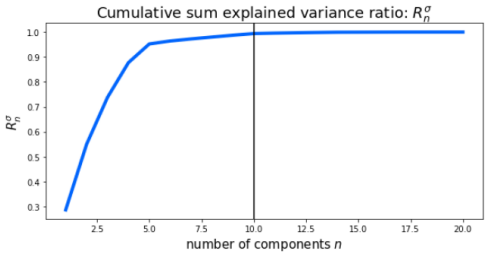

Figure 2.2: PCA on the Density Matrix: Cumulative sum of the explained variance ratio.

Once determined the number of components needed for the complete reconstruction, let us look explicitly at them (see Fig. 2.6). The first thing to be noticed is that the 1-RDMs under analysis have the non-vanishing entries strongly dependent on the corresponding non-vanishing values of the density (see Fig. 1.7). As a consequence it is to be expected that the strongest variations in the N_g^2 dimensional space in which the principal directions of the 1-RDM are defined occur in the subspace of the densities. For this reason it makes sense to compare the principal components of the density with the ones of the density matrix. In Fig. 2.6 it is possible to compare the principal components of the 1-RDM (green) with the ones of the density (red). The vertical black lines identify the only entries along which the principal directions of the density have values, i.e. the subspace associated to the density. Two major remarks are worth being done:

- All of the informative principal components of the density[1] correspond to the respective principal components of the 1-RDM apart from a multiplicative factor that is extremely close to 1 in the 8 grid-points system. This means that there exist a one-to-one mapping between these principal directions;
- When considering the 1-RDM these components carry also off-diagonal information.

In order to quantify the one-to-one mapping, that can be observed to be a scaling factor, for each principal direction of the density the ratio between the entries and the corresponding entries of the associated component of the 1-RDM has been computed. This yield N_g values for each component and a good one-to-one mapping can be defined if the values contained in this vector do not vary much from their average value. In Fig. 2.3 it can be observed that for $N_g = 8$ the scaling factor is close to one for all of the components of the density. Furthermore, the interval of accuracy, defined as three times the standard deviation of the vector associated to each component, is quite small if compared to the amplitude of the average scaling factor.
This multiplicative factor will be essential in the development of the PCA-functional. The reason for the existence of the one-to-one correspondence can be found in the fact that, for

[1] The first five.

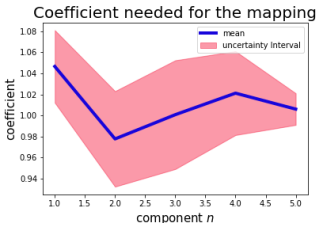

Figure 2.3: Coefficient mapping the principal components of the 1-RDM with the ones of the density for the $N_g = 8$ system.

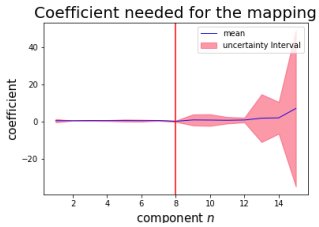

Figure 2.4: Equivalent of Fig. 2.3 for $N_g = 20$. This picture testifies the breaking of the one-to-one mapping between the 7-th and the 8-th principal components.

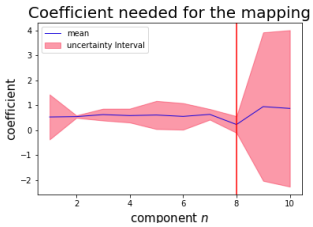

Figure 2.5: Detail of Fig. 2.4 better showing the moment in which the mapping falls apart.

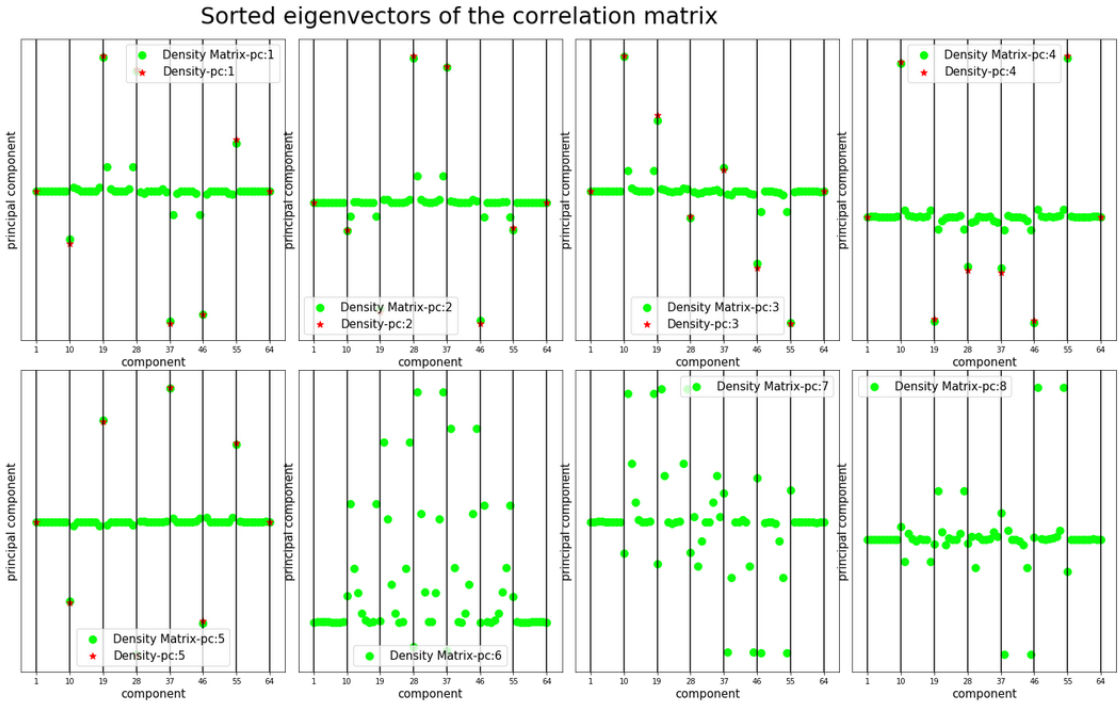

Figure 2.6: First eight principal components of the *flattened* Density Matrix data-set for $N_g = 8$: The first principal directions of the 1-RDM (green) have been compared to the corresponding directions of the density (red). Each principal component of the *flattened* matrix is a N_g^2 vector and, considering the first ones of them, while they resemble the density in its sub-space (black lines, corresponding to the positions of the diagonal of the matrix once flattened) they also carry off-diagonal information.

small numbers of grid-points, the `iDEA` code is working with large lattice spacing. For this reason, the sites are in first approximation independent systems and, the off-diagonal terms farther than the first neighbors are small if compared to the nearest ones. This means that small grid-point systems will have 1-RDMs strongly dominated by the diagonal terms. Consequently, the principal directions are straightforwardly identified with versors identifying the hyper-plane described by $\sum_{i=1}^{N_g} \gamma_{i,i} = N_e$. This statement can be summarized by noticing that the cumulative

sum of the explained variance ratio at the 5-th component is equal to 0.964, meaning that a big portion of the information is carried in the density components.
In section 2.2 we will show how this relevance of the density and the one-to-one mapping of the principal components can be exploited for constructing a functional. Before to proceed, however, it is essential to deepen the previous observations on the existing mapping between the components as a function of the number of grid-points.

Let us now focus on the $N_g = 20$ system. In Fig. 2.7 it is possible to compare the principal components of the density and of the 1-RDM. This time, the latter has been re-normalized in the density subspace[2]. Looking at Fig. 2.4 and at Fig. 2.5 it is possible to find the previously defined plot of the average ratio between the principal components of the density and of the 1-RDM in the density subspace. In Sec. 2.2 the mapping will be mathematically explained but, for now, the most important thing to be noticed is that it holds only up to the 7-th component. By contrast, as soon as the 8-th component is concerned, the ratio changes significantly from the previous average values. In a few components the accuracy interval increases dramatically in width, giving rise to the fall of the mapping. The most plausible explanation of the fact that the one-to-one mapping does not hold for all of the components of the density, at odd with what happened for the $N_g = 8$ grid-points system, is the passage from strongly quantized space to the continuum limit. More explicitely, by adding sites while keeping the width of the system fixed, we experience a transition from a system strongly dominated by local effects to a system in which the transition from a site to the other is less expensive. In such a system the likelihood for an electron to jump from one site to another close to it is much higher and many more entries of the density matrix turn out to be non-negligible. The consequence of this can be directly perceived by looking at the results obtained by performing the PCA. On one hand, the PCA on the density and on 1-RDMs of small number of grid-points system contains in the first $N_g - 1$ components all of the details on the variation of the density, since it is the most important characteristic. On the other hand, when the continuum is approached, the matrices become almost block-diagonal with the off-diagonal entries non-negligible in correspondence of non-negligible diagonal entries. It is still true that the first ν principal components describe the variation in the density but, starting from the $(\nu+1)$-th principal component, while the PCA on the density can focus on the remaining details characterizing the density, the PCA on the 1-RDM needs to start to describe more consistent variations in the off-diagonal terms and the details on the density are diluted in the remaining components. Despite this limitation, it turns out that the first ν components contain a great amount of information. For instance, in the 20 grid-points system the cumulative sum of the explained variance ratio at the 7-th component is

$$R^{\sigma}_{\nu=7}(N_g = 20) = 0.95$$

and, analogously, for the 64 grid-points system we found that the mapping breaks down at the 8-th component, corresponding to

$$R^{\sigma}_{\nu=8}(N_g = 64) = 0.91.$$

The most important point is the existence of a mapping between the PCA on the density and the PCA on the density matrix for a number of component containing the vast majority of the

[2]The principal components of the 1-RDM are not normalized in the conventional way. The modulus squared of a component does not sum to one, what sums to one is the modulus squared of its subset of entries corresponding to the kernel function.

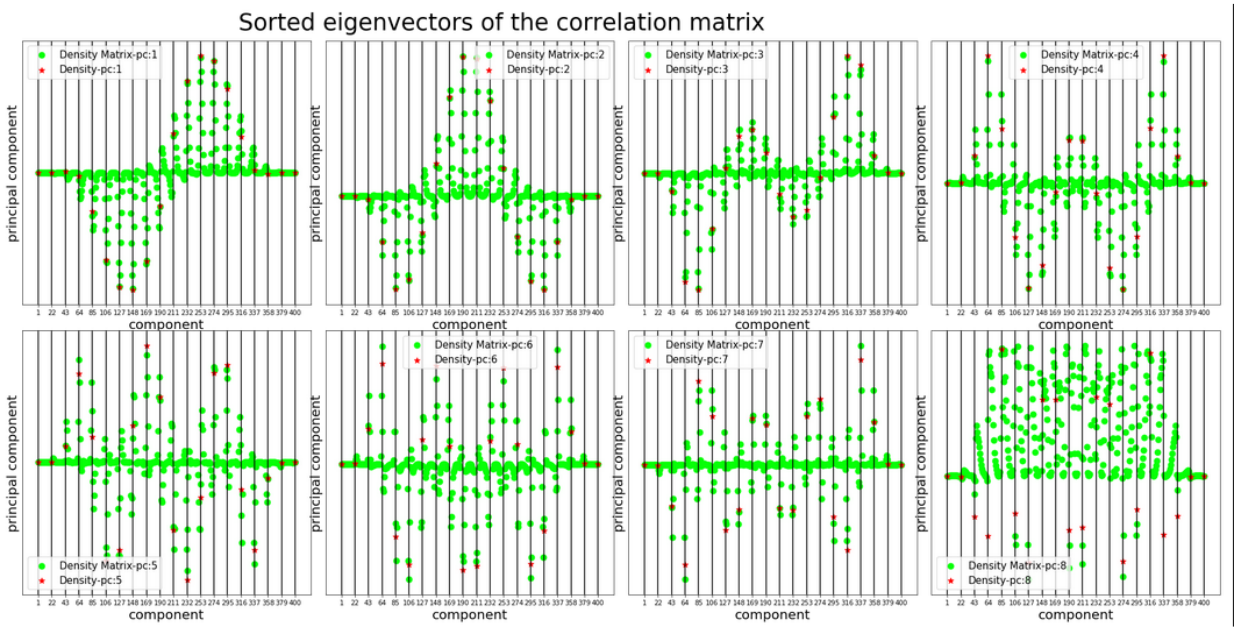

Figure 2.7: First eight principal components of the *flattened* Density Matrix data-set for $N_g = 20$: The first principal directions of the 1-RDM (green) have been compared to the corresponding directions of the density (red). Each principal component of the full matrix is a N_g^2 vector and, considering the first ones of them, while they resemble the density in its sub-space they also carry off-diagonal information.

information. By making explicit the fact that the principal components on the 1-RDM contain off-diagonal information (see Fig. 2.7 and Fig. 2.2) we determined the PCA functional.

2.2 Learning functionals from constraints

Given the insight gained in section 1.3.1, it is now time to develop the functional $\gamma[n]$ for the N_g point data-set. The desired functional can always be split into a linear (L), and non-linear (NL) term:

$$\gamma[n] = \gamma_{\mathrm{L}}[n] + \gamma_{\mathrm{NL}}[n]. \tag{2.5}$$

In the following we will perform explicitly this decomposition. While the linear term will be presented as an explicit functional of the density, we will treat the non-linear one as a perturbation to be deep learned (see section 2.3). In Fig. 2.2 and 2.7 it is possible to observe that each component carries both diagonal and off-diagonal information. In particular, the diagonal of the 1-RDM components has a significant correspondence to the density components. For a given number of grid points, this correspondence holds for the first ν components, where this value is determined by analysing the cumulative sum of the explained variance ratio. The purpose of this section is to exploit this correspondence in order to find a linear approximation of $\gamma[n]$. The starting point will be the formalization of the connection between the two data-sets. Firstly the principal component decomposition of the 1-RDM in the $\mathscr{B}_e$-basis will be performed (see section 1.3.1) and then, starting from the matrix representation of the density data-set, the mapping between the density components and the 1-RDM ones will be analyzed. The starting point is the expression of the 1-RDM components in terms of the known projections of the

principal components onto the basis defining the entries of the matrix (see section 1.3.1).

$$\begin{aligned}\gamma_{i,j} &= \langle e_{s[i,j]}|\gamma\rangle = \\ &= \langle e_{s[i,j]}|\gamma_0\rangle + \langle e_{s[i,j]}|\tilde{\gamma}\rangle = \\ &= (\gamma_0)_{i,j} + \sum_{k,s'=1}^{N_g^2} \langle p_k|e_{s'}\rangle\langle e_{s'}|\tilde{\gamma}\rangle\langle e_{s[i,j]}|p_k\rangle\end{aligned}$$

Where the $\langle e_s|p_i\rangle$ coefficients are known after the evaluation of the eigenvectors of the covariance matrix.
Before proceeding, the density vectors are to be introduced:

$$\underline{n} = [\gamma_{1,1},0,\cdots,0,\gamma_{2,2},0,\cdots,\gamma_{N_g,N_g}] \in \mathbb{R}^{N_g^2} \tag{2.6}$$

together with their data-set

$$P = \begin{bmatrix} \underline{n}^{(1)} \\ \vdots \\ \underline{n}^{(T)} \end{bmatrix}. \tag{2.7}$$

Performing a PCA on this data-set allows one to determine the average density $|n_0\rangle$, the decomposition $|n\rangle = |\tilde{n}\rangle + |n_0\rangle$ and the corresponding principal components

$$\{|p_i^n\rangle\}_{i=1}^{N_g^2}.$$

There are N_g^2 components since they must form an orthonormal basis of the vector-space. However, only the first $N_g - 1$ of them will be informative due to the sparseness of the object defined and due to the normalization of the density. By direct comparison of the principal directions in the two data-sets (see Fig. 2.2 and 2.7), it is possible to observe that the first ν principal directions derived from the Γ data-set can be put in a scaled one-to-one correspondence with the first ν principal directions of the sub-data-set P. In particular, it is possible to define the modified principal directions and to normalize them

$$|q_i\rangle = \sum_{j=1}^{N_g} \langle e_{s[j,j]}|p_i\rangle|e_{s[j,j]}\rangle \quad i = 1,\cdots,N_g-1 \rightarrow |q_i^n\rangle = \frac{1}{\sqrt{\langle q_i|q_i\rangle}}|q_i\rangle.$$

This defines an orthonormal basis for describing the diagonals of the matrices in the ensemble. When the matrices under analysis are such that the non-vanishing off-diagonal terms are mainly the ones closer to the corresponding non-vanishing diagonal terms, it must be true that $|q_i^n\rangle \simeq \pm|p_i^n\rangle$[3]. Where the equality has been observed to be exact for the first ν principal components since the presence in the density matrix of the off-diagonal terms leads to a reduction in priority of the variation along the density. In fact, the main variations in the density are also those more strikingly characterizing the 1-RDM. However, from the $(\nu+1)-th$ component on, while the PCA on the density can provide more details on the remaining changes in the density, orthogonal to the previous ones, the PCA on the density matrix starts describing the variations along the off-diagonal terms and the mapping between the two breaks down. The reason of this can be

[3]The $\pm$ is due to the possible differing convention of the arbitrary directions in the PCA.

explained by noticing that the details on the density, being less evident than the ones on the off-diagonal terms, are contained in a diluted way in the remaining components. At this point all of the information is ready for determining the actual expression of the linear functional. First, the mean-adjusted 1-RDM can be separated in four terms, distinguishing the diagonal from the off-diagonal contributions and taking into account the different information content of the first ν principal component with respect to the remaining ones. Later we will define a basis orthonormal in the subspace of the densities while carrying off-diagonal information. This definition will allow to approximate the dominant contribution to the exact functional $\gamma[n]$. Let us start by writing $\tilde{\gamma}$ as the sum of four contributions:

$$|\tilde{\gamma}\rangle = |\tilde{n}_{\leq\nu}\rangle + |\tilde{n}_{>\nu}\rangle + |\delta\gamma_{\leq\nu}\rangle + |\delta\gamma_{>\nu}\rangle$$

These four terms correspond to the shifted density reconstructed with the first ν principal components, to the shifted density reconstructed with the remaining principal components, to the off-diagonal terms obtainable with the first ν principal components, from now on termed *free off-diagonal terms*, and to the remaining off-diagonal contributions. Considering or not these terms corresponds to different levels of approximation. For the specific data-set we have found that the moment in which the one-to-one mapping stops to hold corresponds to the number of principal components ν at which the cumulative sum of the explained variance ratio reaches a value of 0.96 for $N_g = 20$ and of 0.91 for $N_g = 64$. For this reason, neglecting the term $|\tilde{\gamma}_{>\nu}\rangle = |\tilde{n}_{>\nu}\rangle + |\delta\gamma_{>\nu}\rangle$ will be considered as a reasonable first order approximation, and we are left with the task of focusing on the remaining two terms. This having been said, let us define a new set of vectors:

$$|q_i^\gamma\rangle \doteq \frac{1}{\sqrt{\langle q_i|q_i\rangle}}|p_i\rangle \quad i = 1,\cdots,N_g-1 \qquad \langle q_i^n|q_j^\gamma\rangle = \delta_{i,j}$$

These vectors contain the $|q_i^n\rangle$ ones in them and follow their normalization. Thanks to their orthogonality, if the one-to-one mapping were valid for all the first N_g-1 components, they would be a complete basis in the densities-subspace while carrying the information on the free off-diagonal terms in the components not shared with the basis $\{|q_i^n\rangle\}_{i=1}^{N_g-1}$. Even if the mapping is valid only for the first ν principal components, this basis allows nonetheless to construct the approximate 1-RDM carrying some information on the off-diagonal behavior while its diagonal corresponds to the density reconstruction obtained by looking at its ν most remarkable features. Let us add and subtract this term in $\gamma_{i,j}$:

$$\begin{aligned}\gamma_{i,j} &= (\gamma_0)_{i,j} + \langle e_{s[i,j]}|\tilde{n}_{\leq\nu}\rangle + \langle e_{s[i,j]}|\delta\gamma_{\leq\nu}\rangle + \langle e_{s[i,j]}|\tilde{\gamma}_{>\nu}\rangle + \\ &+ \sum_{k=1}^{\nu}\langle e_{s[i,j]}|q_k^\gamma\rangle\langle q_k^\gamma|\tilde{n}\rangle - \sum_{k=1}^{\nu}\langle e_{s[i,j]}|q_k^\gamma\rangle\langle q_k^\gamma|\tilde{n}\rangle = \\ &= (\gamma_0)_{i,j} + \sum_{k=1}^{\nu}\langle e_{s[i,j]}|q_k^\gamma\rangle\langle q_k^\gamma|\tilde{n}\rangle + (\delta\gamma)_{i,j}\end{aligned}$$

where

$$(\delta\gamma)_{i,j} = \langle e_{s[i,j]}|\tilde{n}_{\leq\nu}\rangle + (\delta\gamma_{\leq\nu})_{i,j} - \sum_{k=1}^{\nu}\langle e_{s[i,j]}|q_k^\gamma\rangle\langle q_k^\gamma|\tilde{n}\rangle + (\tilde{\gamma}_{>\nu})_{i,j}$$

This last quantity must be itself a functional of the density, where the functional relation is non-linear and unknown. This having been done, the functional is now expressed in the form

presented in equation 2.5. Considering the non-linear part, the analysis on the principal values legitimates us to neglect the term $(\tilde{\gamma}_{>\nu})_{i,j}$. For what concerns the remaining contribution it is expected to be small since the basis $\{|q_k^\gamma\rangle\}_{k=1}^{N_g-1}$ has been defined with the exact intent of privileging the exact restoration of the density, being the biggest contribution, while estimating the free off-diagonal terms. By neglecting the $\gamma_{\mathrm{NL}}[n] = \delta\gamma$ term and by writing the resulting expression in terms of the know projections of the principal components onto the $\mathscr{B}_e$-basis, the linear functional is obtained

$$\begin{aligned}\gamma_{i,j} &= (\gamma_0)_{i,j} + \sum_{s':\langle e_{s'}|\tilde{n}\rangle\neq 0}\sum_{k=1}^{\nu}\langle e_{s[i,j]}|q_k^\gamma\rangle\langle q_k^\gamma|e_{s'}\rangle\langle e_{s'}|\tilde{n}\rangle \\ &= (\gamma_0)_{i,j} + \sum_{m=1}^{N_g}(n_m-(n_0)_m)\sum_{k=1}^{\nu}\langle e_{s[i,j]}|q_k^\gamma\rangle\langle q_k^\gamma|e_{s'[m,m]}\rangle\end{aligned}$$

corresponding to:

$$\gamma_{i,j}[n] = (\gamma_0)_{i,j} + \sum_{m=1}^{N_g}(n(r_m)-n_0(r_m))\Delta r\sum_{k=1}^{\nu}\langle q_k^\gamma|e_{s'[m,m]}\rangle\langle e_{s[i,j]}|q_k^\gamma\rangle \tag{2.8}$$

where γ_0 is the average density matrix from the data-set (due to the PCA convention to transform between mean-adjusted data). In the first line of Fig. 2.8 the first 5 PCA reconstructions are reported and they can be compared with the exact density matrix in the bottom row.

2.3 Denoising Autoencoder

In chapter 1 autoencoders have been introduced and it has been argued that they are Neural Network architectures able to learn how to compress the input when trained for reconstructing it. A particular class of autoencoders is the one of Denoising AEs (DAE), corresponding to convolutional AEs used to perform noise reduction in image processing [54]. In presence of a noisy data-set, the convolutional AE can be trained to construct the clean version of it. Afterwards, when given a noisy image not used for training the model, the DAE can reconstruct the image removing the noise from it. The DAE architecture acts as a low pass filter that can be trained for removing the noise present in a specific class of images. Since something needs to be discarded when encoding the input in the reduced number of features at disposal in the latent space, the machine learns to detect what are distortion from the true pattern and neglects them. In the specific case of the $N_g = 20$ system we used a convolutional autoencoder in which both the encoder and the decoder are composed of 5 convolutional layers of 20 filters each, obtained using kernels of size 3×3. For the latent space I chose a dense layer of 35 neurons and the non-linearity has been introduced via the ReLu activation function, except in the last layer, in which the Sigmoid activation function has been used. Training with a batchsize equal to 32 for 200 epochs using the Mean absolute percentage error (MAPE) as a loss function and the Adadelta optimizer results in the following errors:

$$\begin{cases} Loss^{MAPE} = 16\% \\ Loss^{MAE} = 0.0013\,(a.u.) \end{cases} \tag{2.9}$$

Rather than training the DAE directly on the linear approximation, a pre-processing was performed by taking the absolute value of the 1-RDM[4] and we normalized the matrix in such a way that the diagonal sums to N_e. The result of the denoising procedure together with the steps of the pre-processing, represented via the operator $R(\cdot)$, can be observed in Fig. 2.8. A further optimization of the network together with a training performed for an higher number of epochs would allow to further reduce the difference between the reconstruction and the true 1-RDM. However, the purpose of this analysis was to show that ML tools can give insight on the structure of the object under analysis, allowing the "model maker" to generate an approximation based on the observation of the features. Moreover, any model approximating the exact result up to a certain accuracy can be further improved by treating the absence of the correction as noise to be removed[5] via pure ML techniques.

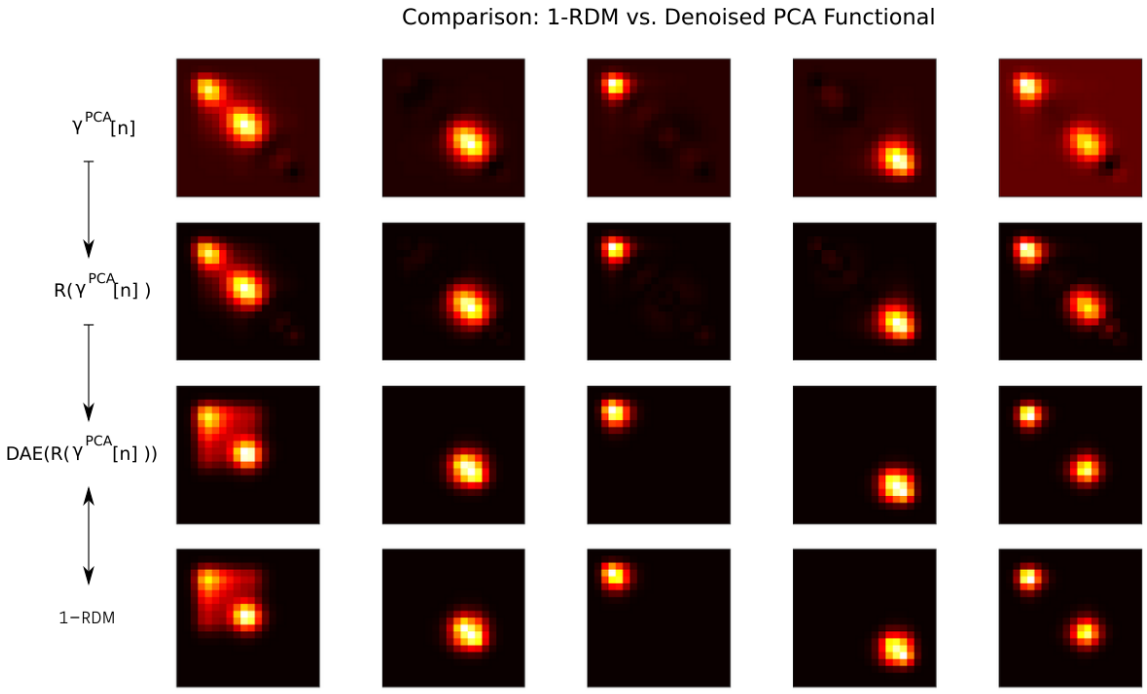

Figure 2.8: Denoised PCA-based functional compared with the exact 1-RDM for five example systems. The first row is the pure PCA functional of the density, the second row corresponds to the pre-processed version of the same and, finally, the third row is the output of the trained DAE when feeding it with the matrices in row 2.

2.4 The origin of the result

The functional proposed was introduced in a rougher version at the very beginning of the thesis, when I was using PCA to obtain information on the 1-RDM. The astonishingly predominant presence of linear constraints witnessed by the good performances of PCA when compared to

[4] the truncation of the principal component decomposition introduces some negative values.

[5] By adding the correction.

the results obtained with AEs led us to study in more depth the nature of the linearity in the constraints. The idea I proposed was based on the fact that the principal components of the density matrix were extremely peaked in correspondence of the density directions, as it has been observed in Fig. 2.6. For this reason I extracted the entries of the principal components corresponding to the N_g-dimensional density subspace obtaining functions that I named *masks* and, by multiplying these functions to the density, it was possible to obtain a weight to be used for the adding of the corresponding principal component, also carrying off-diagonal information. The idea was abandoned when I moved to study the non-linearity in small grid-points system[6] and Jack moved to more advanced applications involving DAEs for the transformation of the non-interacting 1-RDM into the interacting one with the same potential. Trying to construct a numerical functional led him to re-propose the same idea but with two essential adjustments, yielding a consistent increase in accuracy. The first consideration was related to the loss of the validity of using the *masks* after a certain principal component and the second was the need of normalizing the *masks*. In light of the suggestion Lucia Reining did on the importance to express the finding in terms of a matrix expansion Jack and I developed in parallel two different justifications of the functional. While he focused more on the representation in terms of a functional Taylor expansion, I mainly worked on the pure principal component decomposition and in this chapter I have presented this approach. The formalization was developed in light of the essential changes introduced by Jack and some of the results obtained in the process.

2.5 Summary

In this chapter the first functional we developed was presented. It is worth remarking the important role given to the understanding of the contraints in the process of defining this functional. The knowledge of the way the entries of the matrix are related has been shown to allow for a reduction of the actual independent variables to be estimated from the density. We have found that understanding the constraints corresponds to shed light on the mathematical structure of the object under analysis, reducing the difficulty of the task of finding the functional. In fact, as pointed out in Sec. 1.3.1, the existence of constraints results in a compression of the information. The number of independent variables is thus reduced and, being able to estimate them from the density, has been shown to allow for determining the remaining ones.
The PCA-functional is the first example of how the machine can be used to increase the human knowledge on a system. Starting from the pure definition of principal component analysis (PCA) and using the way it structures the data, we managed to derive an analytic representation of the functional. Moreover, the observation that the informative principal components of the density (see Fig. 2.7) resemble modulated sinusoidal functions of a Fourier-like expansion could be further studied to reduce even more the dependency of the model on the data-set.
Finally, the applicability of the work done is expected to be twofold:

1. The results can be directly applied to find the 1-RDM of any system admitting as a reasonable description the system we have analyzed.

2. The methodology proposed can be repeated for different simple systems that allow for a numerically exact solution.

[6]The results of which will be presented in chapters 3,4 and 5.

In any case the important concept of *auxiliary system* appears. It may be that this system could describe some physics of molecules with a valence number equal to two, like the Hydrogen molecule, and starting from the next chapter it will be treated a rare case of experimentally realizable 1D system. Nevertheless, many systems will be far from being one dimensional and will be likely to be populated by more than two electrons. However, as pointed out in Sec. 1.4.1, it may still be possible to map a real system to an *auxiliary system*, i.e. an exactly solvable fictitious systems characterized by the properties of the real system, and sharing with it a desired electronic property.

Chapter 3

Hubbard Dimer in two limiting cases

When the number of points in space is reduced to two, the problem of finding the density functional of the one-body reduced density matrix (1-RDM) is simplified to determining a one variable function. Indeed, the 1-RDM becomes a two by two symmetric matrix whose diagonal is normalized to the number of electrons. Hence, the task becomes the determination of the non-linear functional dependence of the only independent off-diagonal entry in terms of the only independent diagonal one. In this chapter I will first exactly diagonalize the Hamiltonian of the Hubbard Dimer (HD) in two special cases: the symmetric potential and the non-interacting electron cases. This analysis will be particularly useful for subsequent studies. Later I will investigate in detail the finding of the desired density functional for the *asymmetric*[1] HD in two limiting situations: the non-interacting and the strongly interacting cases. In these cases the analytical relation between off-diagonal and diagonal elements of the 1-RDM was already present in literature. Therefore, along the process, I will just outline the main steps leading to these essential results while the details of the calculation will be given in appendix. These analytical results also represent the starting point for studying how to simplify the machine learning architecture on the basis of our knowledge of the problem. Following the concept of *feature engineering*, I introduce a *logarithmic perceptron*. This will show that, with an appropriate pre-processing of the inputs, it is possible to minimize the complexity of the neural network architecture needed to learn the two limiting cases.

3.1 Motivations

As mentioned before, the problem of deriving the functional $\gamma[n]$ corresponds to the problem of deriving the way the off-diagonal elements of the 1-RDM are related to the diagonal ones. This amounts to say that DFT guarantees the existence of $N_g^2 - N_g$ independent functional constraints connecting all of the off-diagonal elements to the density. In the previous chapter the exact linear constraints, present in all of the matrices of the data-set, have been described. Moreover, in addition to these, it has been shown that, for our specific data-set, a large portion of the functional

[1] The symmetric case is trivial due to the fact that the Hamiltonian can be exactly diagonalized.

constraints guaranteed by DFT can be well approximated to be linear, resulting into the PCA-functional. In this chapter only the exact known constraints will be exploited to minimize in an exact way the number of dependent and independent variables into play. By contrast, all of the remaining constraints will no more be approximated as linear but the very same nature of the non-linearity will be studied. The purpose of this chapter is to study the nature of the non-linear dependency of the off-diagonal terms on the density components. In order to do that, we decided to focus on the simplest version of the system, i.e. the effective two points system[2]. The leading motivation was that, in this case, the density matrix has only one independent off-diagonal term due to symmetry. Therefore, the whole purpose of finding the functional $\gamma[n]$ becomes the problem of finding the way of parametrizing the only one off-diagonal term as a function of the density $\gamma_{2,1}[\gamma_{1,1},\gamma_{2,2}]$. Moreover, the density is subject to the normalization condition. Hence, the off-diagonal term is basically only a function of the density at one site $\gamma_{2,1}(\gamma_{1,1})$. This completes the insertion in the solution of the problem of the known linear constraints, leaving only the non-linear ones to be investigated.
Willing to find this relation we started from the Hamiltonian diagonalized in the two points system by the `iDEA` code, transformed from the real space grid version used in the `iDEA` code into its second quantization equivalent:

$$\hat{H} = -t \sum_{\sigma\in\{\uparrow,\downarrow\}} (\hat{c}^{\dagger}_{1,\sigma}\hat{c}_{2,\sigma} + \hat{c}^{\dagger}_{2,\sigma}\hat{c}_{1,\sigma}) + U\sum_{i=1}^{2}\hat{n}_{i,\uparrow}\hat{n}_{i,\downarrow} + U'(\hat{n}_{1,\uparrow}\hat{n}_{2,\downarrow} + \hat{n}_{1,\downarrow}\hat{n}_{2,\uparrow}) + \sum_{i=1}^{2} v_i\hat{n}_i \quad (3.1)$$

The term U' corresponds to the repulsion of the electrons when populating different sites. Nevertheless, the chosen distance between the points is approximately 10 atomic units. For this reason, the repulsion between electrons can be considered to be negligible with respect to the on-site repulsion and the system is equivalent to an in-homogeneous (or asymmetric) Hubbard-Dimer model [55]:

$$\hat{H} = -t \sum_{\sigma\in\{\uparrow,\downarrow\}} (\hat{c}^{\dagger}_{1,\sigma}\hat{c}_{2,\sigma} + \hat{c}^{\dagger}_{2,\sigma}\hat{c}_{1,\sigma}) + U\sum_{i=1}^{2}\hat{n}_{i,\uparrow}\hat{n}_{i,\downarrow} + \sum_{i=1}^{2} v_i\hat{n}_i \quad (3.2)$$

$$= \hat{H}_t + \hat{H}_u + \hat{H}_v \quad (3.3)$$

Where the attribute in-homogeneous is referred to the term $\hat{H}_v$, responsible for the breaking of the symmetry between the two sites. If it was possible to diagonalize this matrix and to find the Ground-State vector, it would then be possible to directly compute the 1-RDM from it. Unfortunately, the exact diagonalization is possible only in limiting cases. The goal is then to extract the laws presented in figure 3.1 for the strongly-interacting limit and for the non-interacting limit. Matteo Gatti noticed the existence in literature of these two relations, defining the boundaries of the v-representability domain [25, 56]. We wanted to understand if the way these results were obtained could have been generalized to larger lattices and for intermediate values of the interaction between the electrons. Therefore, I worked on the analytics of the Hubbard Dimer and this chapter is mainly aimed at reporting the main results I derived and that turned out to be useful for the definition of the following models. Firstly, due to the simplicity of the Hamiltonian, I worked on its explicit diagonalization in some specific subsets of Hamiltonians. Following the paper [25] on lattice density functional theory by Töws and Pastor I

[2]The confining nature of the potential makes the 4 points system an effective 2 points system.

then performed the derivation of the functional in the two limiting cases, by doing explicitly the calculations they prescribed and stressing the meaning of each step. These derivations, despite the fact that they were aimed at reproducing results existing in literature, were essential for better understanding the model and for trying to determine whether it was possible to use similar reasonings for more than two grid-points.
This chapter is thus mainly focused on the derivation of results in the context of Lattice Reduced Density matrix Functional Theory [25, 56], leading to the formulas for the two limiting cases of non-interacting electrons and of strongly-interacting ones, with some details of the calculations reported in appendix. On the other hand, at the end of the chapter a more original piece of information will be presented by introducing the machine learning concept of *feature engineering* (FE). This result came from a discussion we had on the way the NN architecture could have been structured in order to interpret the learned features as more complex mathematical operations like integrals and derivatives. Among the other approaches we considered, I mainly worked on the task of modifying the input space in order to minimize the complexity of the architecture, leading to the concept of FE. Thanks to the simplicity of the application I will use it for better describing the role we were willing to give to ML, in contrast with the idea of brute force machine learning.

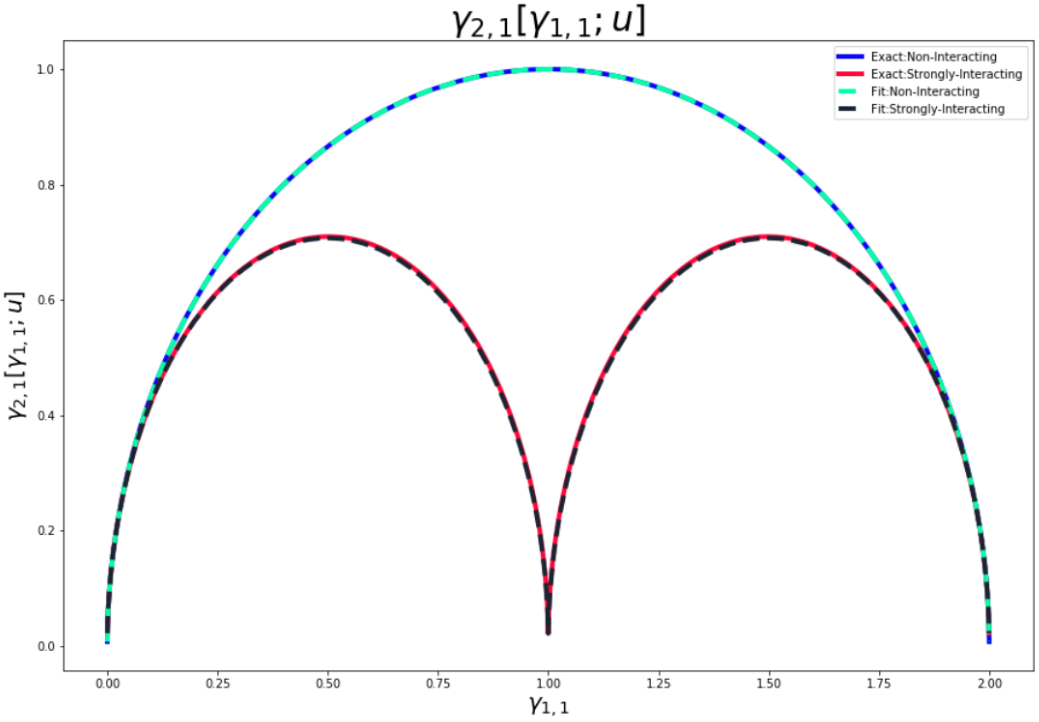

Figure 3.1: The off-diagonal terms $\gamma_{2,1}$ of the 1-RDMs present in the data-set are plot as a function of $\gamma_{1,1}$, the only independent variable in the density thanks to the Eq. 2.2. In addition, the exact laws for the interacting and non-interacting electrons are plot to show the perfect matching between the $N_g = 4$ system solved by the `iDEA` code and the Hubbard Dimer.

3.2 Hubbard Dimer

The Hubbard model for the two sites system, named Hubbard Dimer, is the building block of the Fermi-Hubbard model. Beside the fact that it is possible to experimentally create this system, by using two trapped ultracold ^6Li atoms [57], this system may be interesting for constructing bottom-up theories for more complex Hubbard models. In any case, its simplicity has led to countless applications of it: It has been used as a model for the Hydrogen molecule [58], its symmetric version has been used to estimate quantities on larger Hubbard lattices via scaling hypotheses [59] and for creating bottom up approaches for the solution of the homogeneous Hubbard model in d dimensions [60].
Let us start by describing the system. There are two sites and two electrons populating them: one has a upward-pointing spin and the other is downward-pointing. If the two are on the same site and the interaction is switched on, they interact via a repulsion whose magnitude is U. To each site it is associated a local energy cost due to the external potential and the transition itself is characterized by an energy contribution that dictates the correlation. Being willing to describe effects, a hierarchy must be chosen for ordering the Hilbert space. The ordering chosen is the following :

- The highest priority to the first site;
- The second highest priority to the upward-pointing spin.

That, as a chain of importance reads:

$$1 > \uparrow > 2, \downarrow$$

Having forced the electrons to have opposite spins, we can limit to study the Fock subspace corresponding to a total spin $S_z = 0$, $N_e = 2$. The basis is chosen to be the same as the one chosen in [61], i.e.

$$\mathscr{B} = \begin{cases} |\phi_1\rangle = |1\uparrow 1\downarrow\rangle = \hat{c}^\dagger_{1,\uparrow}\hat{c}^\dagger_{1,\downarrow}|\rangle = |\uparrow\downarrow;\rangle \\ |\phi_2\rangle = |1\uparrow 2\downarrow\rangle = \hat{c}^\dagger_{1,\uparrow}\hat{c}^\dagger_{2,\downarrow}|\rangle = |\uparrow;\downarrow\rangle \\ |\phi_3\rangle = |1\downarrow 2\uparrow\rangle = \hat{c}^\dagger_{1,\downarrow}\hat{c}^\dagger_{2,\uparrow}|\rangle = |\downarrow;\uparrow\rangle \\ |\phi_4\rangle = |2\uparrow 2\downarrow\rangle = \hat{c}^\dagger_{2,\uparrow}\hat{c}^\dagger_{2,\downarrow}|\rangle = |;\uparrow\downarrow\rangle \end{cases} \tag{3.4}$$

Where the ladder operators have been introduced in Sec. 1.1, completely defining the 4 dimensional Hilbert space. The data-set has been generated in such a way that the state vector belongs to the singlet subspace, in accordance with the actual experimental realization [57]. In order to build such a subspace, let us define the spin-exchange operator $\hat{\Pi}$ [62], whose action on a state is such that

$$\hat{\Pi}|i\sigma j\sigma'\rangle = \hat{c}^\dagger_{i,\pi(\sigma)}\hat{c}^\dagger_{j,\pi(\sigma')}|\rangle = \hat{c}^\dagger_{i,\sigma'}\hat{c}^\dagger_{j,\sigma}|\rangle = |i\sigma' j\sigma\rangle.$$

The difference between a vector belonging to the singlet or to the triplet subspace can then be expressed as follows

$$\begin{cases} \hat{\Pi}|\varphi_i\rangle = -|\varphi_i\rangle & \Leftrightarrow |\varphi_i\rangle \in \mathscr{H}_{singlet} \\ \hat{\Pi}|\varphi_i\rangle = |\varphi_i\rangle & \Leftrightarrow |\varphi_i\rangle \in \mathscr{H}_{triplet} \end{cases} \tag{3.5}$$

By applying this operator on the previous basis, it is possible to construct the following basis vectors for the two subspaces:

$$\mathscr{B}_{singlet} = \begin{cases} |\varphi_1\rangle = |1\uparrow 1\downarrow\rangle \\ |\varphi_2\rangle = \frac{1}{\sqrt{2}}(|1\uparrow 2\downarrow\rangle - |1\downarrow 2\uparrow\rangle) \\ |\varphi_3\rangle = |2\uparrow 2\downarrow\rangle \end{cases} \quad \mathscr{B}_{triplet} = |\varphi_4\rangle = \frac{1}{\sqrt{2}}(|1\uparrow 2\downarrow\rangle + |1\downarrow 2\uparrow\rangle)$$

Among these we are only interested in the linear span $\mathscr{L}(\mathscr{B}_{singlet})$, and the most general Ground state vector in the 3-sites problem reads

$$|\Psi\rangle = \sum_{i=1}^{3} a_i |\varphi_i\rangle$$

where $\sum_{i=1}^{3} a_i^2 = 1$. This having been said, it is possible to focus on the 1-RDM that, for a lattice model, we have already argued to be

$$\gamma_{r,r'} = \langle\Psi| \sum_{\sigma} \hat{c}^{\dagger}_{r,\sigma}\hat{c}_{r',\sigma}|\Psi\rangle \tag{3.6}$$

where $r, r' \in \{1,2\}$ are the two possible sites. In the following sections, the action of similar operators will occur many times. In order to speed up the derivation, let us now discuss a general way to do this kind of calculations.
Let us consider a generic operator $\hat{O} = \hat{c}^{\dagger}_{p,\sigma}\hat{c}_{q,\sigma}$ acting on a generic state $\hat{c}^{\dagger}_{r,\sigma'}\hat{c}^{\dagger}_{s,-\sigma'}|\rangle$. By using the CAR, the resulting state becomes:

$$\begin{aligned} \hat{O}\hat{c}^{\dagger}_{r}\hat{c}^{\dagger}_{s}|\rangle &= \hat{c}^{\dagger}_{p,\sigma}\hat{c}_{q,\sigma}\hat{c}^{\dagger}_{r,\sigma'}\hat{c}^{\dagger}_{s,-\sigma'}|\rangle = \\ &= \hat{c}^{\dagger}_{p,\sigma}(\hat{c}^{\dagger}_{s,-\sigma}\delta_{\sigma,\sigma'}\delta_{q,r} - \hat{c}^{\dagger}_{r,-\sigma}\delta_{\sigma,-\sigma'}\delta_{q,s})|\rangle \end{aligned}$$

Thanks to the orthogonality induced by the delta functions on the spin only one of the two will be true. In words, whenever acting with an operator that destroys a particle in the site q and with spin σ for reconstructing it at unvaried spin in the site p, if there is no electron with the same spin as the one in q the result is the vacuum state. Whereas, if there is an electron with the same spin as in q, the two sites need to be substituted. It is essential to remark that, after having obtained the final result, the order of the Hilbert space needs to be imposed. These rules will be implicitly used in all of the following derivations. In particular, for what concerns the 1-RDM it is straightforward to obtain the following results:

$$\begin{cases} \gamma_{1,1} = 2|a_1|^2 + |a_2|^2 \\ \gamma_{2,2} = 2|a_3|^2 + |a_2|^2 \end{cases} \text{and} \begin{cases} \gamma_{2,1} = \sqrt{2}(a_1 a_2^* + a_2 a_3^*) \\ \gamma_{1,2} = \sqrt{2}(a_2 a_1^* + a_3 a_2^*) \end{cases} \tag{3.7}$$

Or, since the 1-RDM is real and symmetric for the sub-class of problems we are considering,

$$\gamma_{2,1} = \sqrt{2}a_2(a_1 + a_3) \tag{3.8}$$

3.2.1 Expressing the Hamiltonian in the singlet basis

Before to diagonalize the Hamiltonian, it must be represented in the chosen basis. The first term to be constructed is the hopping term:

$$\hat{H}_t = -t(\hat{c}^{\dagger}_{1,\uparrow}\hat{c}_{2,\uparrow} + \hat{c}^{\dagger}_{2,\uparrow}\hat{c}_{1,\uparrow} + \hat{c}^{\dagger}_{1,\downarrow}\hat{c}_{2,\downarrow} + \hat{c}^{\dagger}_{2,\downarrow}\hat{c}_{1,\downarrow})$$

Whenever it acts on a basis component of a certain state, it is able to destroy a particle with a certain spin and to recreate it with the same spin but on the other site. In so doing, it gives to the newly obtained state an energy reward for having been able to tunnel to the other state.
Let us construct the kinetic term:

$$\begin{aligned}\hat{H}_t|\varphi_1\rangle &= \hat{H}_t\hat{c}^\dagger_{1,\uparrow}\hat{c}^\dagger_{1,\downarrow}|\rangle = \\ &= -t(\hat{c}^\dagger_{2,\uparrow}\hat{c}_{1,\uparrow}+\hat{c}^\dagger_{2,\downarrow}\hat{c}_{1,\downarrow})\hat{c}^\dagger_{1,\uparrow}\hat{c}^\dagger_{1,\downarrow}|\rangle = \\ &= -t(\hat{c}^\dagger_{1,\uparrow}\hat{c}^\dagger_{2,\downarrow}|\rangle - \hat{c}^\dagger_{1,\downarrow}\hat{c}^\dagger_{2,\uparrow}|\rangle) = -t\sqrt{2}|\varphi_2\rangle\end{aligned}$$

analogously

$$\begin{aligned}\hat{H}_t|\varphi_3\rangle &= \hat{H}_t\hat{c}^\dagger_{2,\uparrow}\hat{c}^\dagger_{2,\downarrow}|\rangle = \\ &= -t(\hat{c}^\dagger_{1,\uparrow}\hat{c}_{2,\uparrow}+\hat{c}^\dagger_{1,\downarrow}\hat{c}_{2,\downarrow})\hat{c}^\dagger_{2,\uparrow}\hat{c}^\dagger_{2,\downarrow}|\rangle = \\ &= -t(\hat{c}^\dagger_{1,\uparrow}\hat{c}^\dagger_{2,\downarrow}|\rangle - \hat{c}^\dagger_{1,\downarrow}\hat{c}^\dagger_{2,\uparrow}|\rangle) = -t\sqrt{2}|\varphi_2\rangle\end{aligned}$$

and, finally

$$\begin{aligned}\hat{H}_t|\varphi_2\rangle &= \hat{H}_t\frac{1}{\sqrt{2}}(\hat{c}^\dagger_{1,\uparrow}\hat{c}^\dagger_{2,\downarrow}|\rangle - \hat{c}^\dagger_{1,\downarrow}\hat{c}^\dagger_{2,\uparrow}|\rangle) \\ &= -t(\hat{c}^\dagger_{2,\uparrow}\hat{c}_{1,\uparrow}+\hat{c}^\dagger_{1,\downarrow}\hat{c}_{2,\downarrow}+\hat{c}^\dagger_{1,\uparrow}\hat{c}_{2,\uparrow}+\hat{c}^\dagger_{2,\downarrow}\hat{c}_{1,\downarrow})\frac{1}{\sqrt{2}}(\hat{c}^\dagger_{1,\uparrow}\hat{c}^\dagger_{2,\downarrow}|\rangle - \hat{c}^\dagger_{1,\downarrow}\hat{c}^\dagger_{2,\uparrow}|\rangle) = \\ &= -t\sqrt{2}(\hat{c}^\dagger_{2,\uparrow}\hat{c}^\dagger_{2,\downarrow}|\rangle + \hat{c}^\dagger_{1,\uparrow}\hat{c}^\dagger_{1,\downarrow}|\rangle) = -t\sqrt{2}(|\varphi_1\rangle + |\varphi_3\rangle)\end{aligned}$$

Where, in the process, the anti-commutation relations of the ladder operators and the number operator have been used

$$\{\hat{c}_{i,\sigma}, \hat{c}^\dagger_{j,\sigma}\} = \delta_{i,j} \tag{3.9}$$

and

$$\hat{n}_{i,\sigma} = \hat{c}^\dagger_{i,\sigma}\hat{c}_{i,\sigma}$$

The kinetic Hamiltonian becomes

$$\hat{H}_t = \begin{pmatrix} 0 & -\sqrt{2}t & 0 \\ -\sqrt{2}t & 0 & -\sqrt{2}t \\ 0 & -\sqrt{2}t & 0 \end{pmatrix}$$

For what concerns $\hat{H}_u$ it will be nonzero only for the basis vector such that both the electrons are in the same site. The matrix then becomes

$$\hat{H}_u = \begin{pmatrix} U & 0 & 0 \\ 0 & 0 & 0 \\ 0 & 0 & U \end{pmatrix}$$

And finally, also the last contribution will be diagonal being it expressed as a function of the number operator

$$\hat{H}_v = \begin{pmatrix} 2v_1 & 0 & 0 \\ 0 & v_1+v_2 & 0 \\ 0 & 0 & 2v_2 \end{pmatrix}$$

Yielding the total matrix

$$\hat{H} = \begin{pmatrix} U+2v_1 & -\sqrt{2}t & 0 \\ -\sqrt{2}t & v_1+v_2 & -\sqrt{2}t \\ 0 & -\sqrt{2}t & U+2v_2 \end{pmatrix} = \begin{pmatrix} U+\Delta v & -\sqrt{2}t & 0 \\ -\sqrt{2}t & 0 & -\sqrt{2}t \\ 0 & -\sqrt{2}t & U-\Delta v \end{pmatrix} + (v_1+v_2)\mathbb{I}_3$$

$\Delta v \doteq v_1 - v_2$ is the difference in the potentials and the last term is just a shift in the energy. From a theoretical point of view, the explicit diagonalization of the Hamiltonian would then require to impose the following

$$det(\hat{H} - E\mathbb{I}_3) \doteq 0$$

from which we finally obtain the third order equation to be solved for E

$$E(U-E)^2 + (2t)^2(U-E) - E(\Delta v)^2 = 0 \tag{3.10}$$

This equation does not allow for a general solution but some limiting cases are of a certain interest.

3.2.2 Non-interacting electrons case

By imposing the absence of interaction, equation 3.10 becomes analytically exactly solvable with a ground state eigenvalue equal to

$$E^o_{GS} = -\sqrt{(2t)^2 + (\Delta v)^2} \tag{3.11}$$

where the (o) stands for non-interacting. By solving for the eigen-vector, it is possible to finally obtain the ground state

$$|\Psi^o_{GS}\rangle = -\frac{1}{\sqrt{2}}\left(|\psi_1\rangle + \frac{2t}{\sqrt{(2t)^2+(\Delta v)^2}}|\varphi_2\rangle - \frac{\Delta v}{\sqrt{(2t)^2+(\Delta v)^2}}|\psi_3\rangle\right) \tag{3.12}$$

Where $|\psi_1\rangle \doteq \frac{1}{\sqrt{2}}(|\varphi_1\rangle + |\varphi_3\rangle)$ and $|\psi_3\rangle \doteq \frac{1}{\sqrt{2}}(|\varphi_1\rangle - |\varphi_3\rangle)$.
With the further assumption that the sites are sufficiently far apart, consistent with the approximation of no repulsion between electrons located at the two sites, we can assume

$$2t \ll \Delta v$$

and, in this limit

$$|\Psi^o_{GS}\rangle \sim |\psi_1\rangle - \frac{\Delta v}{|\Delta v|}|\psi_3\rangle = \begin{cases} |\varphi_1\rangle = |\uparrow\downarrow;\rangle & \text{if } v_1 < v_2, \\ |\varphi_3\rangle = |;\uparrow\downarrow\rangle & \text{if } v_2 < v_1 \end{cases} \tag{3.13}$$

That corresponds with the intuition that, when there is a sufficient energy difference between two states, in absence of tunneling, the two electrons tend to localize together in the deepest well.

3.2.3 Symmetric potential case

Also the case $\Delta v = 0$ is an exactly solvable one. This fact is extremely interesting because it corresponds to the flat potential. $\Delta v = 0$, in fact, corresponds to $v_1 = v_2 = v$. This introduces a symmetry in the two points system, that identifies straightforwardly this case with the condition $\gamma_{1,1} = \gamma_{2,2} = 1$ since a difference in the density would correspond to a not justified breaking of the symmetry. The importance of this condition lays in the fact that, by looking at Fig.3.1, it is possible to observe that the 1-RDMs having $\gamma_{2,1} = 0$ were exactly those corresponding to this specific condition. Hence, the analytical results in this case can explain the reason why, in the data-set under analysis, the off-diagonal term vanishes.
Now equation 3.10 becomes

$$(U-E)((U-E)E + (2t)^2) = 0 \tag{3.14}$$

and the ground state eigenvalue is

$$E_{GS} = \frac{U}{2} - \sqrt{\left(\frac{U}{2}\right)^2 + (2t)^2}$$

corresponding to a Ground state

$$|\Psi_{GS}^{sym}\rangle = z\left(|\varphi_1\rangle - \frac{2\sqrt{2}t}{E_{GS}}|\varphi_2\rangle + |\varphi_3\rangle\right) \tag{3.15}$$

with z being the normalization factor

$$z^2 = \frac{1}{2}\frac{1}{1+\left(\frac{2t}{E_{GS}}\right)^2} \tag{3.16}$$

This having been done, it is possible to compute the off-diagonal term of the 1-RDM by using the following formula:

$$\begin{aligned}
\gamma_{2,1}^{sym} = \gamma_{2,1}[\gamma_{1,1} = 1; u] &= \sqrt{2}a_2(a_1 + a_3) = \\
&= -2z^2\frac{4t}{E_{GS}} = \\
&= -\frac{4tE_{GS}}{E_{GS}^2 + (2t)^2} = \\
&= -4t\left\{\frac{U/2 - \sqrt{(U/2)^2 + (2t)^2}}{(2t)^2 + [U/2 - \sqrt{(U/2)^2 + (2t)^2}]^2}\right\} = \\
&= -\frac{U/4t - \sqrt{(U/4t)^2 + 1}}{1 + (U/4t)^2 - U/4t\sqrt{(U/4t)^2 + 1}} = \\
&= -\frac{u - \sqrt{u^2+1}}{1 + u(u - \sqrt{u^2+1})}
\end{aligned}$$

where the dimensionless interaction strength parameter $u \doteq \frac{U}{4t}$ has been introduced and accounts for how strong the on-site repulsion is felt, relatively to the hopping term intensity. In Fig.3.2 the behavior of this function can be observed.

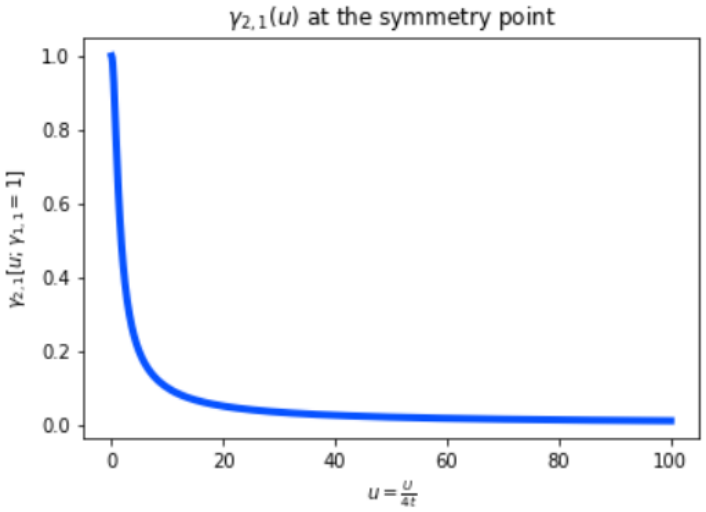

Figure 3.2: Behavior of the off-diagonal term as a function of the interaction strength at the symmetry point ($\gamma_m = \gamma_{1,1} = \gamma_{2,2} = 1$ and $v_1 = v_2$).

From the functional behavior, a few remarks are worth being done:

- Strongly interacting electrons: $\gamma^{\infty}_{2,1} = lim_{u\to\infty}\gamma_{2,1} = 0$
- Non-interacting electrons: $\gamma^{0}_{2,1} = \gamma_{2,1}(0) = 1$
- The function is injective. The parameter u is in one-to-one correspondence with the values assumed by $\gamma_{2,1}$ between the two limiting cases $\gamma^{\infty}_{2,1} \leq \gamma_{2,1} \leq \gamma^{o}_{2,1}$

For relatively low values of the interaction, this quantity is different from zero since, when an electron leaves one site, there will be a finite probability for it to end up exploring the other site. By contrast, as soon as the interaction strength enters in the strong regime, the two electrons will repel so much that the only possible configuration is the one in which the electrons are one per site. Moreover, if an electron leaves its site there will be no way for it to reach the other one due to the strong repulsion with the electron populating that site. The off-diagonal will thus be zero in the strongly interacting electrons case. The strong interaction limit, is then characterized by a vanishing off-diagonal term at the symmetry point. Being this the only case in which this happens, this formula allowed us classify the data generated with the `iDEA` code as being characterized by a strong interacting behavior, and this allowed us to explain the additional node appearing when switching on the interaction. The obtained equation

$$\boxed{\gamma_{2,1}[\gamma_{1,1}=1;u] = -\frac{u-\sqrt{u^2+1}}{1+u(u-\sqrt{u^2+1})}} \tag{3.17}$$

Is worth being remembered because it provides a parametric description of the functional behavior of $\gamma_{2,1}$ for the symmetric potential, when varying the parameter u. Deriving explicit this functional behavior was essential since its knowledge led me to determine the parametric description of $\gamma_{2,1}$ in the range of values $\gamma^{\infty}_{2,1} \leq \gamma_{2,1} \leq \gamma^{o}_{2,1}$. This will be discussed in chapter 4. Nonetheless, before to do that, it is necessary to find an analytical formula for $\gamma^{o}_{2,1}[\gamma_{1,1}]$ and $\gamma^{\infty}_{2,1}[\gamma_{1,1}]$.

3.3 Analytical behavior from Reduced Density Matrix Functional Theory on a lattice

Before to proceed it is worth recalling some concepts about Reduced Density Matrix Functional TheoryRDMFT. In this section we will follow the work done by Pastor, Saubanère Töws and all of their collaborators ([25, 35, 63]) in the presentation of the results needed for the discussion of new approaches. Among the presented references, [25] presents a determination of the density matrix for the single impurity Anderson model. That model can be put in one to one correspondence with a two level system that, in turn, can be mapped to the Hubbard Dimer. In the following we will explicitly derive the results of interest following the procedure they prescribed in [25]. The calculation were done explicitly since some observations on the meaning of some steps are worth being deepened. In the main text only the results will be reported while, for a more detailed discussion, the reader can find the details in appendix A.1. The approach is directed toward the determination of the functional of the 1-RDM. Later, in chapter 4 they will be used for the construction of a parametric functional.

The main idea in RDMFT is that, for lattice Hamiltonians, the density matrix happens to be the natural object on which to build the functionals. Let us work in the context of the Hubbard Hamiltonian:

$$\begin{aligned}\hat{H} &= \sum_{i,j,\sigma} t_{ij}\hat{c}^{\dagger}_{i,\sigma}\hat{c}_{j,\sigma} + \sum_{i} U_i \hat{n}_{i,\uparrow}\hat{n}_{i,\downarrow} + \sum_{i,\sigma} v_i \hat{n}_{i,\sigma} = \\ &= \sum_{i,j} t_{ij} \sum_{\sigma} \hat{c}^{\dagger}_{i,\sigma}\hat{c}_{j,\sigma} + \sum_{i} U_i \hat{n}_{i,\uparrow}\hat{n}_{i,\downarrow} + \sum_{i} v_i \sum_{\sigma} \hat{c}^{\dagger}_{i,\sigma}\hat{c}_{i,\sigma}\end{aligned}$$

An essential remark needs to be done concerning this Hamiltonian. One of the biggest approximations is that the many body contribution is approximated to be only an on-site repulsion, i.e. the softened Coulomb repulsion is written as a sum of local contributions. The method developed in the following, in fact, can only be applied to Hamiltonians where the coulomb interaction between the electrons is predominantly confined to an extremely close neighborhood of the lattice site associated to their Wannier wave-function. The locality of the Coulomb interaction is at the basis of the following derivation, which allows to find the off-diagonal term of the 1-RDM in terms of the density. In this framework, the common energy functional reads

$$\begin{aligned}E[|\Psi\rangle] &= \langle\Psi|\hat{H}|\Psi\rangle = \\ &= \sum_{i,j} t_{ij}\langle\Psi|\sum_{\sigma}\hat{c}^{\dagger}_{i,\sigma}\hat{c}_{j,\sigma}|\Psi\rangle + \langle\Psi|\sum_{i} U_i \hat{n}_{i,\uparrow}\hat{n}_{i,\downarrow}|\Psi\rangle + \sum_{i} v_i \langle\Psi|\sum_{\sigma}\hat{c}^{\dagger}_{i,\sigma}\hat{c}_{i,\sigma}|\Psi\rangle\end{aligned}$$

And, by recalling the definition of the 1-RDM in lattice theory (see Eq. 1.19) and that the purpose is a minimization of such a functional, we can express the energy functional in terms of the density matrix

$$E[\gamma] = \sum_{i,j} t_{ij}\gamma_{i,j} + \sum_{i} v_i \gamma_{i,i} + W[\gamma] \tag{3.18}$$

where

$$W[\gamma] \doteq min_{\Psi\to\gamma}\left\{\langle\Psi|\sum_{i} U_i \hat{n}_{i,\uparrow}\hat{n}_{i,\downarrow}|\Psi\rangle\right\}. \tag{3.19}$$

The determination of this functional requires, in the process, the determination of the expression of the components of the density matrix. For what concerns the Hubbard Dimer, the analytics can be performed and a closed form can be obtained in two specific limits.
For the Hubbard Dimer $U_i = U \; \forall i$. Hence, the quantity to be minimized becomes

$$\begin{aligned} W[\gamma] &= min_{\Psi\to\gamma}\left\{ U\langle\Psi|\sum_i \hat{n}_{i,\uparrow}\hat{n}_{i,\downarrow}|\Psi\rangle \text{ s.t. } \gamma \text{ is a valid representation} \right\} \\ &\doteq U\langle\Psi[\gamma]|\sum_i \hat{n}_{i,\uparrow}\hat{n}_{i,\downarrow}|\Psi[\gamma]\rangle \\ &= U\sum_i \omega_i[\gamma] \end{aligned}$$

Where $\omega_i[\gamma]$ is

$$\omega_i[\gamma] \doteq \langle\Psi[\gamma]|\hat{n}_{i,\uparrow}\hat{n}_{i,\downarrow}|\Psi[\gamma]\rangle \tag{3.20}$$

that corresponds to the expectation value of the double occupancy of the i-th site, where the expectation value is performed using the ground state[3] yielding the 1-RDM γ that minimizes $W[\gamma]$.
For what concerns the Hubbard Dimer, we can observe that

$$\hat{n}_{2,\sigma} = 1 - \hat{n}_{1,\sigma} \tag{3.21}$$

Hence, the functional to be minimized becomes

$$\begin{aligned} W[\gamma] &= U\langle\Psi[\gamma]|\hat{n}_{1,\uparrow}\hat{n}_{1,\downarrow} + \hat{n}_{2,\uparrow}\hat{n}_{2,\downarrow}|\Psi[\gamma]\rangle \\ &= U\langle\Psi[\gamma]|\hat{n}_{1,\uparrow}\hat{n}_{1,\downarrow} + 1 - \hat{n}_1 + \hat{n}_{1,\uparrow}\hat{n}_{1,\downarrow}|\Psi[\gamma]\rangle \\ &= U(1-n_1) + 2U\langle\Psi[\gamma]|\hat{n}_{1,\uparrow}\hat{n}_{1,\downarrow}|\Psi[\gamma]\rangle \\ &\simeq 2U\,\omega_1[\gamma] \to \omega_1[\gamma] \end{aligned}$$

In fact, once fixed γ also n_1 is fixed, being associated to $\gamma_{1,1}$. The only quantity to be minimized is, therefore, the average double occupancy of the first site that, for the Hubbard Dimer, contains all of the information on the system, at least for what concerns the coulomb repulsion.

Once having recognized $\omega_1[\gamma]$ to be the functional with which to work, the derivation of the functional $\gamma_{2,1}[\gamma_{1,1}, \gamma_{2,2}]$ described in the paper [25] proceeds as follows:

1. As a first thing they wrote explicitly the functional to be minimized, corresponding to the local double occupancy constrained via the Lagrange multipliers method. The constraint corresponds to forcing the ground state to yield a certain 1-RDM, which is assumed to be known at this stage;

2. Then they gave the result of the variational minimization. They defined an appropriate variational vector, corresponding to our ground state, and they wrote both ω_1 and the constraints in terms of the parameters of the variational ground-state vector;

[3] To be determined in the variational procedure.

3. The constraints become conditions to be satisfied by the parameters of the state vector and, among all of the possible parameters, the correct choice is the one minimizing the expression of ω_1 in terms of the coefficients. They gave only the results of the minimization and I performed explicitly the steps;

4. Once obtained $\omega_1[\gamma] = \omega_1[\gamma_{1,1}, \gamma_{2,1}]$, it is finally possible to study the strong interaction limit, searching for the relationship existing between the elements of the 1-RDM and yielding the minimum value of $\omega_1[\gamma]$ as a function of $\gamma_{2,1}$. Obtained the relationship between the matrix elements, it is finally possible to explicit $\gamma_{2,1}$ in terms of $\gamma_{1,1}$, finding the desired functional. In the same way, they found the law in the non-interacting case, by looking at the maximum double occupation.

Once again I would like to stress that the results were present in literature ([25]) together with the prescription for deriving them. What I did was to follow the prescription, extremely well suited for our case, and doing autonomously the calculations. Therefore, what follows is the detailed derivation in which the different steps have been commented with as much physical insight as possible. Due to the intellectual belonging of the results to other researchers the details of the calculation are reported in appendix and in this chapter I will just describe the prescription together with some additional comments.

1: Writing the functional to be minimized:

$$\begin{aligned}\omega_1^c[|\Psi\rangle] \doteq \omega_1[\gamma] - \varepsilon(\langle\Psi|\Psi\rangle - 1) + \\ + \lambda_{11}\big(\langle\Psi|\sum_\sigma \hat{c}^\dagger_{1,\sigma}\hat{c}_{1,\sigma}|\Psi\rangle - \gamma_{1,1}\big) + \\ + \lambda_{12}\big(\langle\Psi|\sum_\sigma \hat{c}^\dagger_{1,\sigma}\hat{c}_{2,\sigma}|\Psi\rangle - \gamma_{1,2}\big) + \\ + \lambda_{21}\big(\langle\Psi|\sum_\sigma \hat{c}^\dagger_{2,\sigma}\hat{c}_{1,\sigma}|\Psi\rangle - \gamma_{2,1}\big)\end{aligned}$$

It is to be noticed that working in the subspace of the possible γs corresponding to $N_e = 2$ implies $\gamma_{1,1} + \gamma_{2,2} = 2$. By assuming to work in this subspace and using the constraint along the derivation, there is no need to introduce a Lagrange multiplier also for $\gamma_{2,2}$. In fact this would require a further Lagrange multiplier for imposing the constraint on the trace.

2: Finding the parametric variational state vector and writing ω_1 and the constraints in terms of its parameters: Now the purpose is to extract some information from a variational approach. The ground state vector, written as a linear span of the singlet basis, can be interpreted as a parametric representation of the variational ground state:

$$|\Psi\rangle = a_1|\varphi_1\rangle + a_2|\varphi_2\rangle + a_3|\varphi_3\rangle \tag{3.22}$$

Where the coefficients can be chosen to be real ($a_i \in \mathbb{R}$) since we are considering the ground state of a system. Starting from this vector, the expression of the 1-RDM in terms of the parameters has already been found to be

$$\begin{cases}\gamma_{1,1} = 2|a_1|^2 + |a_2|^2 \\ \gamma_{2,2} = 2|a_3|^2 + |a_2|^2 \\ \gamma_{2,1} = \sqrt{2}a_2(a_1 + a_3)\end{cases} \tag{3.23}$$

moreover, the functional to be minimized was observed to be:

$$\omega_1 = \langle \Psi | \hat{n}_{1\uparrow} \hat{n}_{1\downarrow} | \Psi \rangle = |a_1|^2$$

3: Finding the relation the parameters need to satisfy and performing the minimization to obtain $\omega_1[\gamma]$: At this point, the remaining thing to be done is to solve the nonlinear set of equations for $|a_1|^2$.

$$\begin{cases} |a_2|^2 = \gamma_{1,1} - 2\omega_1 \\ |a_3|^2 = (2 - \gamma_{1,1} - |a_2|^2)/2 = 1 - \gamma_{1,1} + \omega_1 \\ \omega_1 = \left(\frac{\gamma_{2,1}}{\sqrt{2}a_2} - a_3\right)^2 \end{cases} \tag{3.24}$$

Substituting $|a_2|^2(\omega_1)$ and $|a_3|^2(\omega_1)$ in the third equation, and performing the square, one obtains an equation for ω_1

$$\frac{\gamma_{2,1}^2}{2(\gamma_{1,1} - 2\omega_1)} + 1 - \gamma_{1,1} - \sqrt{2}\gamma_{2,1}\frac{\sqrt{1 - \gamma_{1,1} + \omega_1}}{\sqrt{\gamma_{1,1} - 2\omega_1}} = 0 \tag{3.25}$$

By looking at the minimum solution of this equation it is possible to obtain

$$\omega_1 = \frac{\gamma_{1,1}}{2} - \frac{\gamma_{2,1}^2/4}{1 - \sqrt{\gamma_{1,1}(2 - \gamma_{1,1}) - \gamma_{2,1}^2}} \tag{3.26}$$

The details of the derivation can be found in appendix (see A.1).

4: Extracting the functional $\gamma_{2,1}[\gamma_{1,1}]$ in some limiting cases: What eq.3.26 does is to generate a functional relation between the average double occupancy of the first site and the matrix elements of the 1-RDM. This equation is essential because it can be used for finding the desired functionals of the density matrix in terms of the density.
As a first thing, by using the coulomb repulsion as a parameter fixed at some value, it is possible to assume that, by tuning in a proper way the external potential, it is possible to prepare the system under analysis with all the $\gamma_{1,1}$ in the range $\gamma_{1,1} \in [0,2]$. The distinctive variable between the different many body interaction strengths will then be the off-diagonal term, which will be an indicator of the way the two sites are correlated. Having highlighted the one-to-one correspondence between the many-body effects and the off-diagonal term, one expects that different limiting conditions of the many-body strength correspond to different limiting functional behaviors of $\gamma_{2,1}$ as a function of $\gamma_{1,1}$. For this reason, $\gamma_{1,1}$ is fixed as a parameter and the previous equation is considered as a function of $\gamma_{2,1}$. Minima and maxima will be the previously introduced limiting cases.
Given these premises, the two limiting cases to be considered are the non-interacting case and the strongly-interacting case. For what concerns the strongly interacting, $u \to \infty$, when a strong on-site repulsion is present the average double occupancy is expected to be extremely small since the most favorable configuration for the two electrons will correspond, on average, to the condition in which the electrons stay one per each side. Whatever is the perturbation that may happen on the site i, the site j will be perturbed in the minimal way allowed by the stability of the

corresponding density[4]. The strong interacting limit, therefore, will correspond to the minimal average occupation number ω_1^∞ among all the possible ones. By contrast, the non-interacting limit will correspond to a maximum of the double occupancy ω_1^o since whatever is the coulomb repulsion, it will never be as likely for the two electrons as in the non-interacting case to be in the same site. For this reason,

$$\omega_1^\infty \leq \omega_1 \leq \omega_1^o$$

In Fig.3.3, it is plotted the average occupation number as a function of $\gamma_{2,1}$ and the minima, corresponding to the strongly interacting case, has been found numerically. From this plot it is possible to do two major considerations:

1. The minimum, corresponding to the strongly interacting limit, can be found analytically by imposing the gradient to vanish;

2. The maximum of ω_1, corresponding to the non-interacting case, must be at a value higher than the strongly interacting one since the strong repulsion tends to overpower the correlations. For this reason it is possible to expect

   $$\gamma_{2,1}^\infty \leq \gamma_{2,1} \leq \gamma_{2,1}^o$$

   and the maximum is located at the $\gamma_{2,1}$ corresponding to the right border of the domain, as shown in Fig.3.3.

[4]Different densities will correspond to a different stability of the configuration. For some vales of the density, corresponding to some external potential given the strength of the repulsion, the state will be stabler than in others, killing completely the fluctuation (symmetric potential) while for others some form of correlation will be stronger. Anyway, in the strong interacting limit, the correlation will certainly be the minimal possible and associated to the minimal double occupation

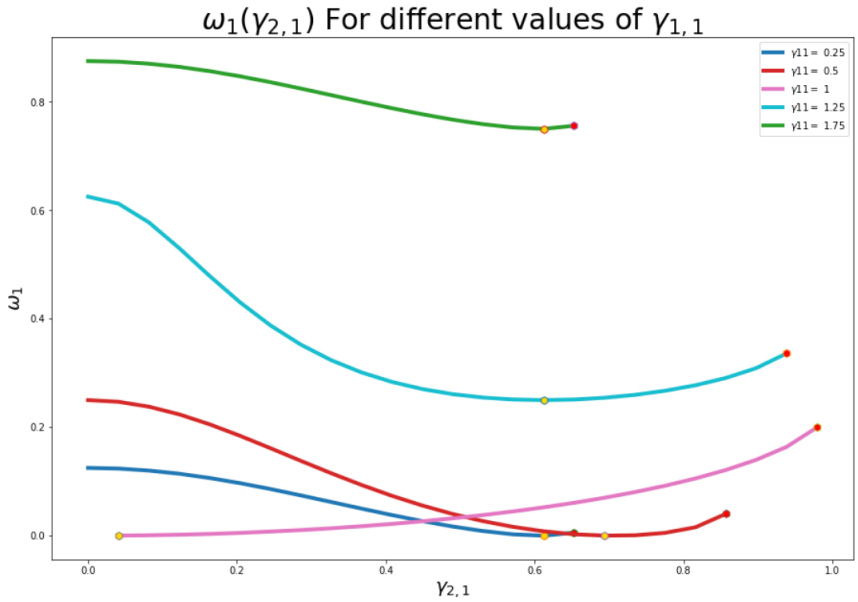

Figure 3.3: Average occupation number (Eq. 3.26) as a function of $\gamma_{2,1}$. Each line corresponds to a different value of $\gamma_{1,1}$. The golden point marks the minimum of the curve, corresponding to the minimal double occupancy and, as a consequence, to the strongly interacting limit. By contrast the red point is associated to the maximum compatible with the golden point being the strongly-interacting case.

Considering figure 3.3 it is possible to evince that the strongly interacting case can be obtained by forcing the derivative to vanish while the non-interacting case is a boundary condition. The details of the derivation can be found in appendix A.2. For the non-interacting case the result is a second derivation of the result

$$\boxed{\gamma^{o}_{2,1} = \sqrt{\gamma_{1,1}(2-\gamma_{1,1})}}$$

already derived in the introductory chapter (see 1.4) while for the strongly interacting case the result is found to be

$$\gamma^{\infty}_{2,1} = \begin{cases} \sqrt{2(\gamma_{1,1}-1)(2-\gamma_{11})} & \text{if } \gamma_{1,1} \geq 1 \\ \sqrt{2\gamma_{1,1}(1-\gamma_{11})} & \text{if } \gamma_{1,1} < 1, \end{cases}$$

that can also be rewritten as

$$\boxed{\gamma^{\infty}_{2,1} = \sqrt{2|\gamma_{1,1}-1| \cdot min\{\gamma_{1,1}, 2-\gamma_{1,1}\}}} \tag{3.27}$$

By comparing this function with the `iDEA` interacting 1-RDMs the matching is perfect, as it can be observed in Fig.3.1.

Remark: The symbol ∞ has been used with a slight abuse of notation. If the electrons were not strongly interacting but infinitely interacting, when varying the potential landscape the density would no more experience all of the values in between 0 and 2 but it would rather experience a sharp transition from 0 to 1 and from 1 to 2. This is better described in appendix B. So in the infinitely interacting limit the formula is still correct but the only experienced value of $\gamma_{2,1}$ is 0.

3.4 Feature Engineering and the Logarithmic Perceptron

Once having derived these two limiting cases I started to ponder what was the best way to make the machine learn these two limiting cases. The overall purpose was to use the gained knowledge for modifying the Neural Network architecture needed for learning the model and the question led me to investigate a procedure whose cornerstone is *feature engineering* (FE). It is essential to remark that, contrary to what happened in the PCA functional, in which the machine taught us additional informations on the data, we are now informing the topology of the machine using human analytical insight. Before to proceed, I will now introduce the concept of FE, that will later be applied for learning the two limiting cases.

3.4.1 Feature Engineering: The exclusive or problem

Let us go back to NN architectures. The main reason why MLPs were included was due to the existence of problems requiring the introduction of a non-linearity for being solved. One of the main classical problems of this kind it learning the *exclusive OR* function (XOR): $(\cdot \oplus \cdot) : \{0,1\} \times \{0,1\} \to \{0,1\}$. This logic function is true (1) if and only if its two inputs have

v_1	v_2	$v_1 \wedge v_2$	$v_1 \oplus v_2$
0	0	0	0
0	1	0	1
1	0	0	1
1	1	1	0

Table 3.1: Truth table of the AND function $v_1 \wedge v_2$ compared to the one of the XOR function $v_1 \oplus v_2$.

opposite logic value (true/false or $0/1$). Its truth table can be compared to the one of the AND logic function in Tab. 3.1. As discussed in Sec. 1.3, what the linear perceptron learns is basically a vector to be multiplied to the input. The projection of the input on this vector gives a number that can be used for regression or for classification tasks. The learning of a logic function belongs to the second category since the task is to learn the truth class to which the pair of inputs belongs.

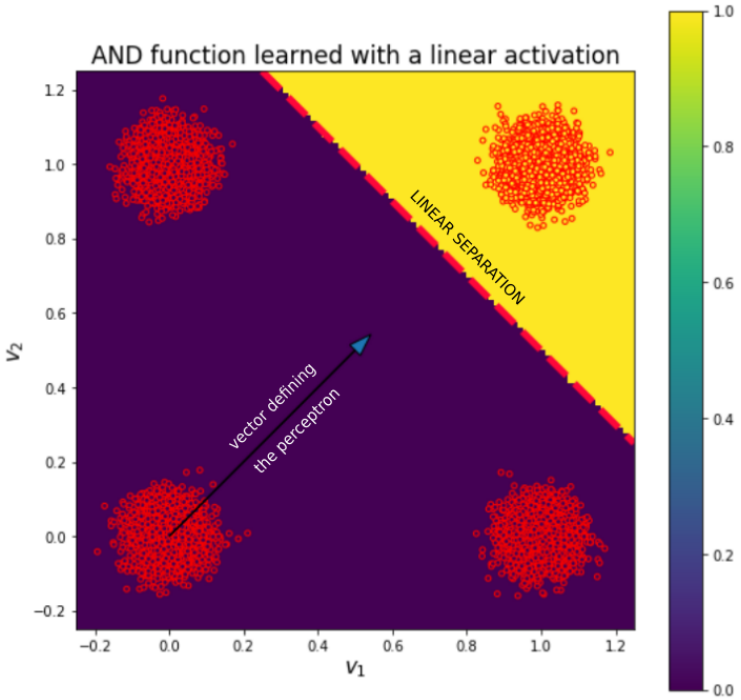

Figure 3.4: AND function and division in domains that can be learned with a perceptron. The points with the red edge correspond to the dataset, an ensemble of points in the set $\{0,1\}\times\{0,1\}$ with some noise on them. The color corresponds to the value of the logic function AND. Dark for 0 and light for 1.

Let us start by considering the AND function. In Fig. 3.4 a data-set of 2D vectors has been sampled. The two components of each point are sampled from a symmetric Bernoulli distribution to which a deviation has been added by sampling it from a gaussian of zero mean and standard deviation 0.05. This is done in order to simulate the kind of logic values that are commonly present in an electronic circuit. From the picture it is clear that the AND classification problem is linearly separable since it is possible to draw a line to separate the two classes. The points laying on the left belong to the *false* class and those on the right to the *true* class. This information can be encoded in the vector $|\theta\rangle$, orthogonal to the line, and in a number $\bar{b}=-b$ due to the parametrization of that line

$$\begin{aligned}\langle\theta|v\rangle &= \bar{b}\\ \sum_{k=1}^{2}\langle\theta|f_k\rangle\langle f_k|v\rangle &= -b\\ v_1\theta_1+v_2\theta_2 &= -b\\ v_1\theta_1+v_2\theta_2+b &= 0\end{aligned}$$

Therefore, the AND can be found to be exactly writable as a (non-linear) Heaviside function

$$v_1\wedge v_2 = f^{\sigma}\left(v_1\theta_1+v_2\theta_2+b\right)=\begin{cases}0 & \text{if } v_1\theta_1+v_2\theta_2+b<0\\ 1 & \text{if } v_1\theta_1+v_2\theta_2+b>0\end{cases} \tag{3.28}$$

Corresponding to the equation defining a perceptron.
On the other hand, as it can be read in the book [64], the XOR cannot be linearly separated as it

is possible to evince in Fig. 3.5. There does not exist any linear manifold that could allow to divide the domain in two classes.

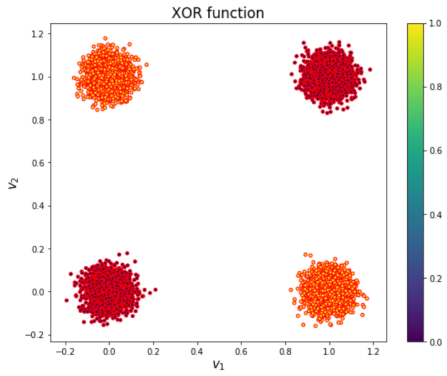

Figure 3.5: XOR function. The points with the red edge correspond to the dataset, an ensemble of points in the set $\{0,1\} \times \{0,1\}$ with some noise on them. The color corresponds to the value of the logic function XOR. Dark for 0 and light for 1

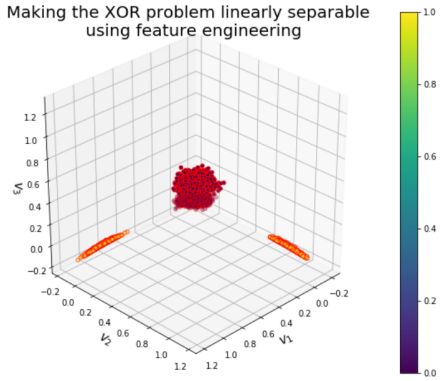

Figure 3.6: Linear separation of the XOR function using feature engineering. While the v_1 and v_2 axes are unvaried, the feature engineered variable v_3 is introduced. Augmenting the space using pre-existing knowledge allows for a reduction of the complexity of the network that would be necessary for learning the non-linearity here simplified by the external.

At this point there are two possibilities to machine learn the XOR. First, the universal approximation theorem [65] guarantees that a MLP with a sufficiently large hidden layer can fit any function. Therefore we could just add as many perceptrons as needed to reach the required non-linearity. Alternatively, it is possible to work on the input for obtaining new variables, better encoding the non-linearity of the problem. This second approach is commonly denoted as *feature engineering* and is what we are interested in. In fact, by defining new *engineered* variables, it is possible to map the problem to a linearly separable problem. This is possible only if some insight is given on the function to be learned. For instance, a common way of making the problem linearly separable is by introducing a new variable $v_3 = v_1 \cdot v_2$. This third dimension can be thought of as an axis orthogonal to the plane. In this augmented space only the points on the top-right of Fig. 3.5 will have $v_3 \sim 1$ and, therefore, will be shifted along the new dimension. This shift automatically induces the possibility of linearly separating the classes as it is possible to evince by looking at Fig. 3.6. Therefore, without the need of adding many neurons, it is possible to solve the problem adding just one input to the previously defined perceptron.

$$v_1 \oplus v_2 = f^{\sigma}\left(v_1\theta_1 + v_2\theta_2 + v_3\theta_3 + b\right) = \begin{cases} 0 & \text{if } v_1\theta_1 + v_2\theta_2 + v_3\theta_3 + b < 0 \\ 1 & \text{if } v_1\theta_1 + v_2\theta_2 + v_3\theta_3 + b > 0 \end{cases} \tag{3.29}$$

where, this time, $|\theta\rangle$ will be the versor orthogonal to the 3D surface that one could use to separate the two classes.

3.4.2 Logarithmic Perceptron

Let us now go back to introducing the gained information to learn the interacting and non-interacting limits. The starting point observation is that any sufficiently complex NN can learn by brute-force ML how to approximate a function by examples. However, in order to obtain an efficient model, it is necessary to determine the best way in which the data should be presented to the machine. FE is at the basis of the whole proposed approach to apply ML to physics, by refusing to consider brute force ML as an acceptable way of doing it. The content of the following lines is to be considered somehow as a manifesto of the underlying adopted approach.

We can start from the functional $\gamma[n]$ for a two points system containing two electrons of opposite spin. As mentioned before the 1-RDM has the charge density along its diagonal and is symmetric, reducing the problem to finding the function

$$\gamma_{21}(\gamma_{11},\gamma_{22}). \tag{3.30}$$

The universal approximation theorem [65] guarantees that a MLP with a sufficiently large hidden layer can fit any function. However, this information is used only as a starting point awareness: *There exist an appropriately complex NN that can approximate the real model*. Starting from this, the purpose of the model-maker is to "dismantle" the complexity of the network. By introducing additional knowledge on the actual law, the network can be progressively simplified, up to the reach of the minimally complex architecture as soon as the model has been understood completely.
Once defined the in-homogeneous Hubbard-Dimer Hamiltonian and the a-dimensional interaction strength $u = \frac{U}{4t}$, the previously performed variational constrained minimization allowed to extract the desired functional in the two limiting cases of non-interacting electrons :

$$\gamma_{21}^{0} = \gamma_{21}(u=0) = \sqrt{\gamma_{11}(2-\gamma_{11})}, \tag{3.31}$$

and of strongly-interacting electrons:

$$\gamma_{21}^{\infty} = \gamma_{21}(u\to\infty) = \begin{cases} \sqrt{2(\gamma_{11}-1)(2-\gamma_{11})} & \text{if } \gamma_{11}\geq 1 \\ \sqrt{2\gamma_{11}(1-\gamma_{11})} & \text{if } \gamma_{11}<1. \end{cases} \tag{3.32}$$

by introducing the variable $\gamma_m = \min\{\gamma_{11}, 2-\gamma_{11}\}$ I then wrote equation 3.32 in one formula

$$\gamma_{2,1}^{\infty} = \sqrt{2\gamma_m(1-\gamma_m)}. \tag{3.33}$$

This allows to drastically reduce the complexity of the network needed for fitting the data. The relations can be written as

$$\gamma_{21}(x_1,x_2) = x_1^{\omega_1}x_2^{\omega_2} = e^{\omega_1\log x_1+\omega_2\log x_2+b}, \tag{3.34}$$

where $\omega_i = 1/2$ and $b = 0$

$$(x_1,x_2) = \begin{cases} (2\gamma_m, 1-\gamma_m) & \text{if strongly-interacting} \\ (\gamma_m, 2-\gamma_m) & \text{if non-interacting.} \end{cases}$$

By defining

$$O_P = f^{\sigma}(\sum_k \omega_k \hat{x}_k + b), \tag{3.35}$$

where $f^{\sigma}(x) = e^x$, $\sum_k \omega_k \hat{x}_k$ is the weighted sum of the inputs, that are defined to be $\hat{x} = \log x$ and the bias is given by b. O_P can be recognized to be the output of a perceptron, which is the simplest neural network, as being composed by one single neuron (see 1.3). This is termed a logarithmic perceptron and it was used in the past for industrial applications [66]. It is important to notice that a brute force MLP could always yield an equally accurate result, but it would require a large hidden layer of many perceptrons. In contrast this model needs only one neuron. The computational burden has been reduced to a three parameter model to be fitted by the logarithm of the original input data.

The logarithmic perceptron has been trained using the mean square error loss function and the Adam optimizer with a learning rate of 10^{-3}. The bias has been initialized to 0 and a norm-2 bias regularizer with a coefficient of 10 has been introduced in order to highly penalize any value of the bias different from zero. The average parameters of 20 training sessions, computed both for the interacting and for the non interacting case are reported in table 3.2. As expected, the machine has learned that the bias is negligible[5] with respect to the ω-parameters, that have been estimated to be $\omega \simeq 0.5$. While for the non-interacting case the result is exact, being the non-interacting condition exactly reproducible, the strongly interacting case only approximately matches the infinitely interacting case, since the limit has not been fully reached.

	ω_1	ω_2	b
γ^0	0.5000 ± 0.0009	0.5001 ± 0.0004	$(2.0 \pm 0.4)10^{-6}$
γ^∞	0.480 ± 0.007	0.480 ± 0.004	$(-0.4 \pm 2.0)10^{-4}$

Table 3.2: Result of the fitting procedure using the logarithmic perceptron as an average over 20 example training sessions, along with the corresponding uncertainty. The uncertainty has been computed as the maximum distance from the mean value.

As a final remark, it is to be noticed that in principle there is no difference in the way the input values have to be presented to the machine since the new function is symmetric in them. However, we noticed that the fitting process benefits in convergence to the correct result from a pre-shuffling of the inputs. In the non-interacting case this corresponds to take $(x_1, x_2) = (\gamma_{1,1}, \gamma_{2,2})$ rather than the formula defined in terms of γ_m.

3.5 Using the logarithmic perceptron as a building block for more complex architectures.

As we mentioned in our paper [24], the *logarithmic perceptron* is engineered to optimally describe the relationship existing between the variables. For this reason it is a candidate building block to construct neural network models for finding the desired functionals when more than two grid-points are concerned. The idea is that it could be possible to take advantage of the capability of this perceptron to introduce the correct non-linearity. Just to mention a preliminary

[5] $b = o(\omega)$ since it is smaller than the precision with which the value of ω is known.

result at the basis of this statement, let us consider the off-diagonal element $\gamma_{3,5}$ of a $N_g = 20$ grid-points system. The density values were substituted with their logarithm and they were feeded to a perceptron with 20 inputs and one output. The logarithmic perceptron with 20 inputs was compared with a simple perceptron with no additional information and having as activation function the hyperbolic tangent, the sigmoid and the linear function. In Fig. 3.7 it is possible to see the boxed plot resulting from performing the training five times, in order to compare the results in a meaningful way. From this plot it is possible to evince that indeed, the logarithmic perceptron dominates many other perceptrons in learning features.

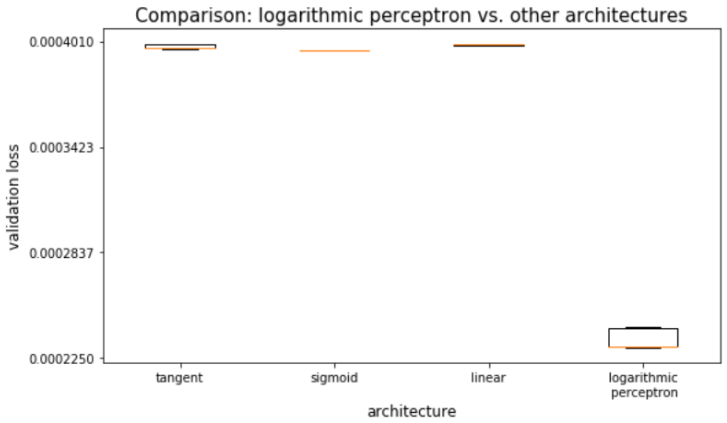

Figure 3.7: Comparison of the logarithmic perceptron with other perceptrons in estimating the value of an off-diagonal entry of the matrix.

3.6 Summary

Summarizing, in this chapter were reported the main results I obtained for the HD. Firstly I derived some information on the 1-RDM from the exact diagonalization of the Hamiltonian. Then, after having obtained the analytical behavior for strongly interacting and non-interacting electrons, I have shown how the ML model can be optimally configured in an engineered minimally complex architecture. In this small system, this yields a network that is vastly simpler than a brute force MLP. The logarithmic perceptron is engineered to optimally describe the relationship between the variables and is thus a candidate building block to construct NN models for finding the desired functionals when more than two grid-points are concerned. This is because it could be possible to take advantage of the capability of this perceptron to introduce the correct non-linearity, while possibly allowing to physically interpret the final architecture as a nested combination of HD for modelling systems with a higher number of grid-points [66]. In chapter 5 I will work on this intuition in order to define HD-based functionals.
Finally, the results obtained in this section could be used for creating dedicated hardware to speed-up calculations. Neural networks are currently implemented in hardware, for instance on Field Programmable Gate Arrays (FPGA). This allows to create dedicated hardware able to efficiently perform the calculations of the implemented NN. If one were able to construct a theory using the HD as an *auxiliary system*, the needed calculations would probably benefit from the fact that we managed to optimize the architecture to its most compact possible form.

Chapter 4

Hubbard Dimer: Beyond the limiting cases

In the present chapter I continue the study of the Hubbard Dimer with the goal of obtaining the density functional for the one-body reduced density matrix (1-RDM). So far we have only considered the limiting cases, in which the interaction strength between the two electrons is either zero or extremely high. By contrast, we will now move to considering the intermediate values of the interaction. First it will be discussed a possible approach that would express the functional as parametrically dependent on the double occupancy parameter, introduced in the previous chapters. Nevertheless, this approach would require a good way to approximate the quantity on which it depends parametrically. Therefore, a different approach will be attempted. The starting point will be to write the functionals associated to the limiting cases in terms of the minimum value of the density. This will allow to obtain simpler expressions, presenting an analogous functional form. Starting from this observation I will then introduce and discuss an analytical approximation to the exact functional. Finally, I will optimize a multilayer perceptron (MLP) to determine the numerical correction to the proposed approximation.

4.1 Double occupancy parametric approach

Once derived eq.3.26, the variational minimization has been completed. For this reason, we decided to use this formula for extracting the desired functional in non-limiting values of the interaction strength. Let us start by defining some quantities

$$\begin{cases} \Delta \doteq \gamma_{1,1} - 2\omega_1 \\ \eta \doteq \sqrt{(\gamma^o_{2,1})^2 - \gamma^2_{2,1}} \rightarrow \gamma_{2,1} = \sqrt{\gamma_{1,1}(2-\gamma_{1,1}) - \eta^2} \end{cases}$$

With these definitions, eq.3.26 can be rewritten as follows[1]:

$$\begin{aligned}
\omega_1 - \frac{\gamma_{1,1}}{2} &= \frac{-\gamma_{2,1}^2}{4\left(1-\sqrt{(\gamma_{2,1}^o)^2-\gamma_{2,1}^2}\right)} \\
2(\gamma_{1,1}-2\omega_1) &= \frac{-\gamma_{2,1}^2}{\sqrt{(\gamma_{2,1}^o)^2-\gamma_{2,1}^2}-1} \\
2\Delta &= \frac{-(\gamma_{2,1}^o)^2+(\gamma_{2,1}^o)^2-\gamma_{2,1}^2}{\sqrt{(\gamma_{2,1}^o)^2-\gamma_{2,1}^2}-1} \\
2\Delta &= \frac{\eta^2-(\gamma_{2,1}^o)^2}{\eta-1} \\
2\Delta(\eta-1) &= \eta^2-(\gamma_{2,1}^o)^2 \\
\eta^2-2\Delta\eta+2\Delta-(\gamma_{2,1}^o)^2 &= 0
\end{aligned}$$

so

$$\begin{aligned}
\eta &= \Delta \pm \sqrt{\Delta^2-2\Delta+1-1+2\gamma_{1,1}-\gamma_{1,1}^2} \\
&= \Delta \pm \sqrt{(\Delta-1-\gamma_{1,1}+1)(\Delta-1+\gamma_{1,1}-1)} \\
&= \Delta \pm \sqrt{4\omega_1(\omega_1+1-\gamma_{1,1})}
\end{aligned}$$

yielding

$$\gamma_{2,1} = \sqrt{(\gamma_{2,1}^o)^2-\eta^2} = \sqrt{\gamma_{1,1}(2-\gamma_{1,1}) - \left[(\gamma_{1,1}-2\omega_1) \pm \sqrt{4\omega_1(\omega_1+1-\gamma_{1,1})}\right]^2}$$

Let us check the validity of this equation while determining the correct sign to be used. According to [56], for instance, ω_1^o is in general $\omega_1^o = \gamma_{1,1,\uparrow}\gamma_{1,1,\downarrow} = \gamma_{1,1}^2/4$.
Substituting this value in the last formula and checking the consistency

$$\gamma_{2,1}^o \stackrel{?}{=} \sqrt{(\gamma_{2,1}^o)^2-\eta^2}$$

This is true if and only if $\eta(\omega_1^o = \gamma_{1,1}^2/4) = 0$.

$$\begin{aligned}
0 = \eta &= \left(\gamma_{1,1} - 2\frac{\gamma_{1,1}^2}{4}\right) \pm \sqrt{4\frac{\gamma_{1,1}^2}{4}\left(\frac{\gamma_{1,1}^2}{4}+1-\gamma_{1,1}\right)} \\
&= \frac{1}{2}\gamma_{1,1}(2-\gamma_{1,1}) \pm \frac{1}{2}\gamma_{1,1}(2-\gamma_{1,1})
\end{aligned}$$

[1] Red terms subsequently cancel

So the consistency is obtained if and only if the sign in the formula for η is a minus, and one is left with the equation

$$\boxed{\gamma_{2,1} = \sqrt{\gamma_{1,1}(2-\gamma_{1,1}) - \left[(\gamma_{1,1}-2\omega_1) - \sqrt{4\omega_1(\omega_1+1-\gamma_{1,1})}\right]^2}} \tag{4.1}$$

A further consistency check can be done on the strongly interacting case, for which, always according to [56], $\omega_1^\infty = max\{\gamma_{1,1}-1,\ 0\}$ that as expected, for $\gamma_{1,1} \geq 1$ is

$$\begin{aligned}\gamma_{2,1}^\infty &= \sqrt{\gamma_{1,1}(2-\gamma_{1,1}) - \left[(\gamma_{1,1}-2\gamma_{1,1}+2) - 2\sqrt{(\gamma_{1,1}-1)(\gamma_{1,1}-1+1-\gamma_{1,1})}\right]^2} \\ &= \sqrt{2(2-\gamma_{1,1})(\gamma_{1,1}-1)}\end{aligned}$$

and, analogously, for $\gamma_{1,1} < 1$

$$\begin{aligned}\gamma_{2,1}^\infty &= \sqrt{\gamma_{1,1}(2-\gamma_{1,1}) - \gamma_{1,1}^2} \\ &= \sqrt{2\gamma_{1,1}(1-\gamma_{1,1})}\end{aligned}$$

Remark Up to this moment we have assumed to have the 1-RDM at hand. By contrast, the only quantity we can work with is the density. Despite this limitation, at this point, a formula linking the off-diagonal terms to the diagonal has been derived. Being able to find a good approximation of it, it could be possible to have directly the functional. Hence, in the Hubbard Dimer problem, finding the functional for the 1-RDM corresponds exactly to the problem of finding the minimal functional of the average double occupation number. The problem corresponds, for this reason, to the problem of finding the best possible approximation of the double occupancy ω_1, i.e. the problem of finding a way to approximate

$$\omega_1[\gamma_{1,1}, \gamma_{2,2}] = \langle \Psi[\gamma] | \hat{n}_{1,\uparrow}\hat{n}_{1,\downarrow} | \Psi[\gamma] \rangle$$

which is the parameter describing the physics of the many-body interaction.
Finding a reasonable approximation of this value would automatically lead to a reasonable approximation for the off-diagonal terms of the 1-RDM. Consequently, it would automatically be possible to compute the kinetic contribution, the local potential contribution and the interaction-energy contribution (this last term directly from the value of ω_1). Nonetheless, rather than proceeding in this direction, the problem will be now formulated in terms of the interaction strength. The basic idea is the same but the following approach will be more directly applicable.

4.2 Interaction strength parametric approach

Let us summarize what it has been found so far for going further:

- From the exact diagonalization the parametric expression for the value of the functional $\gamma_{2,1}[\gamma_{1,1}=1;u]$ is known (eq.3.17), where u is the interaction strength parameter;

- From the limiting cases in the context of Lattice Density matrix functional theory one has the exact parametrization of the functional $\gamma^{o}_{2,1}$ (eq.A.4) and $\gamma^{\infty}_{2,1}$ (eq.A.8)

The purpose of this section is to find a parametric representation of the functional for all of the values of the interaction strength between the limiting cases, yielding the functional in the whole v-representability domain. In order to do that, let us express the functional previously derived in terms of the density of the minor carriers $\gamma_m \doteq min\{\gamma_{1,1},\ 2-\gamma_{1,1}\}$. This is the natural variable of the functions previously introduced, since

$$\gamma^{o}_{2,1}(\gamma_m) = \sqrt{2\gamma_m - 1\gamma_m^2} \tag{4.2}$$

$$\gamma^{\infty}_{2,1}(\gamma_m) = \sqrt{2\gamma_m - 2\gamma_m^2} \tag{4.3}$$

In order to obtain a parametrization in the whole range of the interaction strengths, the ansatz I did corresponds to assuming that a general parametrization exists in the form

$$\gamma_{2,1}[\gamma_m;u] \doteq \sqrt{2\gamma_m - \chi(\gamma_m,u)\gamma_m^2} \tag{4.4}$$

and it must be necessarily true that

$$\begin{cases} \chi(\gamma_m = 1, u = 0) = 1 \\ \chi(\gamma_m = 1, u \to \infty) = 2 \end{cases}$$

The exact expression of $\gamma_{2,1}[\gamma_{1,1} = 1;u] = \gamma_{2,1}[\gamma_m = 1;u]$ was derived in chapter 3 and, consequently, the exact form of $\chi(\gamma_{1,1} = 1,u)$ is known. In fact, by imposing the functional to be correct in the symmetric point $\gamma_m = 1$:

$$\begin{aligned} \gamma_{2,1}[1;u] = \sqrt{2-\chi(1,u)} &\overset{\downarrow}{=} -\frac{u-\sqrt{u^2+1}}{1+u(u-\sqrt{u^2+1})} \\ \to \chi(1,u) &= 2-\gamma_{2,1}(1;u)^2 \\ \to \chi(1,u) &= 2-\left(\frac{u-\sqrt{u^2+1}}{1+u(u-\sqrt{u^2+1})}\right)^2 \end{aligned}$$

Both these versions are extremely useful. Nothing obvious can be said about the γ_m dependence of the function χ but it is always possible to write it as the sum of two terms:

$$\begin{aligned} \chi(\gamma_m,u) &= \chi(\gamma_m = 1,u) + \Delta\chi(\gamma_m,u) \\ &= \chi^{(0)}(u) + \Delta\chi(\gamma_m,u) \end{aligned}$$

and the following functional constraints must be necessarily true

$$\begin{cases} \Delta\chi(\gamma_m = 1,u) = 0 \\ \Delta\chi(\gamma_m,u = 0) = 0 \\ \Delta\chi(\gamma_m,u \to \infty) = 0 \end{cases}$$

The first constraint is valid by definition whatever u in the symmetry point $\gamma_m = 1$. On the other hand the second and the third constraints are due to the fact that $\chi^{(0)}(u = 0) = 1$ and

$\chi^{(0)}(u \to \infty) = 2$. As it must be true on the whole $\gamma_{1,1}$-domain, no correction is needed. While the first term is known, the second is still to be determined.
As a first thing, it is important to determine what is the relevance of the correction to be added to the zero order approximation, which accounts to assume that $\Delta\chi(\gamma_{1,1},u) = 0 \ \forall u, \gamma_{1,1}$. This results in the zero order functional

$$\gamma_{2,1}^{(0)}[\gamma_{1,1};u] = \sqrt{2\gamma_m(1-\gamma_m) + \gamma_{2,1}(1,u)^2\gamma_m^2} \tag{4.5}$$

$$= \sqrt{2\gamma_m(1-\gamma_m) + \left(\frac{u-\sqrt{u^2+1}}{1+u(u-\sqrt{u^2+1})}\right)^2 \gamma_{1,1}^2} \tag{4.6}$$

The 0-order approximation is not expected to be too far from the reality. In fact, we expect that the functionals do not cross in the v-representability domain since to each interaction physics described by the u-parameter must correspond one and only one functional, at least for the simple Hubbard Dimer. By considering that the one-to-one mapping that would be guaranteed by the 0-order approximation must be preserved and that at the borders of the v-representability domain and on the symmetry line the correction must be zero, we expect the correction to be a perturbation. However, in order to confirm this hypothesis and to improve the model, it is necessary to introduce the numerical data and to verify the correctness of the assumption.

4.2.1 Comparison of the exact one-body reduced density matrix with the zero order approximation

Having at hands this model, it is now necessary to check how good it is in describing numerical data. For this reason we generated 30 ensembles of 20000 1-RDMs. Each ensemble is characterized by a different interaction strength (u_{iDEA}), which is a system parameter of the `iDEA` code having the same meaning as the interaction strength parameter u introduced with the Hamiltonian, but having a different range of values. While for both the parameters, being zero correspond to the non-interacting case, the strongly interacting case is reached by the textttiDEA code at $u_{iDEA} = 1$. This is at odd with the theoretical result that, by looking at Fig.3.2, can be noticed to identify the entering of the system in this regime starting from values of u of the order of the tenths.

The proposed procedure for fitting the data-points with the model at hands is the following. Starting from equation 4.5 written as

$$\gamma_{2,1}[\gamma_{1,1};u] = \sqrt{2min\{\gamma_{1,1},2-\gamma_{1,1}\}|1-\gamma_{1,1}| + (\gamma_{2,1}[\gamma_{1,1}=1;u])^2 min\{\gamma_{1,1},2-\gamma_{1,1}\})^2} \tag{4.7}$$

the relationship between the interaction strength of the Hubbard Dimer (u) and the interaction strength of the `iDEA` code (u_{iDEA}) is first ignored for fitting the numerical data with the model. Later this information is used for determining the relationship between the two parameters. In fact, the only u-dependence of the functional is encoded in the dependence of $\gamma_{2,1}[\gamma_{1,1}=1;u]$ on it. However, to each ensemble generated with some u_{iDEA} must correspond a specific value of u and the value of $\gamma_{2,1}[\gamma_{1,1}=1;u(u_{iDEA})]$ can be obtained by interpolating the numerical values $\gamma_{2,1}^{exp}$ and by extracting the intersection with the symmetry line. In Fig.4.1 are presented the numerical points of six density matrix ensembles.

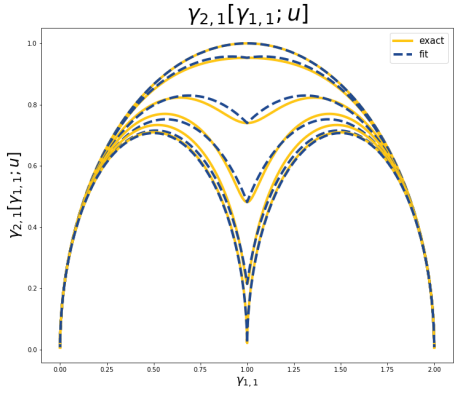

Figure 4.1: Comparison of the zero order model with the exact 1-RDM for different values of the interaction strength.

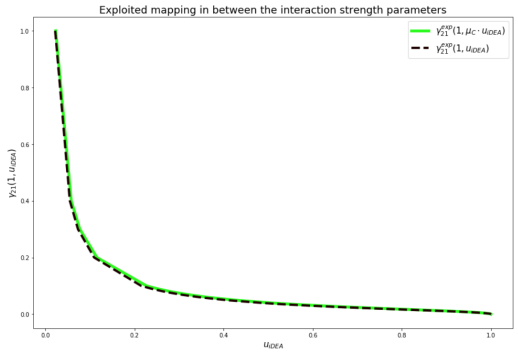

Figure 4.2: Graphical representation of the one-to-one correspondence of the theoretical interaction strength with the corresponding parameter in the `iDEA` code.

This showed that the 0-order model is already quite accurate and that the correction is indeed a perturbation of it (see figure 4.1). However, in order to make the model numerically exact, we then moved to fit the correction, that can be obtained as

$$\Delta\chi(\gamma_{1,1},u) = \chi^{exp}(\gamma_{1,1},u(u_{iDEA})) - \chi^{(0)}(u)$$

However, an essential step before to do that is to understand the link between the interaction strengths. Since the functional relation between $\gamma_{2,1}(1,u)$ and $\gamma_{2,1}^{exp}(1,u_{iDEA})$ is known, all one has to do is to compare the functions $u(\gamma_{2,1}(\gamma_{1,1}=1))$ and $u_{iDEA}(\gamma_{2,1}^{exp}(\gamma_{1,1}=1))$. In Fig.4.2 the mapping is shown and the final purpose is to determine the scaling factor $u = \mu_C \cdot u_{iDEA}$. Using the formula

$$\mu_C = \frac{1}{N}\sum_{\gamma_{2,1}\in\Gamma_{2,1}} \frac{u(\gamma_{2,1})}{u_{iDEA}(\gamma_{2,1})}$$

the factor is found to be $\mu_C \simeq 42.94$, where the accuracy is of the order of $1e-14$ as a witness of the exact correspondence.

Analysis of the correction

Having connected the numerical data with the theoretical one, it is now possible to try to improve the model. The idea is the following: As a first thing, whatever value of the interaction strength considered, when adding the correction, eq.4.7 becomes

$$\gamma_{2,1}[\gamma_{1,1};u] = \sqrt{2\gamma_m(1-\gamma_m) + \gamma_{2,1}[\gamma_{1,1}=1,u]^2\gamma_m^2 - \Delta\chi(\gamma_m,u)\gamma_m^2} \tag{4.8}$$

Where, as always, $\gamma_m \doteq min\{\gamma_{1,1},\ 2-\gamma_{1,1}\}$ is the natural variable containing the information of the symmetries of the system. By inverting 4.8, one can obtain an explicit formula for the correction,

$$\Delta\chi(\gamma_{1,1},u)\gamma_m^2 = 2\gamma_m(1-\gamma_m^2) - \gamma_{2,1}^2 + \gamma_{2,1}(1,u)^2\gamma_m^2 \tag{4.9}$$

Given a data-set, all of the terms on the right hand side of the equation are known and one can obtain the numerical behavior of the correction to be determined.

In Fig.4.3 the specific correction of the $u_{iDEA} = 0.02$ data-set has been plotted in terms of the minority variable γ_m. All of the corrections present the same functional characteristics: from the boundary to the symmetry point the function first reaches a minimum, below zero, then reaches a maximum and finally goes back to zero. This amounts to say that the correction is a function defined on the 2D square

$$(\gamma_m, u_{iDEA}) \in [0,1] \times [0,1]$$

and on this domain the function varies but preserving the same features. Among the differ-

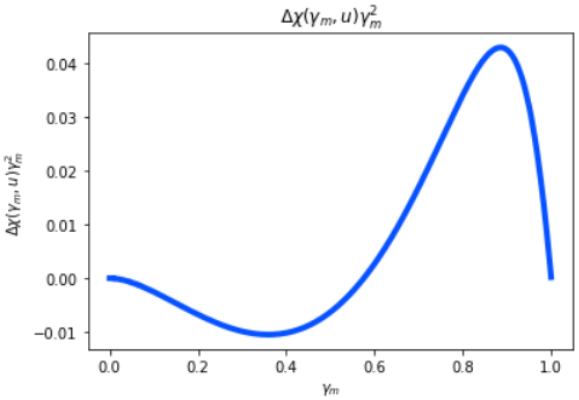

Figure 4.3: Behavior of the correction for the dataset $u_{iDEA} = 0.02$. Function expressed in terms of the variable $\gamma_m = min(\gamma_{1,1}, \gamma_{2,2})$.

ent kinds of fitting procedures one could employ the chosen one has been a fully connected neural network. With this purpose in mind, a data-set containing all of the 600000 couples $(10\gamma_m, 10u_{iDEA})$ previously generated points has been created. The corresponding computed values of $10\Delta\chi(\gamma_m, u_{iDEA})\gamma_m^2$ have been used as labels to be learned in the regression procedure. As commonly done the data-set has been shuffled and divided into a training subset, containing the 80% of the original data and a test subset containing the 20%. The factor 10 has been introduced for assuring to handle data not too small, so that the activation functions can work out from the linear regime and can actually introduce the non-linearity.

Once prepared the data-set, some attempts have been done for determining the easiest architecture yielding a satisfying approximation. A three hidden layer multilayer perceptron (MLP) with an hyperbolic tangent activation function has been found to perform well when using the mean square error as a cost function and training the model for 10 epochs with the Adam optimizer characterized by a learning-rate $lr = 1e-3$. The use of the hyperbolic tangent has been chosen for its capability of reaching negative values.

Chosen the architecture, a grid search has been performed for finding the best combinations of the numbers of neurons in the three layers, in terms of the value of the loss function. The result of the process can be seen in Fig.4.4, in which only the best combinations have not been blacked out.

The best ten architectures have been further compared in terms of the capability of fitting the corrections and the winning network has been found to be the $(12,12,16)$.

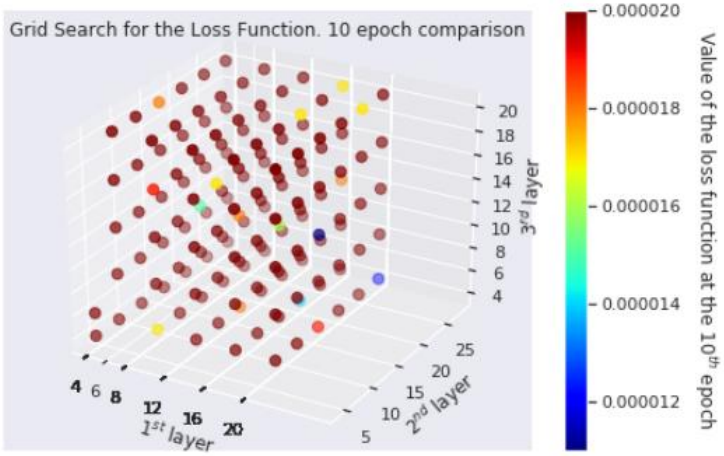

Figure 4.4: Grid Search on the number of neurons in the three hidden layer: Dark red indicates a too high value of the loss function while lighter colors identify candidate models for the fitting.

A schematic representation of the chosen architecture can be observed Fig.4.5

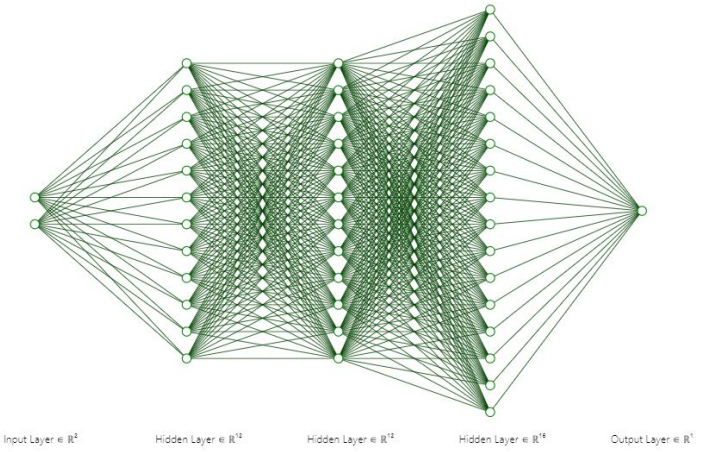

Figure 4.5: Schematic representation of the chosen architecture. A MLP receiving the values of the density as inputs and returning the value of the correction at the output. Three hidden layers appear in the network and the number of neurons appearing in them is, respectively, 12, 12 and 16.

Once trained, by feeding this architecture with $(10\gamma_m, 10u_{iDEA})$ one obtains an estimate of $10\Delta\chi(\gamma_m, u_{iDEA})\gamma_m^2$. In order to impose that whatever estimate meets the constraints previously written, the output of the model is further multiplied by two functions:

$$\begin{cases} (1-e^{-(1-\gamma_m)/0.001}) \\ (1-e^{-u_{iDEA}/0.004}) \end{cases} \tag{4.10}$$

The first function allows to impose, in an analytical way, the vanishing of the approximation at the symmetry point. The second, analogously, forces the correction to be zero when the interaction strength is zero. Forcing these two constraints allows to reduce the complexity of the network being these constraints two of the most difficult things to be learned by the MLP.

By indicating the prediction of the network as $MLP(\gamma_m, u_{iDEA})$, the final approximation can be obtained as

$$\Delta\chi(\gamma_m, u_{iDEA})\gamma_m^2 \simeq \frac{MLP(10\gamma_m, 10u_{iDEA})}{10}(1-e^{-(1-\gamma_m)/0.001})(1-e^{-u_{iDEA}/0.004}) \tag{4.11}$$

In Fig.4.8 the fit of the correction done using this method can be observed. Some of the results may seem disturbing but they are the ones having the smallest amplitude. By further increasing the complexity of the network it would be possible to overcome this deviations but the approximation can be considered acceptable.

This approximation, can now be inserted in 4.8, and the accuracy of the approximation can be checked by comparing the 0-order χ-model (Fig.5.1) with the χ-model with NN-computed correction (Fig.4.7)

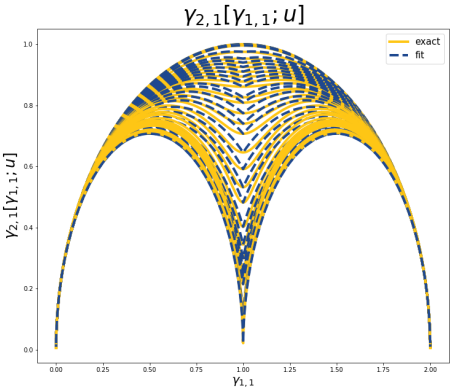

Figure 4.6: Comparison of the zero order model with the exact 1-RDM for different values of the interaction strength. In yellow the exact value and in blue the χ-model functional.

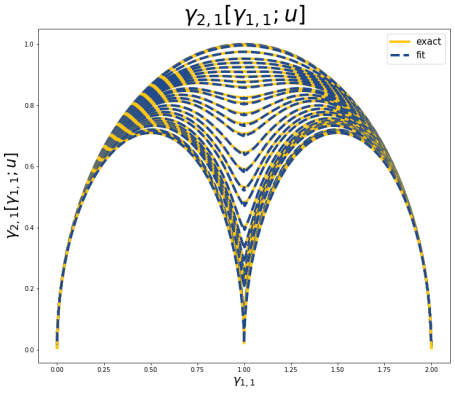

Figure 4.7: χ-model with NN-computed correction for different values of the interaction strength. In yellow the exact value and in blue the χ-model functional.

4.3 Summary

This chapter concluded the characterization of the Hubbard Dimer (HD) model. The main result here obtained was the finding of an analytical approximation to the exact functional, augmented using machine learning techniques. The gained accuracy was extremely satisfying, allowing to dispose of a numerically exact *auxiliary system* uniquely defined by two parameters: the interaction strength and the minimum of the density. The main reason why this finding was considered important was because it allowed to have a numerically exact model in which an extremely small part was blindly learned by the machine. Moreover, the HD can be considered as the physical building block of the Fermi-Hubbard model. Therefore, it is intuitively reasonable that a theory using the HD also as a theoretical building block may be obtainable. Also, given that the Fermi-Hubbard model is widely used for modeling real systems, if one were able to formalize such a theory it would be possible to obtain the 1-RDM of the exact system using the HD as the auxiliary system. For this reason, the disposal of the HD model with an additional

degree of freedom may be useful at a certain point of this mapping. In the following chapters a step forward in the idea of using the HD as an auxiliary system will be done.
Finally, a side comment deserves to be done. The representation of the functionals associated to the two limiting cases and the exact diagonalization at the symmetry point were at the basis of the intuition for the proposal of the functional. Both these results originated from the attempt of finding the most informative variables to present to the machine. Hence, it may be possible to say that the well defined question of finding the best way to structure the machine for learning limiting cases allowed to gain the necessary information for going beyond them.

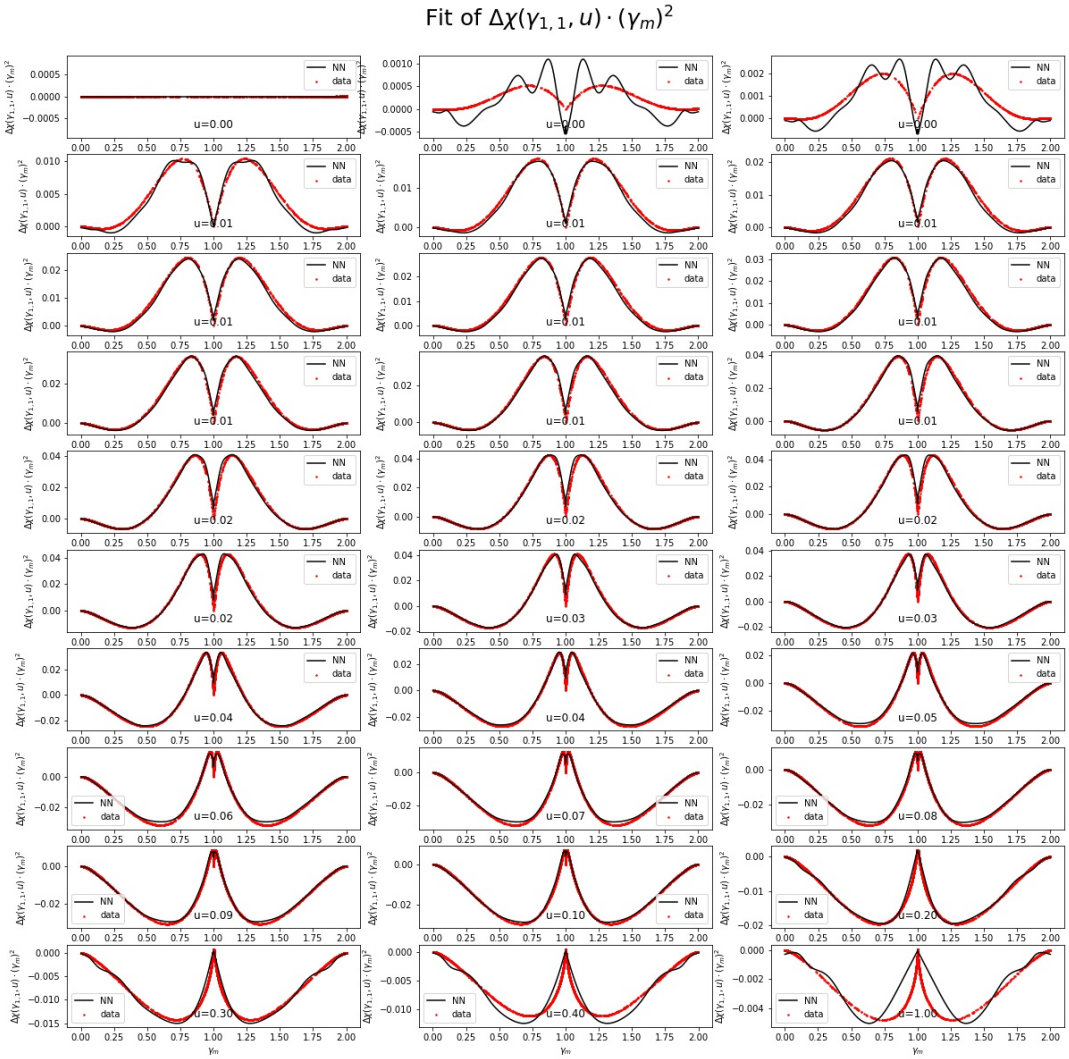

Figure 4.8: Fit of the Correction using ML. Each plot is a different value of the interaction strength. It is worth remarking that the amplitude of the first three and the last two corrections is so small that the deviation of the fit from the exact form does not compromise significantly the accuracy of the final fit.

Chapter 5

Hubbard Trimer from the Hubbard Dimer

After having found the density functional in the Hubbard Dimer (HD), I will now consider its potential applicability for finding the density functional of the one-body reduced density matrix (1-RDM) in the three-site Fermi-Hubbard model, namely the Hubbard Trimer (HT). The idea is to use, for each off-diagonal entry of the 1-RDM of the HT, a different Hubbard Dimer as an auxiliary system, whose parameters can be adjusted, in principle exactly, to obtain the searched element. Following this idea, I will propose and examine two methods for finding the functional: the "forward approach" and the "inverse approach". I will motivate why the latter should be the preferred route to follow and I will discuss results obtained along this line.

5.1 3-Points system: Two approaches

Let us introduce a 3-sites model. The goal is to find the functional relationship between the 1-RDM $\hat{\gamma}^{(3)}$ and its diagonal, the density n.
Starting from the physical description of the system, the potential is sampled at the borders and at 3 equally spaced points $X^{(3)} = \{0, x_1, x_2, x_3, L\}$. Thanks to the confining nature of the potential, the boundaries are not accessible and only the three inner sites can be populated by the two electrons.
The space is less strongly quantized than before but the distance between the sites is still such that the Hubbard model can be supposed to be, in first approximation, a good model for the system. The Hamiltonian then becomes

$$\hat{H}^{(3)} = -t \sum_{\langle i,j \rangle} \sum_{\sigma} \hat{c}^{\dagger}_{i,\sigma} \hat{c}_{j,\sigma} + U \sum_{i} \hat{n}_{i,\uparrow} \hat{n}_{i,\downarrow} + \sum_{i} v_i \hat{n}_i \tag{5.1}$$

As commonly done, the two electrons are chosen to be 'opposite' in terms of spin, which is the `iDEA` jargon for anti-symmetric spin part and symmetric spacial one. For the 2-electron system, this implies a total spin equal to zero $S = 0$ and the ground state belongs to a subspace of the 9-dimensional Hilbert space, corresponding to the singlet subspace.
A good basis for the whole Hilbert space is the following:

$$\mathscr{B}_3 = \{|1\uparrow 1\downarrow\rangle, |1\uparrow 2\downarrow\rangle, |1\uparrow 3\downarrow\rangle, |1\downarrow 2\uparrow\rangle, |1\downarrow 3\uparrow\rangle, |2\uparrow 2\downarrow\rangle, |2\uparrow 3\downarrow\rangle, |2\downarrow 3\uparrow\rangle, |3\downarrow 3\uparrow\rangle\}$$

and, starting from this, it is possible to build a basis for the singlet subspace, as it was done in Chapter 3

$$\mathscr{B}_{singlet} = \begin{cases} |\varphi_1\rangle = |1\uparrow 1\downarrow\rangle \\ |\varphi_2\rangle = \frac{1}{\sqrt{2}}(|1\uparrow 2\downarrow\rangle - |1\downarrow 2\uparrow\rangle) \\ |\varphi_3\rangle = |2\uparrow 2\downarrow\rangle \\ |\varphi_4\rangle = \frac{1}{\sqrt{2}}(|1\uparrow 3\downarrow\rangle - |1\downarrow 3\uparrow\rangle) \\ |\varphi_5\rangle = \frac{1}{\sqrt{2}}(|2\uparrow 3\downarrow\rangle - |2\downarrow 3\uparrow\rangle) \\ |\varphi_6\rangle = |3\uparrow 3\downarrow\rangle \end{cases} \qquad \mathscr{B}_{triplet} = \begin{cases} |\varphi_7\rangle = \frac{1}{\sqrt{2}}(|1\uparrow 2\downarrow\rangle + |1\downarrow 2\uparrow\rangle) \\ |\varphi_8\rangle = \frac{1}{\sqrt{2}}(|1\uparrow 3\downarrow\rangle + |1\downarrow 3\uparrow\rangle) \\ |\varphi_9\rangle = \frac{1}{\sqrt{2}}(|2\uparrow 3\downarrow\rangle + |2\downarrow 3\uparrow\rangle) \end{cases}$$

Among these we are only interested in the span $\mathscr{L}(\mathscr{B}_{singlet})$, and the most general ground state vector in the 3-sites problem reads

$$|\Psi\rangle = \sum_{i=1}^{6} a_i |\varphi_i\rangle$$

where $\sum_{i=1}^{6} a_i^2 = 1$.
This having been done we have a parametric representation of the ground state vector. Using the definition of the 1-RDM terms, it is finally possible to obtain the following systems

$$\begin{cases} \gamma_{1,1} = 2a_1^2 + a_2^2 + a_4^2 \\ \gamma_{2,2} = 2a_2^2 + a_2^2 + a_5^2 \\ \gamma_{3,3} = 2a_6^2 + a_4^2 + a_3^2 \\ \gamma_{1,1} + \gamma_{2,2} + \gamma_{3,3} = 2 \end{cases} \iff \begin{cases} \gamma_{2,1} = \sqrt{2}a_2(a_1 + a_3) + a_4 a_5 \\ \gamma_{3,1} = \sqrt{2}a_4(a_1 + a_6) + a_2 a_5 \\ \gamma_{3,2} = \sqrt{2}a_5(a_3 + a_6) + a_2 a_4 \end{cases}$$

where, as expected, $\sum_{i=1}^{3} \gamma_{i,i} = 2$
These two systems contain the very heart of the Hubbard Trimer problem. On the left there are the known variables, namely the density components, and the equations connecting them to the six parameters introduced in the description. On the other hand, the right system contains the relationship between the unknowns and the six projections. Being able to solve exactly the system on the left, possibly introducing some additional information, would correspond to parametrize the ground-state vector in terms of the ground-state density ($\{a_i(n)\}_{i=1}^{6}$) and consequently solving also the system on the right. If no such information can be introduced, the existing relations can still be used for estimating the values of the unknowns given the information on the left.
The double arrow indicates the existence of two possible approaches that I will follow in this chapter. They will be named the *forward* and the *inverse* approaches.

5.2 The forward approach

The rightward pointing arrow accounts for the forward approach in the problem of finding the functional of the 1-RDM in terms of the density. By using the Schrödinger equation, or other sources of additional information, it is possible to make the system on the left approximately solvable. The ideal result of this approach is the determination of the laws $\{a_i[n]\}_{i=1}^{6}$, to be substituted in the right system in order to obtain the desired functional $\hat{\gamma}[n]$. Choosing this

approach corresponds to look for a parametrization of the ground state in terms of the density and, afterwards, to use this new information for writing any observable as a functional of the density. In the following I will present a limiting case in which this procedure can be done exactly. Interestingly, it will be shown that it offers a reasonable description of at least the 35% of the 1-RDMs present in the `iDEA` data-set. In a second moment, using the variational approach, the coefficients will be parametrized in terms of the interaction strength and of the potential. What is missing is the functional $v[n]$, that would complete the description.

5.2.1 Flat potential and infinite repulsion

Let us start by analyzing the flat potential landscape, where

$$V(x_1) \simeq V(x_2) \simeq V(x_3)$$

when this is the case and the electrons are strongly repulsive there is no way the two electrons will populate together the x_2-site. By contrast, it will be much more likely that they will populate the two remaining sites. Indeed, they will attempt to lower the interaction energy as much as possible. Due to this tendency, the density in x_2 is almost zero in the strongly-interacting limit. Therefore, we can expect that the domain of applicability of the following reasonings could be further extended to the case in which sites x_1 and x_3 are equally likely probable, independently on the value of $V(x_2)$, i.e. the symmetric potential case. More precisely, this is expected to be true unless the value of $V(x_2)$ is so low to dominate over the electronic repulsion and forcing the two electrons to populate the central site with a finite probability
The amplitude of each coefficient a_i is linked to the probability of the two electrons to be in the state described by the basis vector $|\varphi_i\rangle$. For this reason, following the previous arguments, for strongly interacting electrons in the flat potential case (and approximately in the symmetric potential case), it is to be expected that $a_1 \simeq a_3 \simeq a_6 \simeq 0$ since any double occupancy is minimally probable in such a condition. The removal of 3-variables out of the 6 into play makes the system on the left exactly solvable:

$$\begin{cases} \gamma_{1,1} = a_2^2 + a_4^2 \\ \gamma_{2,2} = a_2^2 + a_5^2 \\ \gamma_{3,3} = a_4^2 + a_5^2 \end{cases} \qquad \begin{cases} \gamma_{2,1} = a_4 a_5 \\ \gamma_{3,1} = a_2 a_5 \\ \gamma_{3,2} = a_2 a_4 \end{cases}$$

As said before one must solve the left system

$$\begin{cases} \gamma_{1,1} - \gamma_{2,2} = a_4^2 - a_5^2 \\ \gamma_{3,3} - \gamma_{2,2} = a_4^2 - a_2^2 \\ \gamma_{2,2} = a_2^2 + a_5^2 \end{cases} \rightarrow \begin{cases} a_2 = \sqrt{|\gamma_{1,1} - \gamma_{3,3} + \gamma_{2,2}|/2} \\ a_4 = \sqrt{|\gamma_{1,1} + \gamma_{3,3} - \gamma_{2,2}|/2} \\ a_5 = \sqrt{|\gamma_{3,3} - \gamma_{1,1} + \gamma_{2,2}|/2} \end{cases}$$

And the right system becomes

$$\begin{cases} \gamma_{2,1} = \sqrt{|(\gamma_{1,1} + \gamma_{3,3} - \gamma_{2,2})||(\gamma_{3,3} - \gamma_{1,1} + \gamma_{2,2})|}/2 \\ \gamma_{3,1} = \sqrt{|(\gamma_{1,1} - \gamma_{3,3} + \gamma_{2,2})||(\gamma_{3,3} - \gamma_{1,1} + \gamma_{2,2})|}/2 \\ \gamma_{3,2} = \sqrt{|(\gamma_{1,1} - \gamma_{3,3} + \gamma_{2,2})||(\gamma_{1,1} + \gamma_{3,3} - \gamma_{2,2})|}/2 \end{cases}$$

These equations are in principle exact only for $\gamma_{1,1} = \gamma_{3,3} = 1$ and $\gamma_{2,2} = 0$ but, since it is almost impossible to have perfect symmetry, it is to be expected that they will be reasonably

good to approximate almost symmetric potentials. The absolute value has been introduced to take into account the deviations of $\gamma_{1,1}$ and $\gamma_{3,3}$ from the values for which the formula would be exact. This deviation, in fact, may yield a negative value under the square-root sign.
This example is relevant due to the fact that almost the 35% of the data-set satisfies this condition. In table 5.1 are reported the first three matrices satisfying the condition. The precision is almost the same for all of them.

$\gamma_{11} = 0.9998602634880824$	$\gamma_{33} = 0.9999077342997227$
$\gamma_{21} = 0.01181885741414091$	$\gamma_{21}^{th} = 0.011819648587740502$
$\gamma_{31} = 0.000541994445941969$	$\gamma_{31}^{th} = 0.00011354684991836512$
$\gamma_{32} = 0.009612817694872012$	$\gamma_{32}^{th} = 0.009604389331484973$
$\gamma_{11} = 0.9953922154053608$	$\gamma_{33} = 0.9998553741143202$
$\gamma_{21} = 0.06768260493274257$	$\gamma_{21}^{th} = 0.06771917387890024$
$\gamma_{31} = 0.004451632512504369$	$\gamma_{31}^{th} = 0.0008163362836613604$
$\gamma_{32} = 0.012532806150840178$	$\gamma_{32}^{th} = 0.011997439897957268$
$\gamma_{11} = 0.9999376793465036$	$\gamma_{33} = 0.9999007871574284$
$\gamma_{21} = 0.007903948077441018$	$\gamma_{21}^{th} = 0.007893705506502742$
$\gamma_{31} = 0.0004495049864955163$	$\gamma_{31}^{th} = 7.86321129329664e-05$
$\gamma_{32} = 0.009955702042411953$	$\gamma_{32}^{th} = 0.009959759855253707$

Table 5.1: The first three 1-RDMs satisfying the symmetry condition out of the 17614 1-RDMs alike. For each of them the first line shows the belonging of the 1-RDM to the flat/symmetric potential case while the remaining rows compare the accuracy of the formula previously introduced with the numerical value.

This is a very particular case since it is possible to obtain exactly solvable sets of equations. The general idea is to find a way to make the left system exactly solvable in the general case or, at least, an approximation of it.

5.2.2 Completing the system using the variational approach

The purpose of this subsection is to find the two missing equations from the variational approach. The Ground-state vector previously introduced

$$|\Psi\rangle = \sum_{i=1}^{6} a_i |\varphi_i\rangle$$

is exact because of the belonging of the ground-state to the singlet subspace. However, the coefficients are unknown and it is possible to think about the formula as a variational state vector, to be found. One can then introduce the functional

$$E[|\Psi\rangle] = \langle\Psi|\hat{H}|\Psi\rangle - \mu\langle\Psi|\Psi\rangle,$$

whose minimum is the ground state energy and the corresponding vector is the ground state vector. As a first thing, let us apply the Hamiltonian to the basis

$$\begin{cases} \hat{H}|\varphi_1\rangle = (U+2v_1)|\varphi_1\rangle - t\sqrt{2}|\varphi_2\rangle \\ \hat{H}|\varphi_2\rangle = (v_1+v_2)|\varphi_2\rangle - t\sqrt{2}|\varphi_1\rangle - t\sqrt{2}|\varphi_3\rangle - t|\varphi_4\rangle \\ \hat{H}|\varphi_3\rangle = (U+2v_2)|\varphi_3\rangle - t\sqrt{2}|\varphi_2\rangle - t\sqrt{2}|\varphi_5\rangle \\ \hat{H}|\varphi_4\rangle = (v_1+v_3)|\varphi_4\rangle - t|\varphi_5\rangle - t|\varphi_2\rangle \\ \hat{H}|\varphi_5\rangle = (v_2+v_3)|\varphi_5\rangle - t|\varphi_4\rangle - t\sqrt{2}|\varphi_6\rangle - t\sqrt{2}|\varphi_3\rangle \\ \hat{H}|\varphi_6\rangle = (U+2v_3)|\varphi_6\rangle - t\sqrt{2}|\varphi_5\rangle \end{cases}$$

Starting from this, the functional to be minimized becomes

$$\begin{aligned} E[\{a_i\}_{i=1}^6] = {} & a_1^2(U+2v_1) + a_3^2(U+2v_2) + a_6^2(U+2v_3) + \\ & + a_2^2(v_1+v_2) + a_4^2(v_1+v_3) + a_5^2(v_2+v_3) + \\ & - 2\sqrt{2}t(a_1a_2 + a_3a_2 + a_6a_5 + a_3a_5) - 2t(a_4a_5 + a_4a_2) + \\ & - \mu\sum_{i=1}^{6} a_i^2 \end{aligned}$$

And, forcing the gradient to vanish leads to

$$\begin{cases} \partial_{a_1}E = 2a_1(U+2v_1-\mu) - 2\sqrt{2}ta_2 \overset{\downarrow}{=} 0 \\ \partial_{a_2}E = 2a_2(v_1+v_2-\mu) - 2\sqrt{2}ta_1 - 2\sqrt{2}ta_3 - 2ta_4 \overset{\downarrow}{=} 0 \\ \partial_{a_3}E = 2a_3(U+2v_2-\mu) - 2\sqrt{2}ta_2 - 2\sqrt{2}ta_5 \overset{\downarrow}{=} 0 \\ \partial_{a_4}E = 2a_4(v_1+v_3-\mu) - 2ta_5 - 2ta_2 \overset{\downarrow}{=} 0 \\ \partial_{a_5}E = 2a_5(v_2+v_3-\mu) - 2\sqrt{2}ta_6 - 2\sqrt{2}ta_3 - 2ta_4 \overset{\downarrow}{=} 0 \\ \partial_{a_6}E = 2a_6(U+2v_3-\mu) - 2\sqrt{2}ta_5 \overset{\downarrow}{=} 0 \end{cases}$$

The full solution would yield the ground state details but all we are looking for are two equations to make the previously introduced system solvable. Among them, the first and the last ones express a very clearly readable information:

$$\begin{cases} a_2 = \frac{U+2v_1-\mu}{\sqrt{2}t}a_1 =: \Delta_1 a_1 \\ a_5 = \frac{U+2v_3-\mu}{\sqrt{2}t}a_6 =: \Delta_6 a_6 \end{cases}$$

From which the factor μ can be interpreted as a chemical potential, introducing a reference in the description.
These two equations express a proportionality relation between two probabilities. The first one states that the probability that the two electrons are one in x_1 and the other in x_2 (a_2^2) is proportional to the probability that both the electrons are in x_1. In formulas $a_2^2 \propto a_1^2$ and, analogously $a_5^2 \propto a_6^2$. The proportionality factors contain the value of the potential at the target site referred to the chemical potential μ. Once found two additional equations, it is now possible

to insert them in the system, that becomes

$$\begin{cases} \gamma_{1,1} = 2a_1^2 + a_2^2 + a_4^2 \\ \gamma_{2,2} = 2a_3^2 + a_2^2 + a_5^2 \\ \gamma_{3,3} = 2a_6^2 + a_4^2 + a_5^2 \\ \sum_{i=1}^{6} a_i^2 = 1 \\ a_2 = \Delta_1 a_1 \\ a_5 = \Delta_6 a_6 \end{cases} \rightarrow \begin{cases} \gamma_{1,1} = 2a_1^2 + \Delta_1^2 a_1^2 + a_4^2 \\ \gamma_{2,2} = 2a_3^2 + \Delta_1^2 a_1^2 + \Delta_6^2 a_6^2 \\ \gamma_{3,3} = 2a_6^2 + \Delta_6^2 a_6^2 + a_4^2 \\ a_4^2 = 1 - a_1^2(1+\Delta_1^2) - a_6^2(1+\Delta_6^2) - a_3^2 \end{cases}$$

that leads to three equations in three unknowns

$$\begin{cases} \gamma_{1,1} = 1 + a_1^2 - a_3^2 - a_6^2(1+\Delta_6^2) \\ \gamma_{2,2} = 2a_3^2 + \Delta_1^2 a_1^2 + \Delta_6^2 a_6^2 \\ \gamma_{3,3} = 1 + a_6^2 - a_3^2 - a_1^2(1+\Delta_1^2) \end{cases} \rightarrow \begin{cases} a_3^2 = (\gamma_{2,2} - \Delta_1^2 a_1^2 - \Delta_6^2 a_6^2)/2 \\ \gamma_{1,1} = 1 + a_1^2 - a_6^2(1+\Delta_6^2) - (\gamma_{2,2} - \Delta_1^2 a_1^2 - \Delta_6^2 a_6^2)/2 \\ \gamma_{3,3} = 1 + a_6^2 - a_1^2(1+\Delta_1^2) - (\gamma_{2,2} - \Delta_1^2 a_1^2 - \Delta_6^2 a_6^2)/2 \end{cases}$$

$$\begin{cases} \gamma_{l,l} := \gamma_{1,1} + \frac{\gamma_{2,2}}{2} = a_1^2(1+\frac{\Delta_1^2}{2}) - a_6^2(1+\frac{\Delta_6^2}{2}) + 1 \\ \gamma_{r,r} := \gamma_{3,3} + \frac{\gamma_{2,2}}{2} = a_6^2(1+\frac{\Delta_6^2}{2}) - a_1^2(1+\frac{\Delta_1^2}{2}) + 1 \end{cases} \rightarrow \boxed{a_6^2 = (\gamma_{l,l} - 1)\frac{2+\Delta_1^2}{2+\Delta_3^2} a_1^2 = \beta a_1^2}$$

finally

$$\begin{cases} a_1^2 = \dfrac{\gamma_{1,1} - \gamma_{3,3}}{2 + \Delta_1^2 - \beta(2+\Delta_6^2)} = \dfrac{\gamma_{1,1} - \gamma_{3,3}}{(2+\Delta_1^2)(2-\gamma_{l,l})} = \dfrac{\gamma_{1,1} - \gamma_{3,3}}{(2+\Delta_1^2)\gamma_{r,r}} \\ a_3^2 = \dfrac{\gamma_{2,2}}{2} - \dfrac{(\Delta_1^2 + \beta\Delta_6^2)a_1^2}{2} \\ a_6^2 = \beta a_1^2 = \dfrac{\gamma_{l,l} - 1}{\gamma_{r,r}} \dfrac{\gamma_{1,1} - \gamma_{3,3}}{2 + \Delta_6^2} \end{cases}$$

Now it turns out that, whatever μ,

$$\sum_{i=1}^{6} a_i^2 = a_1^2 + \frac{1}{2}[\gamma_{2,2} - (\Delta_1^2 - \beta\Delta_6^2)a_1^2] + \beta a_1^2 + (\Delta_1^2 + \beta\Delta_6^2)a_1^2 + 1 - a_1^2\left[1 + \frac{\Delta_1^2}{2} + \beta(1 + \frac{\Delta_6^2}{2})\right] = 1$$

Thanks to these equations the coefficients are known exactly as $a_i = a_i(\gamma_{1,1}, \gamma_{2,2}, \gamma_{3,3}, v_1, v_3)$. The missing information to make the functional purely dependent on the density is the knowledge of $v_i[\{\gamma_{j,j}\}_{j=1}^{3}]$

$$\begin{cases} a_1^2 = \frac{\gamma_{1,1} - \gamma_{3,3}}{(2+\Delta_1^2)\gamma_{r,r}} \\ a_2^2 = \Delta_1^2 a_1^2 \\ a_3^2 = (\gamma_{2,2} - \Delta_1^2 a_1^2 - \beta\Delta_6^2 a_1^2)/2 \\ a_4^2 = 1 - a_1^2[1 + \Delta_1^2/2 + \beta(1 + \Delta_6^2/2)] - \gamma_{2,2}/2 \\ a_5^2 = \beta\Delta_6^2 a_1^2 \\ a_6^2 = \beta a_1^2 \end{cases}$$

Remark: Let us consider the flat potential. As argued before $\gamma_{1,1}$ and $\gamma_{3,3}$ are expected to be almost equal to 1 and $\gamma_{2,2}$ is expected to be small. By substituting these values in the last equations it is possible to see how $a_1 \simeq a_3 \simeq 0$ and $a_2^2 \simeq \gamma_{2,2}/2 \simeq 0$ accordingly to the previous discussion. Previously, it has been shown how all of the a_i^2 can be written as proportional to a_1^2. However, the vanishing of this last factor does not imply the vanishing of all the others thanks to the presence in the proportionality factors of the interaction strength u, which tends to infinity. This fact allows to have $a_i \neq 0$ for $i = 4,5,6$.

Three states models are interesting per se. Nonetheless, the forward approach has not been investigated any further due to the bad scalability of the problem when increasing the number of states[1]. For this reason, the inverse approach is thought to be more promising.

5.3 The inverse approach

The leftward pointing arrow accounts for a more twisted approach, based on the introduction of three auxiliary systems. Starting from each single term on the right system, it is possible to work on the analytical formula and to legitimate the existence of a mapping for the coefficients into the corresponding coefficients of an Hubbard Dimer. In so doing it is possible to create a *connection* of some coefficients of the Hubbard Trimer with the coefficients a Hubbard Dimer. However, this is only a formal knowledge since neither group of coefficients has a known parametrization in terms of the density. The Hubbard Dimer is fully determined by the density and by the interaction strength. For this reason, once found the mapping, it is then possible to move to the left system to estimate the parameters of the newly defined auxiliary system from the density of the Trimer. In the following we will better explain the proposed approach, which has been ideated in the context of the emerging *Connector Theory* (see the seminal paper [67]). As anticipated before, the key component of this approach is the introduction of three Hubbard Dimers, each of which is an auxiliary system to be used for the estimation of a different off-diagonal term. The starting point is to find the two systems of equations for the Hubbard Dimer. The ground states read

$$|\Psi_{l,r}\rangle = b_l|\varphi_l\rangle + b_r|\varphi_r\rangle + b_s|\varphi_s\rangle$$

where (l,r,s) is $(1,3,2)$ for $\gamma_{2,1}$, $(1,6,4)$ for $\gamma_{3,1}$ and $(3,6,5)$ for $\gamma_{3,2}$. By direct calculation the two systems of equations can be found:

$$\begin{cases} \gamma_{l,l} = 2b_l^2 + b_s^2 \\ \gamma_{r,r} = 2b_r^2 + b_s^2 \end{cases} \iff \gamma_{l,r} = \sqrt{2} b_s (b_l + b_r)$$

Let us now rewrite the system we want to solve and focus on the $\gamma_{2,1}$ term

[1] The simple equations obtainable in the variational minimization are always two, corresponding to the first and the last site so the system on the left would have always $N_g + 2$ simple equations. By contrast, already for the 4-points system, the number of unknowns becomes $N_g + \binom{N_g}{2} = \frac{N_g(N_g+1)}{2} = 10$. This means that for solving the equation more complex expressions should be used, loosing the simplicity of the model.

$$\begin{cases} \gamma_{1,1} = 2a_1^2 + a_2^2 + a_4^2 \\ \gamma_{2,2} = 2a_3^2 + a_2^2 + a_5^2 \\ \gamma_{3,3} = 2a_6^2 + a_4^2 + a_5^2 \\ \gamma_{1,1} + \gamma_{2,2} + \gamma_{3,3} = 2 \end{cases} \Longleftarrow \begin{cases} \boxed{\gamma_{2,1} = \sqrt{2}a_2(a_1 + a_3) + a_4 a_5} \\ \gamma_{3,1} = \sqrt{2}a_4(a_1 + a_6) + a_2 a_5 \\ \gamma_{3,2} = \sqrt{2}a_5(a_3 + a_6) + a_2 a_4 \end{cases}$$

The starting point is to work on the three points system expression for $\gamma_{2,1}$ in order to *connect* it to the corresponding equation for the auxiliary system. With this purpose in mind, unless $a_4 a_5 = 0$, it is possible to rewrite it as follows

$$\begin{aligned} \gamma_{2,1} &= \sqrt{2}a_2(a_1 + a_3) + a_4 a_5 = \\ &= \sqrt{2}a_2 \left[a_1 + a_3 + \frac{a_4 a_5}{\sqrt{2}a_2} \right] = \\ &= \sqrt{2}a_2 \left[\left(a_1 + f_1 \frac{a_4 a_5}{\sqrt{2}a_2} \right) + \left(a_3 + f_2 \frac{a_4 a_5}{\sqrt{2}a_2} \right) \right] \overset{\downarrow}{=} \sqrt{2} b_2 (b_1 + b_3) \end{aligned}$$

Where $f_2 = 1 - f_1$ and $f_1 \in [0,1]$ accounts for the fraction of the term $\frac{a_4 a_5}{\sqrt{2}a_2}$ to be considered as the double occupancy in the first site for mapping the trimer to a dimer in the estimation of $\gamma_{2,1}$ Among the different mappings one could choose, a possibility is

$$\begin{cases} b_1 \overset{\downarrow}{=} a_1 + f_1 \frac{a_4 a_5}{\sqrt{2}a_2} \\ b_2 \overset{\downarrow}{=} a_2 \\ b_3 \overset{\downarrow}{=} a_3 + (1 - f_1) \frac{a_4 a_5}{\sqrt{2}a_2} \end{cases}$$

This introduces a mapping between the trimer and the dimer for the estimation of $\gamma_{2,1}$. An auxiliary Hubbard Dimer having these parameters could give the correct off-diagonal term provided that we were able to extract the fraction f_1 and the interaction strength for the dimer from the parameters of the system. This is to say that the problem becomes to find two functions:

$$\begin{cases} f_1 = f_1[n,u] = ? \\ u^{(2)} = g^u[n,u^{(2)}] = ? \end{cases} \tag{5.2}$$

What we need to do is to find (an approximation of) the density of such a dimer and the value of the interaction strength to be used. In fact, knowing these parameters would allow to derive the same result as the one obtainable by knowing the coefficients a_i. This is due to the fact that one can find the off-diagonal term with the previously discussed models for the Hubbard Dimer rather than using the system on the right. These considerations lead to define the purpose as the one of finding an approximation of $\gamma_{1,1}^{(2)}(\gamma_{1,1}, \gamma_{2,2}, \gamma_{3,3})$ and of $\gamma_{2,2}^{(2)}(\gamma_{1,1}, \gamma_{2,2}, \gamma_{3,3})$ and the value of the interaction strength $u^{(2)}$ to be used. Starting with $\gamma_{1,1}^{(2)}$, it is always possible to write it as a

correction of the corresponding value in the three-sites system:

$$\begin{aligned}
\gamma^{(2)}_{1,1} &= 2b_1^2 + b_2^2 = \\
&= 2a_1^2 + a_2^2 + 2\left[\left(f_1\frac{a_4a_5}{\sqrt{2}a_2}\right)^2 + 2f_1\frac{a_4a_5a_1}{\sqrt{2}a_2}\right] \\
&= \gamma^{(3)}_{1,1} + 2\left[\left(f_1\frac{a_4a_5}{\sqrt{2}a_2}\right)^2 + 2f_1\frac{a_4a_5a_1}{\sqrt{2}a_2}\right] - a_4^2 = \\
&= \gamma^{(3)}_{1,1} + \zeta_1.
\end{aligned}$$

Analogously, moving to $\gamma^{(2)}_{2,2}$:

$$\begin{aligned}
\gamma^{(2)}_{2,2} &= 2b_3^2 + b_2^2 = \\
&= 2a_3^2 + a_2^2 + 2\left[\left((1-f_1)\frac{a_4a_5}{\sqrt{2}a_2}\right)^2 + 2(1-f_1)\frac{a_4a_5a_3}{\sqrt{2}a_2}\right] \\
&= \gamma^{(3)}_{2,2} + 2\left[\left((1-f_1)\frac{a_4a_5}{\sqrt{2}a_2}\right)^2 + 2(1-f_1)\frac{a_4a_5a_3}{\sqrt{2}a_2}\right] - a_5^2 \\
&= \gamma^{(3)}_{2,2} + \zeta_2.
\end{aligned}$$

It is worth to remark that, at this point, the HD has been characterized in detail. Therefore, it corresponds to an auxiliary system to be characterized by choosing the values of the density and of the interaction strength, starting from the three sites system parameters. The guarantee that a reasonable choice should exist is based on the fact that the off-diagonal of the HD can vary from 0 to 1, as it can be evinced by looking at the limiting cases, especially in Fig. 3.1. This legitimates the usage of the HD as an auxiliary system not only for the trimer, but also for any lattice in which two electrons live with opposite spin. This statement will be discussed in more details in the next chapter.

The goal has been now moved to express the ζ-functions in terms of the density. In order to do that, it is necessary to do some assumptions. For instance, if the system is non-interacting, the exact result is obtained by forcing $\zeta_1 = \zeta_2 \overset{\downarrow}{=} 0$.
In the following, different assumptions will be considered together with the resulting approximation. This will be done in order to build a reasonable estimate of the 1-RDM. The assumptions will not be derived, they will rather be imposed and it will be motivated afterwards the reason why they turn out to be effective in specific conditions.

Summarizing, given the trimer density $n^{(3)} = \{\gamma^{(3)}_{1,1}, \gamma^{(3)}_{2,2}, \gamma^{(3)}_{3,3}\}$ and the interaction strength $u^{(3)}$, the purpose is to find an approximation of the 1-RDM using Hubbard Dimers. The guarantee of the possibility of finding at least one valid choice for this pair comes from the fact that the image of the off-diagonal of the HD with varying interaction strength spans the whole range $[0,1]$.

For the estimation of $\gamma_{2,1}$ it is possible to use an Hubbard Dimer characterized by:

$$\begin{cases} \gamma^{(2)}_{1,1} = \gamma^{(3)}_{1,1} + \zeta^{2,1}_1[n^{(3)},u^{(3)}] \\ \gamma^{(2)}_{2,2} = \gamma^{(3)}_{2,2} + \zeta^{2,1}_2[n^{(3)},u^{(3)}] \\ u^{(2)} = g^u_{2,1}(u^{(3)},n^{(3)}) \end{cases} \qquad \begin{cases} \zeta^{1,2}_1 = 2\big[\big(f^{2,1}_1 \frac{a_4 a_5}{\sqrt{2}a_2}\big)^2 + 2 f^{2,1}_1 \frac{a_4 a_5 a_1}{\sqrt{2}a_2}\big] - a_4^2 \\ \zeta^{1,2}_2 = 2\big[\big((1-f^{2,1}_1)\frac{a_4 a_5}{\sqrt{2}a_2}\big)^2 + 2(1-f^{2,1}_1)\frac{a_4 a_5 a_3}{\sqrt{2}a_2}\big] - a_5^2 \end{cases}$$

For $\gamma_{3,2}$:

$$\begin{cases} \gamma^{(2)}_{2,2} = \gamma^{(3)}_{2,2} + \zeta^{3,2}_2[n^{(3)},u^{(3)}] \\ \gamma^{(2)}_{3,3} = \gamma^{(3)}_{3,3} + \zeta^{3,2}_3[n^{(3)},u^{(3)}] \\ u^{(2)} = g^u_{3,2}(u^{(3)},n^{(3)}) \end{cases} \qquad \begin{cases} \zeta^{3,2}_2 = 2\big[\big(f^{3,2}_2 \frac{a_2 a_4}{\sqrt{2}a_5}\big)^2 + 2 f^{3,2}_2 \frac{a_2 a_4 a_3}{\sqrt{2}a_5}\big] - a_2^2 \\ \zeta^{3,2}_3 = 2\big[\big((1-f^{3,2}_2)\frac{a_2 a_4}{\sqrt{2}a_5}\big)^2 + 2(1-f^{3,2}_2)\frac{a_2 a_4 a_6}{\sqrt{2}a_5}\big] - a_4^2 \end{cases}$$

and for For $\gamma_{3,1}$:

$$\begin{cases} \gamma^{(2)}_{1,1} = \gamma^{(3)}_{1,1} + \zeta^{3,1}_1[n^{(3)},u^{(3)}] \\ \gamma^{(2)}_{3,3} = \gamma^{(3)}_{3,3} + \zeta^{3,1}_2[n^{(3)},u^{(3)}] \\ u^{(2)} = g^u_{3,1}(u^{(3)},n^{(3)}) \end{cases} \qquad \begin{cases} \zeta^{3,1}_1 = 2\big[\big(f^{3,1}_1 \frac{a_2 a_5}{\sqrt{2}a_4}\big)^2 + 2 f^{3,1}_1 \frac{a_2 a_5 a_6}{\sqrt{2}a_4}\big] - a_2^2 \\ \zeta^{3,1}_3 = 2\big[\big((1-f^{3,1}_1)\frac{a_2 a_5}{\sqrt{2}a_4}\big)^2 + 2(1-f^{3,1}_1)\frac{a_2 a_5 a_6}{\sqrt{2}a_4}\big] - a_5^2 \end{cases}$$

The purpose is to find a way to estimate $g^u_{(i,j)}(u^{(3)},n^{(3)})$ and $\zeta^{i,j}_k[n^{(3)},u^{(3)}]$, where the only certainty is that

$$g^u_{i,j}(0,n^{(3)}) = 0$$

and

$$\zeta^{i,j}_k[n^{(3)},0] = 0$$

Moreover, the existence of at least a pair of values satisfying the required conditions is guaranteed by the range of values assumed by the HD auxiliary system. Remarkably, the whole range would be equally guaranteed by using the non-interacting HD alone. This is in analogy with the Kohn-Sham system since we are arguing that any off-diagonal can be estimated from an effective dimer populated by non-interacting electrons.
Using a more physical jargon, for the estimation of $\gamma_{i,j}$, the two electrons living in the 3-sites system can be substituted with two effective particles that, rather than occupying the three sites, can only occupy the two sites x_i and x_j. The information connecting the two systems is the fact that both of them must yield the same $\gamma_{i,j}$.
The appropriate auxiliary system can be chosen in many different ways due to the degeneracy of the image of the HD at different densities and interaction strengths. In the following, different effective systems will be imposed a-priori. A posteriori, comparing the result with the exact 1-RDMs, it is then possible to understand in which limits each effective dimer is a valid approximation.

5.3.1 Non-interacting Trimer Using non-interacting Dimers

This case is special since the exact solution is known. Let us refer to the three sites in the most generic way possible: x_i,x_j and x_k, where (i,j,k) is a general permutation of $(1,2,3)$.

$$\gamma_{i,i} := \gamma^{(2)}_{i,i} = \gamma^{(3)}_{i,i}$$

The formula used for estimating the off-diagonal term $\gamma_{i,j}$ is

$$\gamma_{i,j}^{th} = \sqrt{\gamma_{i,i}\gamma_{j,j}}$$

In order to test the performances it is possible to define two kinds of error:

- Average absolute error: $\varepsilon_{i,j} := \langle|\gamma_{i,j} - \gamma_{i,j}^{th}|\rangle$
- Average absolute percentage error: $P\varepsilon_{i,j} := \langle\frac{|\gamma_{i,j}-\gamma_{i,j}^{th}|}{\gamma_{i,j}}\rangle$

Where the average is performed on all of the 50000 estimations.
The results are listed in the following table:

	$\gamma_{2,1}$	$\gamma_{3,1}$	$\gamma_{3,2}$
ε	$3.20e-18$	$2.8e-19$	$3.06e-18$
$P\varepsilon$	$(5.7e-17)\%$	$(5.7e-17)\%$	$(5.7e-17)\%$

It is important to notice that, in the special case of non-interacting electrons, the double occupancy of a site is much more likely to occur than in other cases. For this reason, using as an example the element $\gamma_{2,1}$,

$$a_4 a_5 \ll \sqrt{2}a_2(a_1+a_3)$$

That allows to directly identify some parameters of the dimer as the corresponding ones of the trimer

$$\begin{cases} b_1 \simeq a_1 \\ b_2 \simeq a_2 \\ b_3 \simeq a_3 \end{cases}$$

$$\begin{aligned} \gamma_{2,1}^{th} &= \sqrt{(2a_1^2+a_2^2+a_4^2)(2a_3^2+a_2^2+a_5^2)} = \\ &= \sqrt{2a_2^2(a_1+a_3)^2 + O((a_4a_5)^2)} = \\ &\simeq \sqrt{2}a_2(a_1+a_3) = \sqrt{2}b_2(b_1+b_3) \end{aligned}$$

5.3.2 Interacting trimer using interacting dimers density preserving

For what concerns the interacting case let us impose the normalization of the density also in the auxiliary Hubbard Dimer since it is a simple constraint at hand:

$$\begin{aligned} \gamma_{i,i}^{(2)} + \gamma_{j,j}^{(2)} &= \gamma_{i,i}^{(3)} + \gamma_{j,j}^{(3)} + \zeta_i^{i,j} + \zeta_j^{i,j} = \\ &= 2 - \gamma_{k,k}^{(3)} + \zeta_i^{i,j} + \zeta_j^{i,j} \overset{\downarrow}{=} 2 \\ &\rightarrow \zeta_i^{i,j} + \zeta_j^{i,j} = \gamma_{k,k}^{(3)} \end{aligned}$$

It is to be remarked that it is not necessary to impose such a condition since we are working with an auxiliary system. The left system of equations is used since it contains many known relations of the known variables, the density values in the trimer, and the parameters used for mapping the trimer in the auxiliary dimer ($\{a_i\}_{i=1}^6$ and $\{b_i\}_{i\in(l,r,s)}$). However, it is not compulsory to

satisfy all of them. The highest priority must go to the estimation of the off-diagonal term and, for accomplishing this task, one could decide to violate some common properties, at the risk of having a non physical model[2].

If no additional information is introduced it is necessary to estimate both the functions at once. The roughest approximation one can think of in order to solve the system is to assume that

$$\zeta := \zeta_i^{i,j} = \zeta_j^{i,j} \rightarrow \zeta = \frac{\gamma_{k,k}}{2}$$

where no prior information is introduced on the relevance of the two terms. This leads the parameters of the auxiliary Hubbard Dimer to be

$$\begin{cases} \gamma_{i,i}^{(2)} = \gamma_{i,i}^{(3)} + \frac{\gamma_{k,k}^{(3)}}{2} \\ \gamma_{j,j}^{(2)} = \gamma_{j,j}^{(3)} + \frac{\gamma_{k,k}^{(3)}}{2} \end{cases} \tag{5.3}$$

Finally, the dimer proposed is characterized by

$$\zeta_j^{i,j}(n^{(3)}) \simeq \zeta_j^{i,j}(\gamma_{k,k}) = \frac{\gamma_{k,k}}{2}$$

and

$$u^{(2)} = u^{(3)}$$

By defining $\gamma_m^{j,j} = min\{\gamma_{i,i}^{(2)}, \gamma_{j,j}^{(2)}\}$ and assuming to be in the strongly interacting limit:

$$\gamma_{i,j}^{e} = \sqrt{2\gamma_m^{j,j}|1-\gamma_m^{j,j}|}$$

The errors are listed in the following:

	$\gamma_{2,1}$	$\gamma_{3,1}$	$\gamma_{3,2}$
ε	0.47	0.43	0.47
Pε	28%	259%	28%

This is not a good approximation due to the roughness of its assumption and for the not justified requirement of preserving the normalization of the density over the accuracy in the estimation of the off-diagonal term. In order to improve the model it would be sufficient to find a better estimation of these two functions or, possibly, the exact expression, that is the expression of the function $\zeta_i^{i,j}(\{\gamma_{i,i}\}_{i=1}^{(3)}, u^{(3)})$ that, once chosen the physics of the interaction (non-interacting, strongly-interacting or whatever) and the additional information to be used could give the exact value of the off-diagonal term.
It is then possible to do the same thing for the other off-diagonal terms. For what concerns $\gamma_{3,2}$ and $\gamma_{2,1}$ it is to be expected that they will be well approximated by the same auxiliary system (in terms of interaction and approximations of the density). By contrast, the choices for $\gamma_{3,1}$ may be radically different.

[2]In the non-interacting case, for instance, the normalization of the density in the auxiliary system is violated but still the result is exact

5.3.3 Interacting Trimer using non-interacting Dimers

Let us now assume that

$$\zeta_k^{i,j} \simeq 0$$

and

$$u^{(2)} = g_{i,j}^{u}(u, n^{(3)}) = 0$$

This yields

$$\gamma_{i,i} = \gamma_{i,i}^{(2)} = \gamma_{i,i}^{(3)} \rightarrow \gamma_{i,j}^{th} = \sqrt{\gamma_{i,i}\gamma_{j,j}}$$

Resulting in the following errors

	$\gamma_{2,1}$	$\gamma_{3,1}$	$\gamma_{3,2}$
ε	0.28	0.43	0.28
Pε	6%	323%	6%

The approximation of the $\gamma_{3,1}$ is even worse than before, however, the other off-diagonal terms start to present a reasonable percentage error. This is a sign of the fact that, for some kinds of densities, the non-interacting Hubbard Dimers can be used for estimating the off-diagonal term. Let us determine the validity of the assumptions for the estimation of $\gamma_{2,1}$. In Fig.5.1 each point corresponds to a system, identified by its density list $(\gamma_{1,1}, \gamma_{2,2}, \gamma_{3,3})$. The color map is defined by the percentage error when using the non-interacting HD as an auxiliary system. The systems in red will be those characterized by the highest percentage error. This plot teaches us that these Hubbard Dimers will be very bad for estimating $\gamma_{2,1}$ when $\gamma_{1,1} \simeq \gamma_{2,2} \simeq 1$. By contrast, if $\gamma_{1,1}$ is small or if $\gamma_{3,3}$ is close to one, the approximation starts to be good. It is then possible to qualitatively say that, for (i,j) equal to $(1,2)$ and $(3,2)$:

$$\boxed{\gamma_{i,j} \simeq \sqrt{\gamma_{i,i}\gamma_{j,j}} \qquad \text{if } \gamma_{i,i} \text{ small or } \gamma_{k,k} \simeq 1}$$

Also in this case, however, $\gamma_{3,1}$ cannot be properly estimated.

Let us try to understand why this is correct. The region in which the approximation is very bad is for $\gamma_{1,1} \simeq 1$ while $\gamma_{2,2} \in [\sim 0.5, 1]$. These are points in which the third site is less likely to be populated due to the value of the potential in it. The presence in x_1 and x_2 of a big amount of charge means that it is not possible to assume that, when the electrons are in these two sites, they do not interact and, due to the high probability of them populating these two sites, the dominant contribution in the evaluation of the off-diagonal term cannot be well approximated by non-interacting electrons. By contrast, when the population at x_1 or at x_2 or in both the sites becomes less probable, it is to be expected that the regions at low density will be characterized by an high value of the potential. Considering also the fact that the on-site repulsion is high, the double occupancy of any of these two sites as well as finding one electron in x_2 and the other in x_1 will be very unlikely if compared to the other possible configurations. This means that, the exploration of an electron of one of the two sites x_1 or x_2 will be independent from the exploration of the other one. Therefore, if we want to substitute the real system with an HD, a reasonable choice for the electrons are two non-interacting electrons. Symmetric reasonings can be done on the $\gamma_{3,2}$ estimation.

A posteriori, after the previous considerations, it is possible to legitimate

$$\begin{cases} \zeta_1^{2,1} \simeq 0 \\ \zeta_2^{2,1} \simeq 0 \\ u^{(2)} \simeq 0 \end{cases} \qquad \text{when } \neg\{\gamma_{1,1} \in [0.1,1] \wedge \gamma_{2,2} \in [0.1,1.1]\}$$

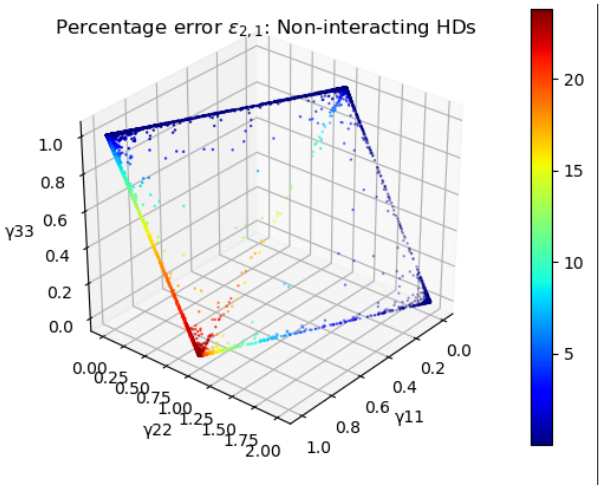

Figure 5.1: Non-interacting dimers: Error in the estimation of the off-diagonal term $\gamma_{2,1}$ in different regions of the density plane

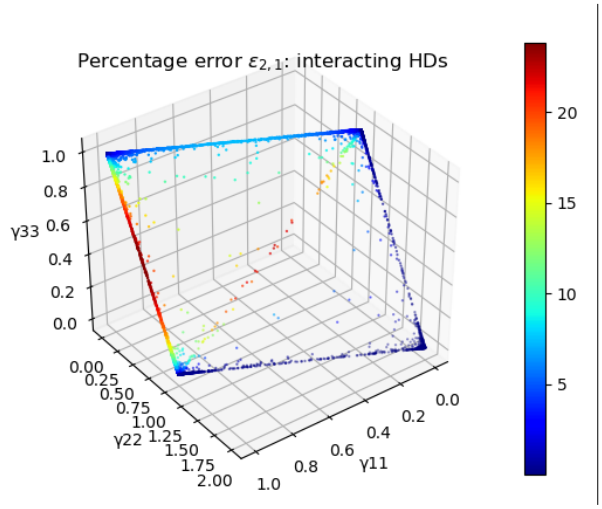

Figure 5.2: Strongly interacting dimers: Error in the estimation of the off-diagonal term $\gamma_{2,1}$ in different regions of the density plane

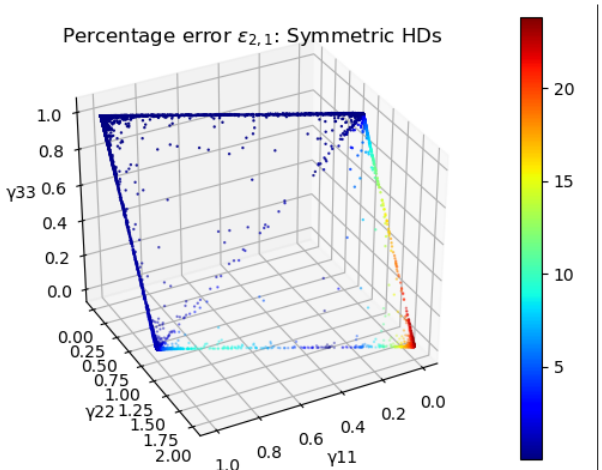

Figure 5.3: Symmetric equations: Error in the estimation of the off-diagonal term $\gamma_{2,1}$ in different regions of the density plane using the negligible double occupancies approximation

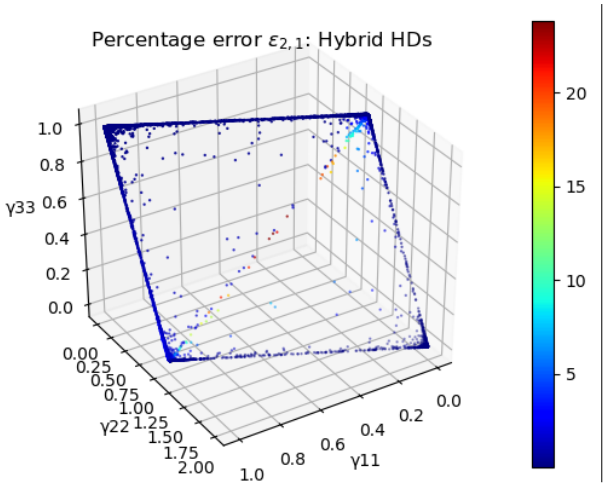

Figure 5.4: Hybrid approach: Error in the estimation of the off-diagonal term $\gamma_{2,1}$ in different regions of the density plane using the Hybrid Approach

5.3.4 Interacting Trimer using equally strongly interacting Hubbard Dimers

Let us now assume that $\zeta_k^{i,j} \simeq 0$ and $u^{(2)} = f^{i,j}(u, n^{(3)}) = u^{(3)}$. In this way, once again,

$$\gamma_{i,i} := \gamma_{i,i}^{(2)} = \gamma_{i,i}^{(3)} \qquad \gamma_m^{j,j} := min\{\gamma_{i,i}, \gamma_{j,j}\} \rightarrow \gamma_{i,j}^{th} = \sqrt{2\gamma_m^{j,j}|1-\gamma_m^{j,j}|}$$

This yields the following errors

	$\gamma_{2,1}$	$\gamma_{3,1}$	$\gamma_{3,2}$
ε	0.039	0.066	0.039
Pε	1.29%	19.33%	1.28%

while the plot representing the accuracy of the approximation can be find in Fig.5.2.
The fact that this case is the best approximation so far is reasonable since we are considering the exact interaction and we are just neglecting one out of the three sites. When that site is not accessible, one should expect that this estimation is almost exact. Let us first comment on the point $(\gamma_{1,1},\gamma_{2,2}) \simeq (1,1)$, that is now well suited for being approximated with this model. More in general, all the points corresponding to $\gamma_{3,3} \simeq 0$ are well described by this approximation. The reason for this is that this condition corresponds to the case in which the value of the potential in x_3 is so high that the electrons will not populate it. They will rather live in x_1 and x_2 accordingly to the value of v_1 and v_2. In this limit the Hubbard Trimer corresponds exactly to an Hubbard Dimer having the sites x_1 and x_2.
Also the cases in which at least one between $\gamma_{1,1}$ and $\gamma_{2,2}$ is small is well approximated. Also the non-interacting model was shown to be effective in these cases but the two things are not in contrast with each-other. In fact, in the real HD, in which the density is normalized, the smallest is the value of the density at one site the more the difference between interacting and non-interacting electrons vanishes. The reason for this can be found in the fact that both in the non-interacting and in the strongly interacting cases, a small value of the density corresponds to a high value of the potential. Locally, in the non-interacting case, as soon as the value of the potential is sufficiently high the two electrons will escape to the other site. It will still be possible for the electrons to visit the penalizing site but, at most, they will do this on their own. Indeed, a double occupancy of the penalizing site would be even more dramatic than an occasional single occupancy. The very same thing happens for strongly interacting electrons. As soon as the value of the potential is sufficiently high the two electrons will escape somewhere else in the lattice, that in this case means to the other site. This is due to the fact that bearing the repulsion may be, at a certain point, more convenient than living in such an high value of the potential. Again the occasional single occupancy of the penalizing site will be possible but there will be no much difference from the non-interacting case at a slightly higher value of the potential. The higher is the potential at that site the smaller will be the value of the density and the more similar will be the non-interacting and the strongly interacting case. This can be graphically observed in Fig. 4.7, in which it is possible to notice the progressive degeneracy of the off-diagonal at small values of the density and for different interaction strengths. On the other hand, when the electrons can escape to more than one site, the phenomenology is more complicated. Nonetheless, what is in common is that locally the site will be progressively less explored when increasing the potential at that site. Therefore, when consider any site sufficiently close to the one penalized, the off-diagonal associated to the two, which measures the likelihood for the electrons to go from one to the other, will tend to be independent on the interaction strength. The reason why this should be true is that the dominant physics is the local value of the potential, which is independent from the interaction strength.
Again, a posteriori

$$\begin{cases} \zeta_1^{2,1} \simeq 0 \\ \zeta_2^{2,1} \simeq 0 \\ u^{(2)} \simeq u^{(3)} \end{cases} \qquad \text{when } \neg\{\gamma_{2,2} \in [0.1,0.9] \wedge \gamma_{3,3} \geq \gamma_{1,1}\}$$

5.3.5 Interacting Trimer using the symmetric equations

Let us go back to the remark that almost the 35% of the 1-RDMs in the data-set are well approximated by the pure symmetric potential assumption. Let us see what is an auxiliary system definable starting from the equations found in this case. The equations for the observable were:

$$\begin{cases} \gamma_{2,1} = \sqrt{|\gamma_{1,1}+\gamma_{3,3}-\gamma_{2,2}||\gamma_{3,3}+\gamma_{2,2}-\gamma_{1,1}|/4} \\ \gamma_{3,1} = \sqrt{|\gamma_{1,1}+\gamma_{2,2}-\gamma_{3,3}||\gamma_{3,3}+\gamma_{2,2}-\gamma_{1,1}|/4} \\ \gamma_{3,2} = \sqrt{|\gamma_{1,1}-\gamma_{3,3}+\gamma_{2,2}||\gamma_{3,3}-\gamma_{2,2}+\gamma_{1,1}|/4} \end{cases} \rightarrow \begin{cases} \gamma_{2,1} = \sqrt{|1-\gamma_{2,2}||1-\gamma_{1,1}|} \\ \gamma_{3,1} = \sqrt{|1-\gamma_{3,3}||1-\gamma_{1,1}|} \\ \gamma_{3,2} = \sqrt{|1-\gamma_{3,3}||1-\gamma_{2,2}|} \end{cases}$$

So let us define

$$\begin{cases} \gamma^{(2)}_{i,i} = |1-\gamma^{(3)}_{i,i}| \\ \gamma^{(2)}_{j,j} = |1-\gamma^{(3)}_{j,j}| \\ u^{(2)} = 0 \end{cases} \rightarrow \gamma^{th}_{i,j} = \sqrt{\gamma^{(2)}_{i,i}\gamma^{(2)}_{j,j}}$$

That results in the following error table

	$\gamma_{2,1}$	$\gamma_{3,1}$	$\gamma_{3,2}$
ε	0.028	0.025	0.029
Pε	0.71%	8.05%	0.72%

The reason for a similar effectiveness may be that the core assumption at the basis of these equations was the vanishing of the probability of double occupancy. It may be true that the symmetric potential is among the most favorable conditions for making prevail the repulsion and making these equations good enough to describe the observable.

However, it is reasonable that a broader ensemble of potential landscapes can be estimated with vanishing double occupancies given that the electrons are strongly interacting. For this reason, these equations become valid in a larger set of systems. The value 35% was obtained by checking which 1-RDM had $\gamma_{1,1} \simeq \gamma_{3,3} \simeq 1$ and by verifying afterwards that the off-diagonal terms were indeed well approximated. Apparently, a much larger number of matrices are described by these equations. As it is possible to evince from Fig.5.3 the symmetry point, corresponding to $\gamma_{1,1} \simeq \gamma_{3,3} \simeq 1$ is indeed well approximated by this auxiliary system. However, the region in which the approximation is good is also extended to a whole other bunch of points. As a matter of fact, the only condition for which it fails is the $\gamma_{1,1} = 0$ region, in which the contribution to $\gamma_{2,1}$ of the double occupancy (a_1) and of a_4 could be comparable and, for this reason, the approximation may fail dramatically .

5.3.6 Interacting Trimer using a piecewise defined approximation

From the previous analysis it is possible to evince that three different auxiliary models turn out to be good approximations for the $\gamma_{2,1}$ term (and consequently for the $\gamma_{3,2}$ one) in partially overlapping regions. In particular:

- The negligible double occupancies model (symmetric potential) is good provided that $\gamma_{2,2} \leq 1$. This condition also includes those systems in which all of the three densities are comparable (center of the plane), at odd with the previous cases;
- The interacting dimers model will be good both for the region at $\gamma_{1,1} \simeq 0$ and for the one at $\gamma_{3,3} \simeq 0$;

- By looking more closely at the non-interacting approximation and comparing its numerical estimations with those obtained with the strongly interacting dimers, it is possible to evince that the non-interacting one turns out to be optimal when $\gamma_{1,1} \leq 0.11$

These remarks lead to an hybrid approximation, defined as follows:

$$\gamma_{2,1} \simeq \begin{cases} \sqrt{\gamma^{(2)}_{1,1}\gamma^{(2)}_{2,2}} & \gamma^{(2)}_{i,i} = \gamma^{(3)}_{i,i} \qquad \text{when } \gamma_{1,1} \leq 0.11 \\ \sqrt{\gamma^{(2)}_{1,1}\gamma^{(2)}_{2,2}} & \gamma^{(2)}_{i,i} = |1-\gamma^{(3)}_{i,i}| \qquad \text{when } \gamma_{2,2} \leq 1 \\ \sqrt{2\gamma^{(2)}_{m}|1-\gamma^{(2)}_{m}|} & \gamma^{(2)}_{m} = min\{\gamma^{(3)}_{1,1}, \gamma^{(3)}_{2,2}\} \qquad \text{otherwise} \end{cases}$$

With these piece-wisely defined auxiliary Hubbard Dimers, the error table becomes

	$\gamma_{2,1}$	$\gamma_{3,1}$	$\gamma_{3,2}$
ε	0.011	0.025	0.010
$P\varepsilon$	0.23%	8.05%	0.23%

Where, for the $\gamma_{3,1}$-term, the symmetric approximation has been used.
The error color-map for the $\gamma_{2,1}$-term can be seen in figure 5.4.

5.3.7 The effect of the increased interaction strength on the approximation of the term $\gamma_{3,1}$

The weakest point of this approximation is the $\gamma_{3,1}$-term. The reason is the fact that there are limiting cases in which the Hubbard Trimer actually behaves as a Dimer when neglecting one of the boundary lattices. By contrast, when the sites x_1 and x_3 are considered, the increased distance and the presence of the site x_2 influence the way the remaining two sites "communicate". The importance of defining an approach for estimating this term lays on the fact that, since the purpose is to increase the number of lattice sites (N_g), the number of terms accounting for the presence of next-nearest neighbors will increase as $N_g - 2$. Furthermore, also correlations between lattice sites farther than 2 lattice sites will appear as soon as the number of grid-points will be higher than 3 and so on. As a consequence, improving the performances is essential for testing the applicability of this model to a larger number of grid-points.
The first thing to be noticed is that the previous models fail in estimating the $\gamma_{3,1}$ term because, in all of the cases, it is overestimated. As said before we assume that, when adding one site to the sampling of the potential, only the on-site repulsion contributes to the coulomb repulsion and the value of U can be considered as fixed. By contrast, the value of t, corresponding to the hopping integral, is a measure of the amplitude of probability of jumping from one site to the other. The farther the sites are the smaller t is, especially if there is an intermediate site. For such a quantized system, the presence of an intermediate site is expected to dominate the transfer of charge from one site to the other, reducing the direct transfer from x_1 to x_3. The lowering of the hopping term results in an increase of the interaction strength with respect to the value it assumes when nearest neighbors are considered.When the interaction strength increases in the strongly-interacting electrons regime, values of the density in the intervals $\gamma_{1,1} \in (0,1)$ and $\gamma_{1,1} \in (1,2)$ become progressively less likely since they would imply a coexistence of the electrons. By contrast, the stronger is the repulsion the more the electrons will be in limiting cases, up to the moment of very strong interaction, in which the density is $\gamma_{1,1} = 2$ if and only if the value of the potential v_1 is extremely advantageous. Similarly, $\gamma_{1,1} = 0$ if and only if the value

of the potential v_2 is extremely advantageous. In all of the other cases the details of the potential loose importance and the densities are forced to be $\gamma_{1,1} = \gamma_{2,2} = 1$, values of the density for which $\gamma_{2,1} = 0$. Pictorially, starting from the strongly interacting curve in Fig. 3.1, to each potential landscape corresponds a point on the double arches of the strongly interacting case and for any finite interaction strength, by generating a sufficiently high number of potential all of the density profiles will be generated. By increasing progressively the value of the interaction strength, the point associated to each potential will move like it was on a rail and, unless the value of v_1 or v_2 is particularly advantageous, the points will tend to go to the symmetry point $\gamma_{1,1} = \gamma_{2,2} = 1$, where the two electrons can stay well separed. As soon as the infinitely-interacting electrons limit is reached, due to the fact that we do not have infinitely deep wells, any detail of the potential is irrelevant, becoming to the eyes of the electrons a flat potential, where the electrons live one per site. In order to well describe this phenomenon, it would be necessary to vary the density profile with the increase of the interaction strength. However, this would require a nontrivial analysis for determining the parametrization on the path experience by every system/potential on the strongly-interacting double arches $\gamma_{2,1}[u > 1]$, leading to the determination of the corresponding density $\gamma_{1,1}(v;u)$. As it is always possible to write the modified value of the off-diagonal term as

$$\gamma_{2,1}(u > 1) = \gamma_{2,1}(u = 1) \cdot \tau(u, v)$$

and considering the fact that the $\gamma_{3,1}$ term is always overestimated, I assumed that the pictorial process previously described happens quickly and, as a first approximation, the function τ is assumed to be a constant, acting as a damping multiplicative term (or enhancement, $\kappa = 1/\tau$). The numerical value is then estimated by averaging over all the matrices the different results obtained with each approximation:

$$\gamma_{3,1} = \tau \cdot \gamma_{3,1}^{HD} \rightarrow \kappa := \left\langle \frac{\gamma_{3,1}^{HD}}{\gamma_{3,1}} \right\rangle$$

The best result in terms of deviation from the average value is obtained for the interacting dimers, for which

HDs	equally int
κ	20 ± 8
ε	0.0032
Pε	0.337%

With this model, the error table of the full hybrid approach becomes

	$\gamma_{2,1}$	$\gamma_{3,1}$	$\gamma_{3,2}$
ε	0.011	0.003	0.010
Pε	0.23%	0.33%	0.23%

This is a good candidate as a noisy version of the actual 3-points 1-RDM and, at this point, a machine learning tool for correcting it could (numerically) complete the model. In Fig.5.5 it is possible to observe a set of original matrices and the artificial ones created by using this hybrid approach.

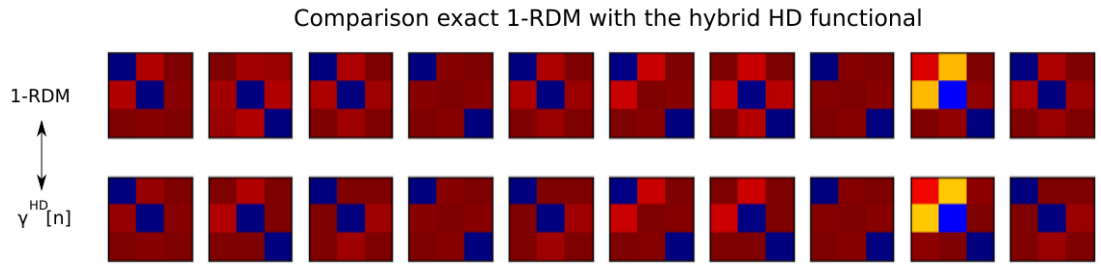

Figure 5.5: Ten examples of 1-RDMs and the result of the HD hybrid functional just defined. The first row is the exact 1-RDM while the second the density functional. Note that the colors associated to the numerical values of the entries has been changed with respect to the rest of the text.

5.4 Summary

The leading motivation of this chapter was to determine whether the HD model could be used as an auxiliary system for the Hubbard Trimer. The HT is the simplest form in which we can add physics to the dimer. Therefore, a success in this task was essential to legitimate further developments of the hypothesized theory, connecting the HD to the Fermi-Hubbard model, and from there to real system problems using 1-RDMs for computing observables. The way it has been done was by associating to each one of the $\binom{3}{2} = 3$ independent off-diagonal entries of the 1-RDM a different HD. The starting point was to express the problem in an exact way, representing the off-diagonals in terms of the occupation probabilities defining the state vector. In order to proceed any further, I have discussed the two approaches I tried for solving the problem: the forward and the inverse approaches. I argued that, the former, is not promising due to a degrading increase in complexity with the number of grid-points. Then, once chosen the latter as the most promising one, I then moved to the actual characterization of the auxiliary systems. The result was the finding of a piece-wise defined functional for the HT. This empirically witness the possibility of using the HD as an auxiliary system for more complex lattices.

Chapter 6

The Hubbard Dimer Functional

This chapter concludes the analysis done on the potential applicability of the Hubbard Dimer (HD) as an auxiliary system. An ensemble of HDs will be used for obtaining the density functional of the one-body reduced density matrix (1-RDM) for the N_g grid-points system. It will be shown that, the smallness of the density makes the interacting and the non interacting dimers equivalent in the description. Moreover, these dimers will be shown to be extremely effective in the estimation of the off-diagonal terms. Finally, analogously to what previously done for the PCA-functional, a denoising autoencoder will be used to correct the errors committed by this functional in the estimation.

6.1 A "Local Density Approximation"

The purpose is to use the HD to find the density functional of the 1-RDM for a 1D system. In Fig. 6.1 it is possible to observe the histogram of the values of the entries in the $N_g = 20$

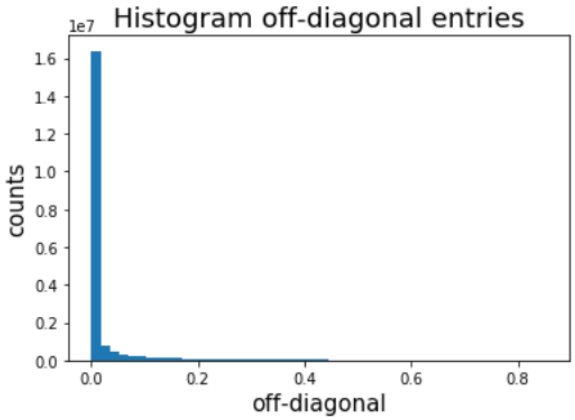

Figure 6.1: Histogram of the off-diagonal entries present in the data-set.

grid-points system. The values of the off-diagonals are always inside the image of the non-interacting Hubbard Dimer ($[0,1]$). Therefore, it will always exist a value of the density such that a non-interacting Hubbard Dimer can estimate the corresponding entry. This legitimates us to use the HD as an auxiliary system. Moreover, it would be desirable to find the interaction strength and the density of the HD from the same parameters of the $N_g = 20$ system alone.

In fact, if we were able to do it, we would straightforwardly obtain the density functional of the 1-RDM for the $N_g = 20$ grid-points system. This is the idea at the basis of the proposed Hubbard Dimer functional. However, it is essential to choose properly the interaction strengths and the densities for the HDs, starting from the same parameters in the 1D system. If we were considering non-interacting electrons, the exact choice would be to use a non-interacting dimer whose density at the two sites corresponds to the one on the real system. The purpose is to understand what is the density and the interaction strength to be used for the dimer when the electrons are interacting.
One of the main results of the previous chapter was the fact that a "local density approximation" was widely effective. This is to say that, many times, it was not necessary to modify the density with respect to the value in the real system, at the interested points to reach a satisfactory accuracy. Following the approach proposed in the previous section, we will therefore start by checking the applicability of the two limiting interaction strengths for the 1-RDM under this approximation.

6.2 Defining the parameters of the auxiliary system

In order to avoid the issue that the densities considered do not sum to the number of electrons it is not safe to express the off-diagonal functional in terms of the γ_m variable since it implies the existence of a symmetry in $\gamma_{i,i} = \gamma_{j,j} = 1$ that does not hold anymore. The functional for the non-interacting dimer will thus be

$$\gamma^o_{i,j} = \sqrt{\gamma_{i,i}\gamma_{j,j}} \tag{6.1}$$

while for the strongly interacting one it will be more reasonable to start from a more general formula derived in appendix (see equation A.6) and to obtain a more general expression for $\gamma_{i,j}$ as a function of the associated non-interacting density matrix term. By using this result for modeling the strongly interacting HD, the model has been chosen to be

$$\gamma^\infty_{i,j}(n, u = 1) = \sqrt{2(1 - (\gamma^o_{i,j})^2)}\sqrt{1 - \sqrt{1 - (\gamma^o_{i,j})^2}} \tag{6.2}$$

In figure 6.2 it is possible to observe that both the functionals give the same result and both of them overestimate in the same way some off-diagonal elements. Moreover, apparently, they well estimate the values of the 1-RDM closest to the diagonal. Before to investigate the accuracy of the model and the reason of the over-estimation, it is worth motivating why the two functionals yield the same result. This can be shown under the hypothesis of small density $\gamma_{i,i}\gamma_{j,j} \ll 1$, that leads to rewrite equation 6.2 as

$$\begin{aligned}\gamma^\infty_{i,j} &\simeq \sqrt{2(1 - (\gamma^o_{i,j})^2)}\sqrt{1 - 1 + \frac{1}{2}(\gamma^o_{i,j})^2} = \\ &\simeq \sqrt{2}\sqrt{\frac{1}{2}(\gamma^o_{i,j})^2} = \gamma^o_{i,j}\end{aligned}$$

Hence, we will use the non-interacting formula to build the desired HD-functional.

This having been said, let us determine what is the accuracy of the model in estimating the 1-RDM. In Fig. 6.3 the columns of the first 1-RDM appearing in Fig. 6.2 have been compared with the corresponding values of the Hubbard Dimer functional at significant rows. For the

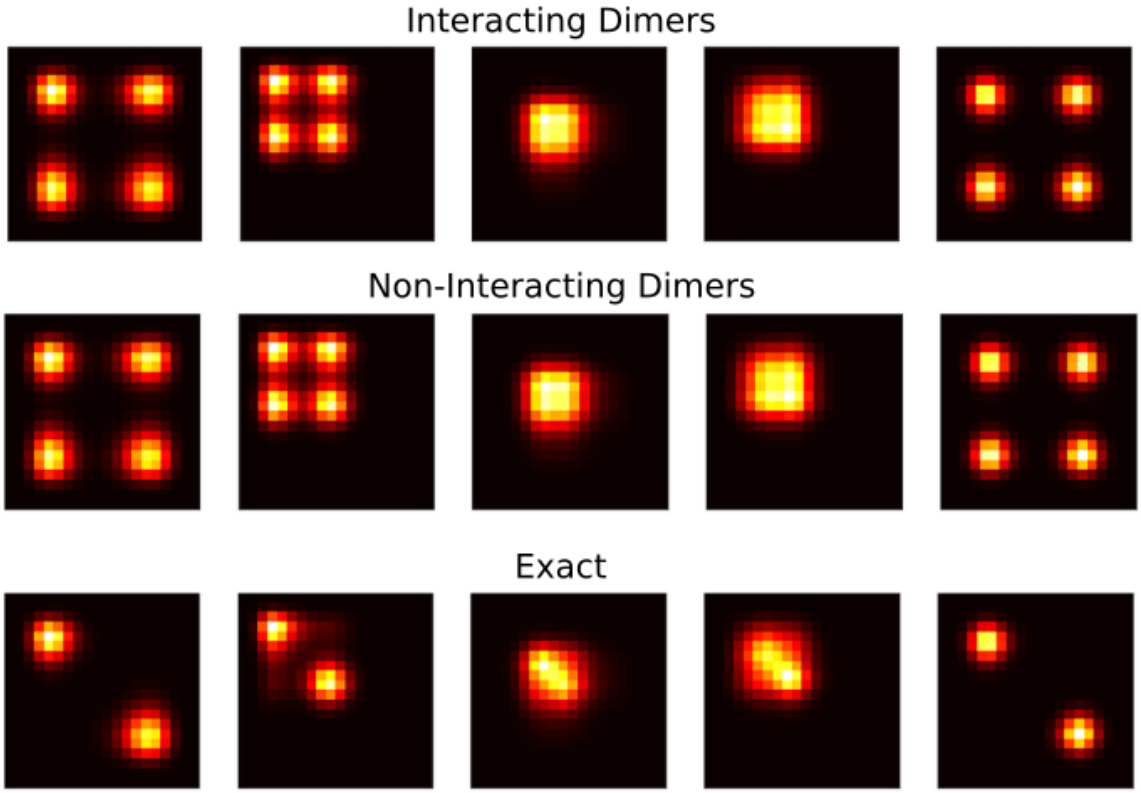

Figure 6.2: Comparison of the matrices obtained using interacting dimers (first row), the one obtained using non-interacting dimers (second row) and the exact one (bottom row).

chosen matrix, as well as for any matrix in the data-set, it is possible to identify the two peaks in the density induced by the repulsion between the electrons. This observation can be explained with the fact that two main single particle orbitals appear at the most distant minima allowed by the depth of the global minimum. In the specific case under analysis the left and right peaks are at the position $p_L = 4$ and $p_R = 14$. They are associated to a middle point $\bar{p} = 9$. The behaviors presented are valid in wide subsets of rows, with the same accuracy in the corrected estimated part. It turns out that the Hubbard Dimer reproduces exactly the entries of the 1-RDM for all the elements $\gamma_{i,j}$ such that $i, j < \bar{p}$ or $i, j > \bar{p}$. In fact, the first image on the left is taken for the row $i = 7$, lower than the intermediate value of the interval. In this case the left-side of the matrix, associated to $j < \bar{p} = 9$ is exactly reproduced while the right side is dramatically overestimated. Symmetric considerations can be done on the right-most image, while the central image represents one of the rows in the small interval in which neither of the peaks can be exactly reproduced. The width of this interval does not exceed 4 up to $N_g = 40$ and it has not been studied for higher numbers of grid-points. Finally, in figure 6.4 it has been plotted the multiplicative factor needed for correcting the amplitude of the two peaks.

As expected the overall shapes are two opposite Fermi-like functions, centered at $\bar{p}$, quantifying the switch between exactness and overestimation, experienced when crossing $\bar{p}$.
In the following, a qualitative reasoning will be proposed for explaining the why this happens. It would be possible to determine the correction in an analytical way, by parametrizing the Fermi-like functions in terms of the density profile. In this work, due to the lack of time, this

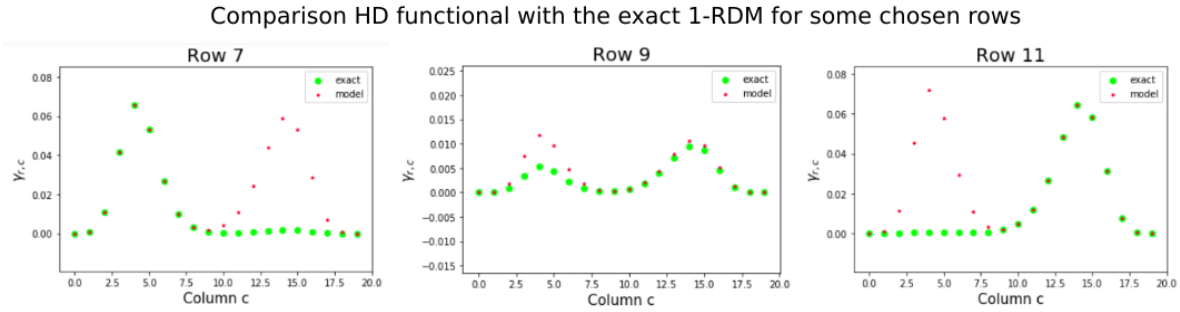

Figure 6.3: Comparison of the behaviors of the peaks as functions of the columns and at fixed rows.

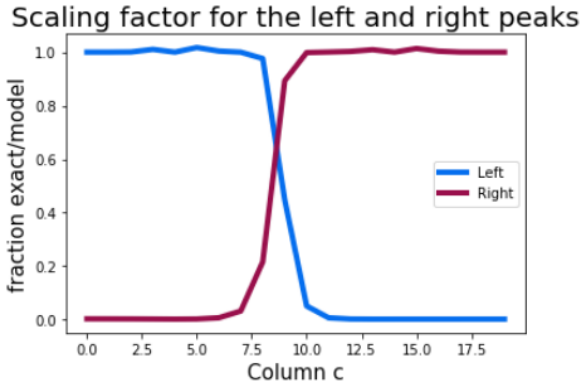

Figure 6.4: Scaling

analytical deepening will be bypassed and, as usual, the systematic error of the model will be treated as a noise to be removed via a DAE. The same architecture as the one used for the PCA functional has been used and, as expected from the well defined properties of the error, with only 50 epochs[1] it has been possible to reach extremely good performances, without the need of any pre-processing

$$\begin{cases} Loss^{MAPE} = 9.24\% \\ Loss^{MAPE} = 0.0011 a.u. \end{cases} \tag{6.3}$$

The resulting functional can be compared with the exact matrices in figure 6.5

6.3 A qualitative motivation of the result

The purpose of this section is to give some intuition on the reason why the formula for the non-interacting HD works well when both the row and column indices are lower or higher than $\bar{p}$ but fail in the remaining cases. Firstly it will be given some qualitative limit explaining why the formula hold. Later, some naive argument will be proposed with the aim of giving some intuition.

[1] For the PCA 200 were needed to reach a worse accuracy.

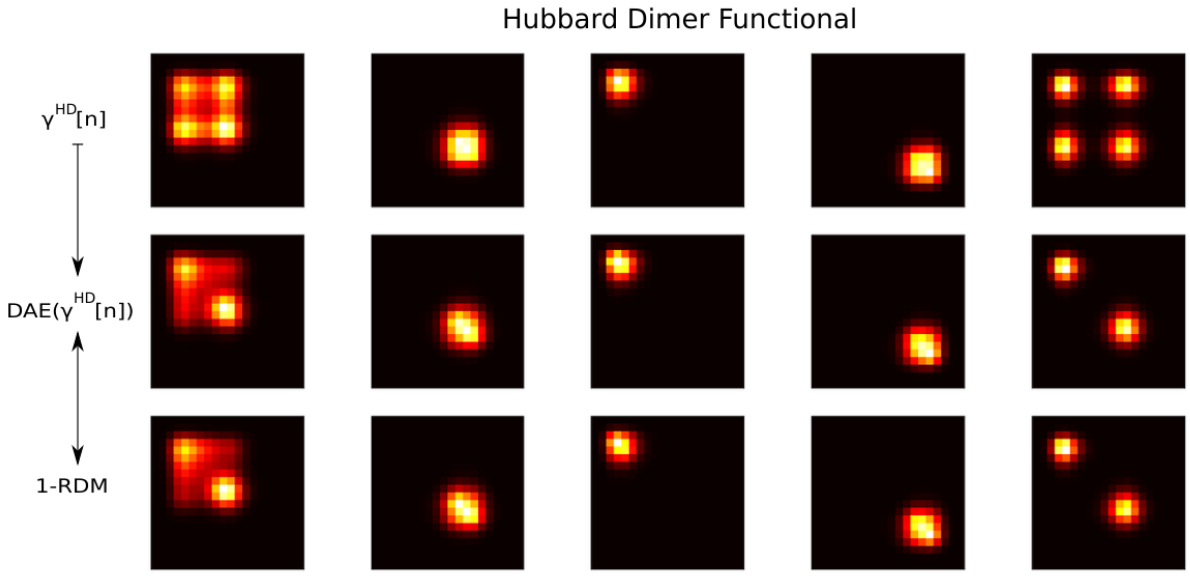

Figure 6.5: Comparison of the HD-functional with the exact 1-RDM for five example matrices. In the first row the pure HD-functional is presented. The overestimation of the blobs is correctly learned by the DAE as it can be noticed by comparing the second row with the exact 1-RDMs, reported in the bottom row.

6.3.1 Some limits

Let us start by considering the full Hamiltonian (see A. C):

$$\hat{H} = \sum_{j,k=1}^{N_g} \sum_{\sigma=\uparrow,\downarrow} t_{j,k} \hat{c}^{\dagger}_{j,\sigma} \hat{c}_{k,\sigma} + \frac{1}{2} \sum_{j,k,l,m} \sum_{\sigma,\sigma'} U_{j,k,l,m} \hat{c}^{\dagger}_{j,\sigma} \hat{c}^{\dagger}_{k,\sigma'} \hat{c}_{l,\sigma} \hat{c}_{m,\sigma'} + \sum_{j=1}^{N_g} v_j \hat{n}_j \tag{6.4}$$

When considering two electrons with opposite spin the most general ground state can be written as

$$\begin{aligned} |\Psi\rangle &= \sum_{s \leq r=1}^{N_g} a_{s,r} |\varphi_{s,r}\rangle = \\ &= \sum_{r=1}^{N_g} a_{r,r} |\varphi_{r,r}\rangle + \sum_{r=2}^{N_g} \sum_{s=1}^{r-1} a_{r,s} |\varphi_{r,s}\rangle \end{aligned}$$

where $a_{r,s} = a_{s,r}$ and, by introducing $m = min(r,s)$ and $M = max(r,s)$

$$|\varphi_{r,s}\rangle = |\varphi_{s,r}\rangle = \begin{cases} \frac{1}{\sqrt{2}} (\hat{c}^{\dagger}_{m,\uparrow} \hat{c}^{\dagger}_{M,\downarrow} - \hat{c}^{\dagger}_{m,\downarrow} \hat{c}_{M,\uparrow}) |\rangle & \text{if } r \neq s \\ \hat{c}^{\dagger}_{r,\uparrow} \hat{c}^{\dagger}_{r,\downarrow} |\rangle & \text{if } r = s \end{cases} \tag{6.5}$$

In order to compute the 1-RDM element $\gamma_{p,q}$, let us introduce the operator $\hat{O}_{p,q} = \hat{c}^{\dagger}_{p,\uparrow} \hat{c}_{q,\uparrow} + \hat{c}^{\dagger}_{p,\downarrow} \hat{c}_{q,\downarrow}$, such that $\gamma_{p,q} = \langle \Psi | \hat{O}_{p,q} | \Psi \rangle$. The application of this operator to the most general ground state can be shown to yield

$$\hat{O}_{p,q} |\Psi\rangle = \begin{cases} \sqrt{2}(a_{p,q} |\varphi_{p,p}\rangle + a_{q,q} |\varphi_{p,q}\rangle) + \sum_{r \neq q,p} a_{r,q} |\varphi_{r,p}\rangle & \text{if } p \neq q \\ 2a_{p,p} |\varphi_{p,p}\rangle + \sum_{r \neq p} a_{r,p} |\varphi_{r,p}\rangle & \text{if } p = q \end{cases} \tag{6.6}$$

leading to the three elements of the 1-RDM

$$\begin{cases} \gamma_{p,q} = \sqrt{2}a_{p,q}(a_{p,p} + a_{q,q}) + \sum_{r\neq p,q} a_{r,p}a_{r,q} \\ \gamma_{p,p} = 2a_{p,p}^2 + \sum_{r\neq p} a_{r,p}^2 \\ \gamma_{q,q} = 2a_{q,q}^2 + \sum_{r\neq q} a_{r,q}^2 \end{cases} \tag{6.7}$$

As mentioned before, the repulsion between the two electrons leads the two of them to localize at the two minima of the potential, resulting in a density characterized by two peaks and in the division of the x-axis into three sub-domains. The intermediate domain Ω_m contains the mean value of the positions of the maxima ($\bar{p}$) and a small neighborhood of it, corresponding to the rows at which the scaling in figure 6.4 is badly defined and it is approximately $\Omega_m \simeq \{\bar{p}-2, \bar{p}-1, \bar{p}, \bar{p}+1, \bar{p}+2\}$. Starting from this definition, the left and the right sub-domain are straightforwardly defined

$$\Omega_L = \{i : (i \notin \Omega_m) \cap (i < \bar{p})\}$$
$$\Omega_R = \{i : (i \notin \Omega_m) \cap (i > \bar{p})\}$$

Due to the presence of a large number of sites in the continuum and since the double occupation of a site is maximally disadvantageous from the coulomb interaction point of view, it is to be expected that, for what concerns the diagonal terms of the matrix, the dominant contribution comes from the sum:

$$\gamma_{p,p} \simeq \sum_{r\neq p} a_{r,p}^2.$$

Moreover, when comparing the probability that the two electrons live in the same sub-domain with the probability that the two of them live far apart, each in a different sub-domain, it is intuitively clear that the sum is further dominated by the indices belonging to Ω_R when $p \in \Omega_L$ and by the indices belonging to Ω_L when $p \in \Omega_R$. Therefore, by introducing the notation

$$\Omega(\neg p) = \begin{cases} \Omega_L & \text{if } p \in \Omega_R \\ \Omega_R & \text{if } p \in \Omega_L \\ \varnothing & \text{if } p \in \Omega_m \end{cases} \tag{6.8}$$

and considering only values of p and q belonging either to Ω_L or to Ω_R, i.e. to the off-digonals well estimated by the HD-functional, it is possible to obtain

$$\gamma_{p,p} \simeq \sum_{r\in\Omega(\neg p)} a_{r,p}^2$$

If we now use an HD for the estimation of the element $\gamma_{p,q}$ and we characterize it by assigning to the two sites the densities $\gamma_{p,p}$ and $\gamma_{q,q}$, it has been shown that the points of the v-representability domain considered are limited to the boundaries of the original HD domain, at which the difference between interacting and non-interacting does not exist (see Fig. 3.1,4.6,4.7). Therefore, using the non-interacting functional, the HD functional becomes

$$\gamma_{p,q}^{HD}[n] = \sqrt{\gamma_{p,p}\gamma_{q,q}} = \sqrt{\sum_{r\in\Omega(\neg p)} \sum_{s\in\Omega(\neg q)} a_{r,p}^2 a_{s,q}^2} \tag{6.9}$$

to be compared with the expression 6.7. When $\Omega(\neg p) = \Omega(\neg q)$, i.e. when q and p are on the same side of $\bar{p}$, it must be true that $a_{p,q} \sim a_{p,p}, a_{q,q}$ when compared to coefficients $a_{r,s}$ such that $(r,s) \in \Omega_L \times \Omega_R$. Therefore, the exact expression for the off-diagonal term becomes

$$\begin{aligned}\gamma_{p,q} &\simeq \sum_{r\in\Omega(\neg p)} a_{r,p}a_{r,q} = \\ &= \sqrt{\sum_{r\in\Omega(\neg p)}\sum_{s\in\Omega(\neg p)} a_{r,p}a_{r,q}a_{s,p}a_{s,q}} = \\ &\simeq \sqrt{\sum_{r\in\Omega(\neg p)}\sum_{s\in\Omega(\neg q)} a^2_{r,p}a^2_{s,q}} = \gamma^{HD}_{p,q}[n]\end{aligned}$$

where the HD-functional has been obtained by noticing that, since p and q are close to each-others and belong to the same sub-domain, it must be true that $a_{r,p} \sim a_{r,q}$.
On the other hand, when $q \in \Omega(\neg p)$ and $p \in \Omega(\neg q)$, i.e. when considering off-diagonal entries that are overestimated by the HD-functional, Eq. 6.9 is to be compared with the following quantity:

$$\gamma_{p,q} = \sqrt{2}a_{p,q}(a_{p,p} + a_{q,q}) + \sum_{r\neq p,q} a_{r,p}a_{r,q}$$

This time the sum will no more be the dominant contribution since one between the two couples (r,p) and (r,q) has the two indices belonging to two different sub-domains while the other has the two indices belonging to the same one. Therefore, the sum and the remaining term are not only comparable, but are of the order of $a_{p,p}$, significantly smaller than the value of $\gamma^{HD}_{p,q}[n]$ in which all of the coefficients appearing involve pair of indices belonging to the two different sub-domains and, therefore, are significantly higher than the double occupancy probabilities.

6.4 Summary

In this chapter the Hubbard Dimer has been used for building a functional for the N_g lattice system in which two electrons live with opposite spin. The non-interacting and the strongly interacting dimers have been shown to coincide in the description of the 1-RDM and both of them show the same overestimation of certain off-diagonal terms while exactly estimating the remaining ones. A qualitative motivation of the reason why this happens has been proposed together with the results of performing the correction using a DAE. The goodness of the model is reflected in the easiness of the machine in learning how to correct the raw functional without any optimization of the network and without the need of training for an high number of epochs. In fact, being the error extremely well structured, the machine easily learns which blobs are overestimated and need to be smoothed out. This concludes the analysis of the ways the Hubbard model can be used for estimating the 1-RDM of extended systems in which two electrons with opposite spins are present. We showed that, from the HD, it is possible to obtain an estimate of the density functional for the 1-RDM of a 1D system, with a non-trivial potential landscape. The easiness with which the machine was able to remove the error, led to understand the way the model fails, paving the road for follow up studies to analytically correct the result. Once having done that, it would then be possible to use the 1D system with two electrons as an auxiliary system for two electrons in more dimensions or for more electrons systems. This defines a bottom-up approach, whose progress would be based on the side-by-side collaboration of the model maker with the machine, so far proved to be effective.

Chapter 7

Gaussian Process Regression as the basis for future works

In this chapter, we shift our focus to how we can use machine learning (ML) to improve the efficiency of experimental measurements of spectra. In particular, I will discuss the applicability of the Gaussian Process Regression (GPR) technique to Inelastic X-ray Scattering (IXS) experiments. In this kind of spectroscopy, the dynamical structure factor $S(q, \omega)$ is measured, which is a function of the momentum transfer q and the energy loss ω. For each momentum transfer q, in order to reduce the noise, the spectrum is obtained by the average of many measurements obtained by scanning the energy ω many times. The original goal of the use of the GPR was twofold: firstly to reduce the number of scans (i.e. the acquisition time) needed to obtain a single spectrum accurately; secondly to reduce the number of measured spectra as a function of q. A key moment of the internship would have been the actual measurement of the spectrum. Unfortunately, adverse conditions hindered it. In the preliminary work here presented two previously measured spectra have been used for Anatase [100] and Rutile [110]. The content of this chapter should therefore be considered as a preliminary study to be used later in July, when we will have the possibility to perform the experiment needed to characterize the regressor.

7.1 Motivations

This chapter addresses the second methodological question at the basis of the thesis: *How can we use ML to augment low resolution calculations and experiments?*
Once more, in analogy to what previously done, the idea is to use the capability of the ML techniques to learn the existence of constraints among the features of the data. Nonetheless, this time, the purpose is not the creation of a density functional but rather the optimization of the information content one can find in the experimental data at hand.
The purpose is to study the possibility of reducing the experimental burden to the absolute essential needed, without loosing in accuracy. This amounts to say that, if the machine was able to reconstruct the high accuracy measurement from a set of low accuracy ones, the experiment would automatically require less time. This would be essential in IXS experiments, in which about two hours are needed for having a single high accuracy scan in energy loss at fixed momentum q.
It is worth mentioning that the twofold goal presented in the introduction was not only interesting

per se. Indeed, the results obtained can be thought of as a witness of the legitimacy of attempting to use the GPR for a more general purpose, for which more accurate data would be needed. In fact, since the high accuracy measurement is equivalent in arbitrary units to the average of many fast scans on the same grid, it would be desirable to have the same final accuracy with a lower number of scans. This is in analogy with what previously done since this "compression" in the amount of information needed to obtain the same final observable is possible if and only if the machine is actually capable of encoding the statistics of the noisy measurement. On one hand, if we will succeed, the study of the way the machine structures the information could be directly studied to understand something more on the properties of spectra. On the other hand, if the machine will not be capable of doing it, it could also be possible that there is nothing to be learned. In fact, if there was no physical information on the way the experimental points are distributed around their average, no ML tool could help. If this was the case the details could emerge only by performing long measurements. The purpose of this chapter is hence to perform some preliminary tests on the potential applicability of the GPR for this task. In particular, we will focus on its capability of learning the spacial correlation of the spectrum at different values of its independent variables.

7.2 An introduction to Gaussian Process Regression

Suppose that there exist a function $S : \mathbb{R}^N \mapsto \mathbb{R}$, possibly containing an intrinsic random component [1], and the purpose is to estimate this law starting from a number of observations of it. In other words the problem we are facing is a generic N to 1 *regression problem* in which the function has an intrinsic randomness. Gaussian Process Regression (GPR) is a ML technique specifically conceived for solving similar tasks. In the following the main results needed will be quickly summarized but, for more information, one may refer to the book [68].
In order to understand how it works, let us consider the independent variable to be one dimensional: $x \in \mathbb{R}$. After having introduced this simplification and by collecting in $\mathbf{X_2} \in \mathbb{R}^{N_2}$ the values of the independent variable at which we want to be able to estimate a realization of the function, the problem becomes to find a generative model for the vector $\mathbf{Y}_2 = \{S(x_i)\}_{x_i \in \mathbf{X_2}} \in \mathbb{R}^{N_2}$. In order to do that, let us assume that we are given a realization of the function at another set of points $\mathbf{Y}_1 = \{S(x_i)\}_{x_i \in \mathbf{X}_1} \in \mathbb{R}^{N_1}$ where $\mathbf{X}_1 \in \mathbb{R}^{N_1}$ is the corresponding vector of independent variables.
The way this is done is by using a Bayesian approach. Firstly a vector for the known variables and one for the unknown ones is defined

$$\mathbf{X} = \begin{bmatrix} \mathbf{X}_1 \\ \mathbf{X}_2 \end{bmatrix} \in \mathbb{R}^N \qquad \mathbf{Y} = \begin{bmatrix} S(\mathbf{X}_1) \\ S(\mathbf{X}_2) \end{bmatrix} = \begin{bmatrix} \mathbf{Y}_1 \\ \mathbf{Y}_2 \end{bmatrix} \in \mathbb{R}^N \tag{7.1}$$

As a prior assumption on the nature of the correlations between different points of the space, it is then assumed that the $\mathbf{Y}$ vector is a multivariate Gaussian random variable of a certain mean and a certain covariance matrix, both parametrized by the $\mathbf{X}$ vector

$$\mathbf{Y} \sim P(\mathbf{Y}|\mathbf{X}) = \mathcal{N}(\mu(\mathbf{X}), \Sigma = k(\mathbf{X}, \mathbf{X}))$$

[1] Corresponding in our case to the measurement uncertainty

Where $\mu(\cdot)$ is the law followed by the mean while $\Sigma_{i,j} = k(x_i, x_j)$ express the correlation between the values of the function at the points x_i and x_j and is called the kernel. The diagonal of this matrix contains the correlation of the function at one point with itself and, therefore, it corresponds to the variance $\sigma^2(x_i)$. Overall, the function at each point can thus be estimated as a mean behavior and its predicted standard deviation from it

$$S(x) = \mu(x) \pm \kappa\sigma(x) \tag{7.2}$$

where κ is a numerical factor usually chosen around 1.9 and, *if one has been able to encode the functional correlation correctly*, the uncertainty interval will always contain any realization of the function for all of the values of x.
After having talked about the general random variable, let us perform the separation into known and unknown data. Since the purpose is to estimate the vector $\mathbf{Y}_2$ and considering the fact that it is a random variable, its generative model corresponds to its probability distribution, given not only the knowledge on the points in which the value of the function is to be sampled but also a sampling of the function at the set of known independent variables

$$\mathbf{Y}_2 \sim P(\mathbf{Y}_2|\mathbf{X}_2, \mathbf{Y}_1, \mathbf{X}_1) =?$$

In order to do that, GPR employs a bayesian approach. The unknown function in fact can be written as

$$P(\mathbf{Y}_2|\mathbf{X}_2, \mathbf{Y}_1, \mathbf{X}_1) = \frac{P(\mathbf{Y}_2, \mathbf{Y}_1, \mathbf{X}_2, \mathbf{X}_1)}{P(\mathbf{Y}_1, \mathbf{X}_1, \mathbf{X}_2)} = \frac{P(\mathbf{Y}_2, \mathbf{Y}_1|\mathbf{X}_2, \mathbf{X}_1)}{P(\mathbf{Y}_1|\mathbf{X}_1, \mathbf{X}_2)} = \frac{P(\mathbf{Y}|\mathbf{X})}{P(\mathbf{Y}_1|\mathbf{X}_1)}$$

By separating explicitly the mean into two parts

$$\mu(\mathbf{X}) = \begin{bmatrix} \mu(\mathbf{X}_1) \\ \mu(\mathbf{X}_2) \end{bmatrix} = \begin{bmatrix} \mu_1 \\ \mu_2 \end{bmatrix} \tag{7.3}$$

and the covariance matrix into the four corresponding sub-matrices

$$\Sigma = k(\mathbf{X}, \mathbf{X}) = \begin{bmatrix} k(\mathbf{X}_1, \mathbf{X}_1) & k(\mathbf{X}_1, \mathbf{X}_2) \\ k(\mathbf{X}_2, \mathbf{X}_1) & k(\mathbf{X}_2, \mathbf{X}_2) \end{bmatrix} = \begin{bmatrix} \Sigma_{1,1} & \Sigma_{1,2} \\ \Sigma_{2,1} & \Sigma_{2,2} \end{bmatrix} \tag{7.4}$$

It is possible to show that

$$\mathbf{Y}_2 \sim P(\mathbf{Y}_2|\mathbf{X}_2, \mathbf{Y}_1, \mathbf{X}_1) = \mathcal{N}(\mu_{2\leftarrow 1}, \Sigma_{2\leftarrow 1})$$

where

$$\mu_{2\leftarrow 1} = \mu_2 + \Sigma_{2,1}\Sigma_{1,1}^{-1}(\mathbf{Y}_1 - \mu_1) \tag{7.5}$$

$$\Sigma_{2\leftarrow 1} = \Sigma_{2,2} - \Sigma_{2,1}\Sigma_{1,1}^{-1}\Sigma_{1,2} \tag{7.6}$$

The step necessary for performing the GPR technique can be then summarized as follows:

- Determine the prior guess of the law of the mean $\mu(\cdot)$;
- Determine the prior guess of the *law* of the kernel, representing the correlation. This guess will depend parametrically on a set of parameters θ: $k(\cdot, \cdot; \theta)$;

- Fit the model by finding the optimal set of parameters θ and update the mean.

Therefore, GPR is a generalization of a linear interpolation in which, depending on the kernel, different functions can be approximated. The law for the mean and for the variance read

$$\mu_{2\leftarrow 1}(x) = \mu(x) + k(x,\mathbf{X}_1)k^{-1}(\mathbf{X}_1,\mathbf{X}_1)(\mathbf{Y}_1 - \mu_1) \tag{7.7}$$

$$\sigma^2_{2\leftarrow 1}(x) = k(x,x) - k(x,\mathbf{X}_1)k^{-1}(\mathbf{X}_1,\mathbf{X}_1)k(\mathbf{X}_1,x) \tag{7.8}$$

Thanks to these expressions it is possible to approximate the desired law as

$$S(x) = \mu_{2\leftarrow 1}(x) \pm \kappa\sigma_{2\leftarrow 1}(x) \tag{7.9}$$

The information content has been moved to the prior knowledge of the kernel function, telling us how are correlated the values of the spectrum at two different values of the independent variable, and on the prior knowledge of the mean. Everything said so far can be generalized to independent variables with higher dimensionality and the optimization procedure is effective up to 20-dimensional input variable. In our case we are interested on 2-dimensional inputs, (ω, q) or, in the worst case scenario, to 4-dimensional inputs $(\omega, \mathbf{q})$

7.3 First Application: Fitting at fixed momentum

Let us start from one dimensional variables by fixing the value of q and considering the energy as the independent variable $x = \omega$. In Fig. 7.2 it can be seen an example. The plot shows the spectrum at momentum fixed to $q = 1.93A^{-1}$ for the Anatase measurements along the crystallographic direction 100, namely for the Anatase [100].

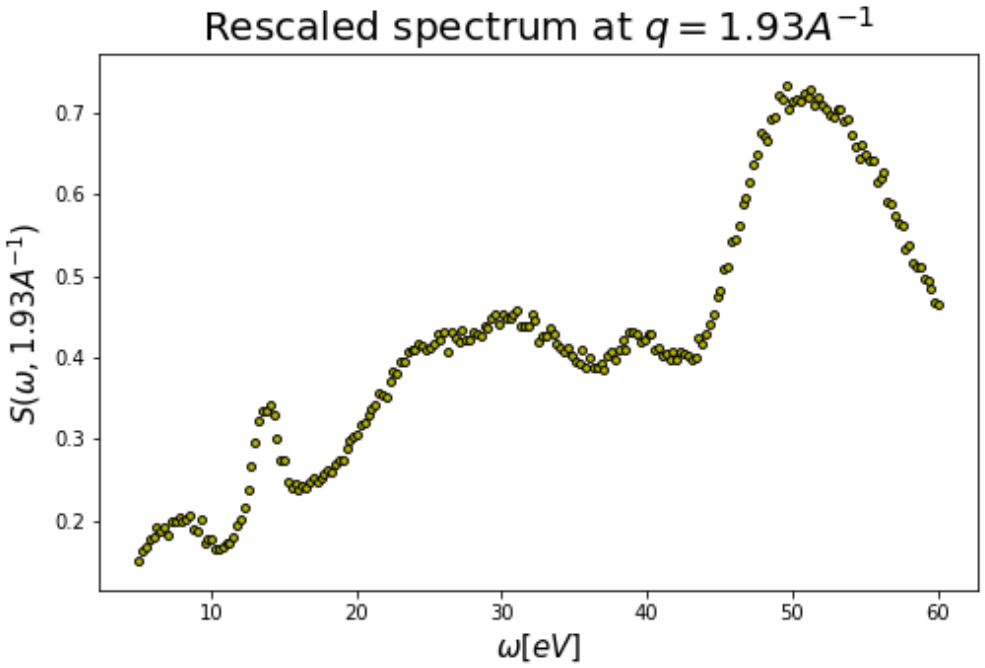

Figure 7.1: Experimental spectrum $S(\omega, q = 1.93A^{-1})$ for the Anatase [100]. The momentum has been fixed and the spectrum has become a function of one variable.

Since no prior information is available on the mean, a possible guess is

$$\mu(x) = 0 \qquad \forall x$$

This having been done, it is also necessary to find a parametric formula for the kernel function. An example is the following:

$$k(x_i, x_j) = Ce^{-\frac{||x_i - x_j||^2}{2\alpha^2}} + \beta\delta(x_i - x_j) \tag{7.10}$$

This kernel is characterized by three parameters $\theta = (\alpha, C, \beta)$ and it is composed of two main terms: the product of a constant kernel with a Radial Basis Function (RBF) kernel and a White Noise (WN) kernel:

1. The first term is the RBF kernel

$$RBF(x_i, x_j; \alpha) = e^{-\frac{||x_i - x_j||^2}{2\alpha^2}} \tag{7.11}$$

   This is a term able to model the correlation between the points. It is parametrized by α, the *lenght scale*, describing the distance at which two independent variables need to be far away from each-other for having the y-values correlated. By looking at the peak at $\omega \simeq 15eV$ in figure 7.2 it is possible to evince that, in order to recover similar variations, the RBF must be more strongly influenced by the values of the function between a range equal to $\Delta\omega \simeq 5eV$. In the optimization process it is possible to specify this information by requiring that α is to be found in a range $\alpha \in (1e-2, 2.5)$.

2. In order to complete the part describing the correlation, a constant kernel C has been introduced;

3. As it can be observed in figure 7.2, there is an underlying structure that is compromised by fluctuations in the measurement. In order to model them, it is to be introduced the White Noise kernel by adding it

$$WK(x_i, x_j; \beta) = \beta\delta(x_i, x_j) \tag{7.12}$$

   where β is the noise level and it can model the noise. In fact, the only information it can carry is the random fluctuation of the observable around the stronger underlying structure, the latter being encoded in the $C \cdot RBF$ part.

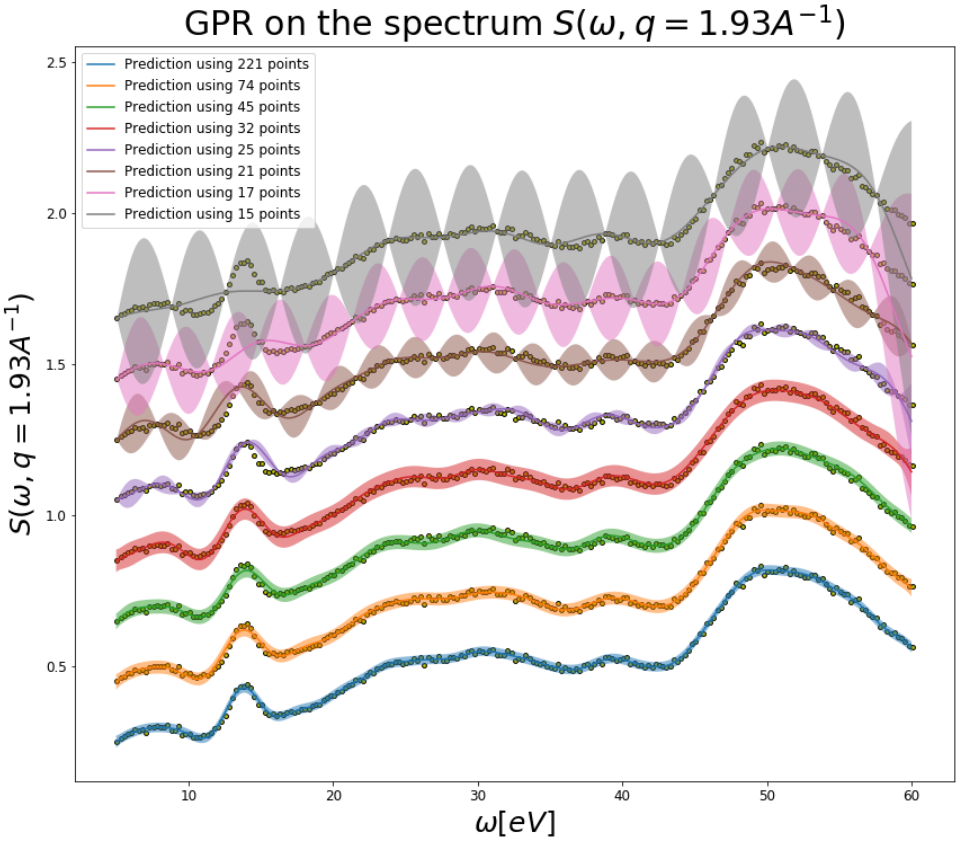

Figure 7.2: Gaussian Process Regression on the Anatase [100]: The momentum q has been fixed to $1.93A^{-1}$ and the result of the fitting of the GPR has been compared using different amounts of data for the fitting. From the bottom to the top the amount of data used has been progressively reduced. The shaded area corresponds to the 95% *confidence interval* around the learned mean values and corresponds to the values that the random function one could sample using the generative model can assume.

In figure 7.2 it is possible to observe the result of the fitting procedure for the spectrum portion of the Anatase [100] at $q = 1.93A^{-1}$. From the bottom to the top the number of energy values used for the estimation have been progressively reduced, with the goal of checking the correctness of the guesses done. The initial kernel has been proposed as

$$kernel = C(1.0, (1e-3, 10)) * RBF(1, (1e-2, 2.5)) + WK(1e-5, (1e-6, 5e-4)) \quad (7.13)$$

This is the way it has to be written in the scikit-learn implementation of the GPR [39]. In particular, for each of the kernels it is to be written the initial guess for the parameter and the range of values in which the machine has to check for the solution. The result per number of energy points used for the estimation is reported in table 7.1.

This simple analysis alone shows that, rather than performing 221 measurements in the range $\omega \in [5,60]$, it could have been possible to reduce the number up to 32 measurements and still well reproducing the position of the peaks and containing, in a reasonable way, the experimental

N_1	C	α	β
221	0.293^2	2.27	$5.62e-05$
74	0.275^2	2.5	$8.41e-05$
45	0.27^2	2.5	$8.58e-05$
32	0.281^2	2.5	$1.76e-04$
25	0.284^2	2.5	$1e-06$
21	0.304^2	2.5	$1e-06$
17	0.327^2	2.5	$1e-06$
15	0.348^2	2.5	$1e-06$

Table 7.1: Result of the fitting procedure

data not used for training the model.
It is worth mentioning that this has been a brute-force approach. No real knowledge on the mean has been introduced and the kernel function has been chosen arbitrarily, with the only requirement of having a model able to describe independently correlations and noise. An improvement of the approach would require both a better guess of the mean and a more legitimate choice of the kernel.

7.4 2D-fitting: Determination of the spectra at not measured momenta

Let us attempt the task of determining the spectrum on the whole 2D plane defined by the energy and the moments, so that the indepent variable becomes $x = (\omega, q)$. This time the Rutile dataset along the crystallographic direction 110, namely Rutile [110], has been considered due to the larger number of available momenta.
As a direct generalization of what done in section 7.3 let us focus on the fitting of the GPR using the whole dataset with the purpose of looking at the way the machine learns how to connect the spectrum function at known values of q, by estimating the intermediate ones. The kernel is slightly different with respect to the one previously introduced since the difference between the functional dependence along the q-axis and the ω-axis has been taken into account using two different length scales parameters along the two axis. The learned kernel is then characterized by the parameters

$$\theta = (\alpha_q = 0.509, \alpha_\omega = 2.55, C = 0.257^2, \beta = 4.84e-5)$$

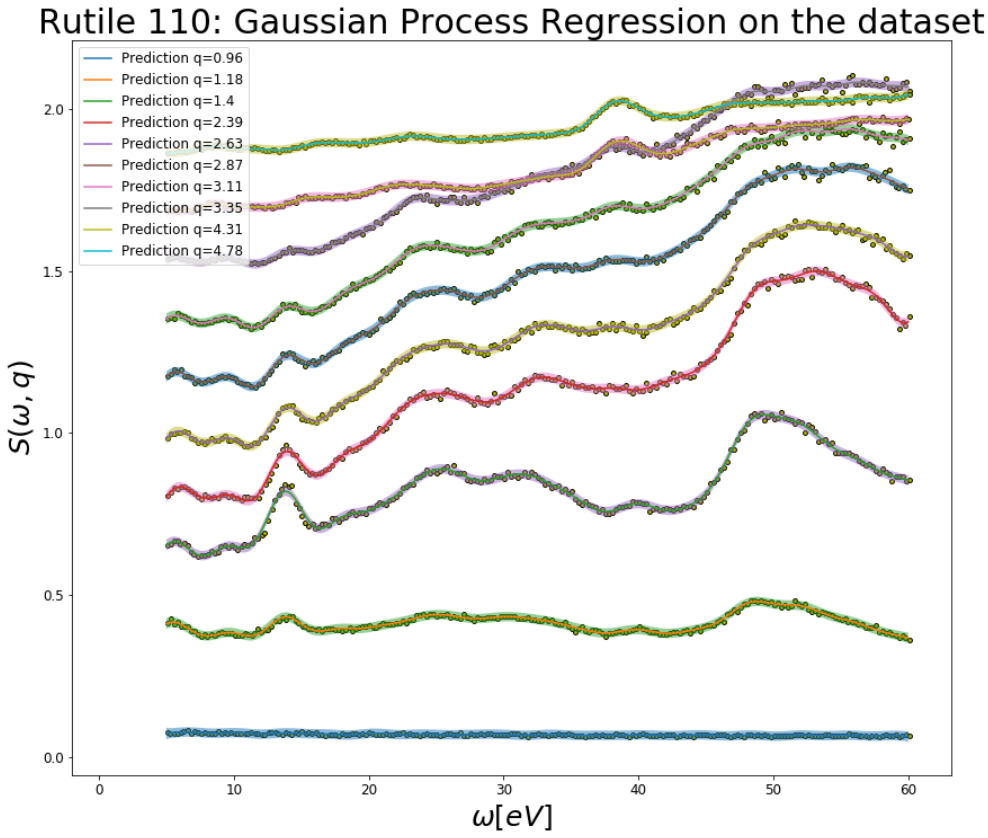

Figure 7.3: Gaussian Process Regression on the whole Rutile 110 data-set. The plots have been shifted to make it easier to understand the result. From the bottom to the top the value of the momentum progressively increases. The shaded area corresponds to the 95% *confidence interval* around the learned mean values and corresponds to the values that the random function one could sample using the generative model can assume.

As it can be observed in Fig. 7.3, the Gaussian process (GP) correctly fits the provided points for the model. Moreover, analogously to what done in Sec. 7.3, it is possible to estimate the behavior of the spectrum at values of q not present in the training set. It is important to notice that when many points are used for fitting the model, it is not essential a good choice of the kernel and of the mean since a lot of constraints will lead many choices to be sufficiently accurate. Things get complicated when the measurements are done on a coarser grid and, in this last case, it is essential to have the best possible parametric model to properly fit the function considered. The same procedure has been done on the Anatase [100] data. In Fig. 7.4 it is possible to observe how starting from the measured $q = 1.65A^{-1}$ and $q = 1.93A^{-1}$ the GPR is able to predict the intermediate points

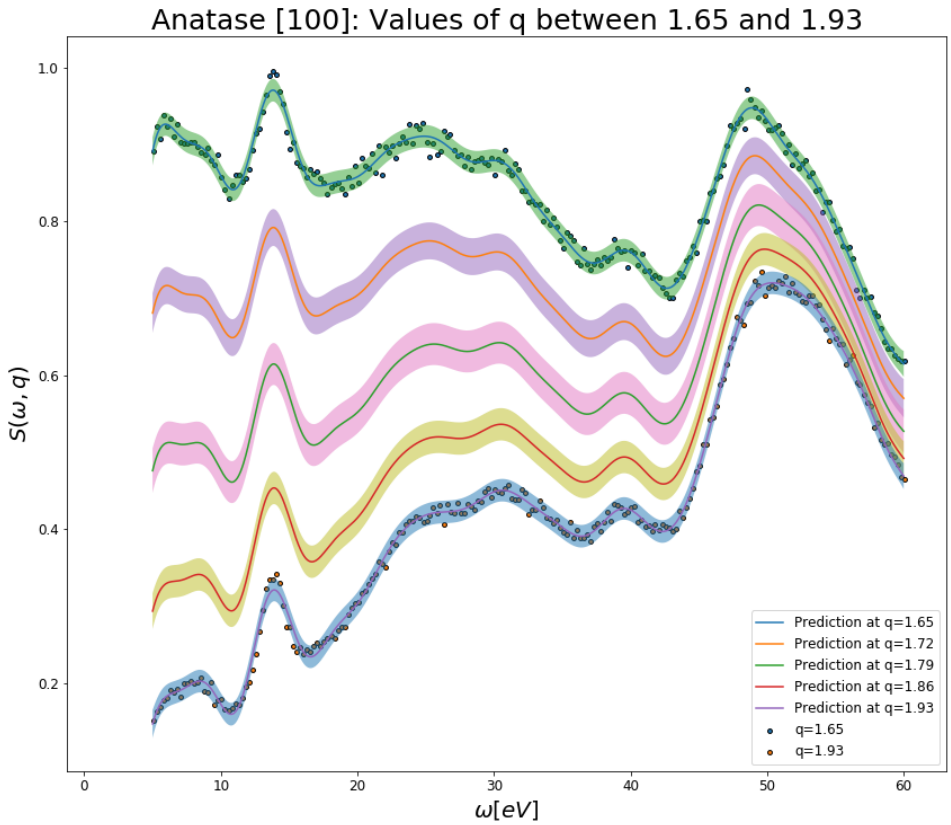

Figure 7.4: Gaussian Process Regression on the Anatase 100 data: estimation of the curves between $q = 1.65$ and $q = 1.93$. The first and the last corresponds to known values of q and the experimental data are plotted in red dots while all of the others are not

At this point it is essential to determine an approach for comparing different kernels and for consequently choosing the best one. This analysis would benefit from a denser measurement but, since no additional data are given, the richest data-set at hands, i.e. the Rutile [110], has been splitted into two parts. Five out of the ten values of q have been used for the fitting phase, defining the vector Q, while the remaining five values, stored in the vector $\bar{Q}$, have been used for validating the model. The two sets of q used are:

$$Q = [0.96,1.4,2.63,3.35,4.78]$$
$$\bar{Q} = [1.18,2.39,2.87,3.11,4.31]$$

The model will correctly fit the functions $S(\omega,q)$ for $q \in Q$ and the $q \in \bar{Q}$ can be used for checking the goodness of the model. The comparison between the different kernels has been done by defining the following error function:

$$\mathscr{E} = \sum_{\omega} \sum_{q \in \bar{Q}} Z(q,\omega), \quad Z(x) = \begin{cases} 0 & \text{if } S^{exp}(x) \in [S_{LB}(x), S_{UB}(x)] \\ min(|S^{exp}(x) - S_{LB}(x)|, |S^{exp}(x) - S_{UB}(x)|) & \text{else} \end{cases} \tag{7.14}$$

where $S_{LB}(x) = \mu(x) - \kappa\sigma(x)$ while $S_{UB}(x) = \mu(x) + \kappa\sigma(x)$. In words, if the experimental data falls inside the accuracy interval of the model there is no cost since the model is reasonable. By contrast, any violation of this rule is to be penalized proportionally to the severity of the violation. The comparison has been done by varying the correlation part. By comparing the an-isotropic RBF and three an-isotropic kernels belonging to a class of kernels named *matérn* and differing between each-others for the value of a parameter ν, that has been fixed to the values 0.5,1.5 and 2.5. Following the Scikit-learn implementation [39]:

$$MAT(x_i, x_j; l, \nu) = \frac{1}{\Gamma(\nu)2^{\nu-1}}\left(\frac{\sqrt{2\nu}}{l}||x_i - x_j||^2\right)^{\nu} K_\nu\left(\frac{\sqrt{2\nu}}{l}||x_i - x_j||^2\right)$$

where $\Gamma(\dot{})$ is the gamma function and $K_\nu(\dot{})$ is the modified Bessel function. The best one in terms of the proposed criterion has turned out to be the *matérn kernel* with $\nu = 0.5$. The result can be checked in figure 7.5

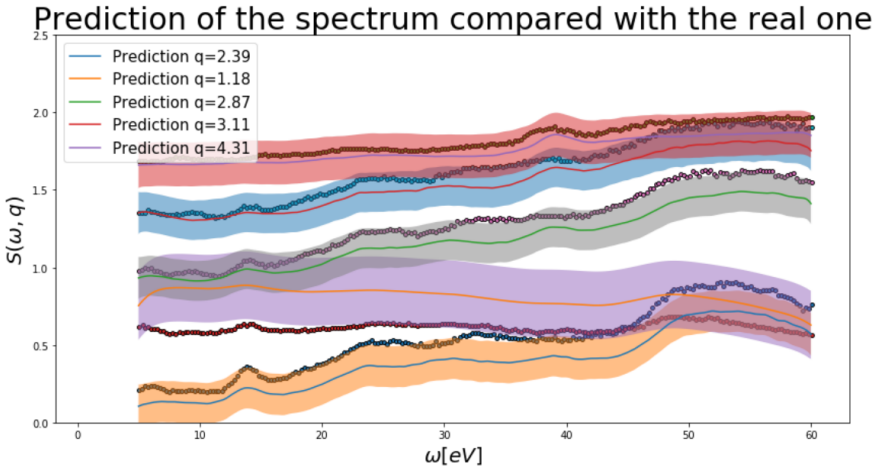

Figure 7.5: Validation of the Gaussian Process Regression for 2D input variables: The plots have been shifted to make it easier to understand the result and the result is presented as the mean value together with the surrounding 95% accuracy interval.

7.5 Future works

In this chapter we introduced the tool that will be later used in more details once it will be possible to perform more detailed experiments. In particular, among the ideas for going further, the following two are the most promising ones:

- So far no real information has been given on the mean, that has been set to zero as an initial guess. It may be possible to increase the accuracy of the prediction by using as a prior information the result of DFT calculations, not necessarily accurate.

- With a more detailed experiment, that will be carried later in July, it should be possible to better study what is the nature of the correlations in more details. In this way it may be possible to optimize the choice of the kernel to be used, consequently increasing the accuracy of the model.

Moreover, the very same concept of using ML for reducing the amount of information needed may also be of interest for theoretical calculations and for numerical simulations. The key idea proposed by the LSI researchers I had the opportunity to work with is that ML techniques may be used for connecting the values of the observables of simple systems, requiring cheap calculations, to the corresponding observables in extremely time requiring calculations. This is a key candidate for a follow up work.

Chapter 8

Conclusions

This work was structured around two methodological questions:

1. *Is it possible for the model maker to learn with the machine?*

2. *How can we use ML to augment low resolution calculations and experiments?*

The former was addressed using as a working table the problem of designing density functionals for the one-body reduced density matrix. The latter, instead, was tackled by studying the potential applicability of Machine Learning (ML) to the problem of fitting spectra from low accuracy measurements. In this chapter we will summarize the main results obtained along the process together with their potential applicability.

8.1 Designing density functionals

In the first part of this work we focused on designing density functionals for one-body reduced density matrices (1-RDMs) using machine learning. The class of problems we considered was the one of 1D systems of two electrons with opposite spin in a randomly generated smooth potential. The apparent oversimplification of the task should not be interpreted as a lack of applicability. In such few electrons systems it is contained a lot of physics that is also present in systems with more electrons. This implies that improvements in the understanding of few electrons systems are essential for increasing our detailed knowledge of matter in a bottom-up learning process. Additionally, the generality of the results may be of an even wider applicability thanks to the concept of *auxiliary system*, i.e. an exactly solvable fictitious system characterized by the properties of the real system, and sharing with it a desired observable. In fact, it may be possible to use the systems considered as auxiliary systems for estimating some observable of a real system.

We started our analysis by introducing the many-body electron problem, at the basis of the modern understanding of matter. In principle, this problem might be completely solved by determining a function containing all of the information of the system, namely the state function. Nonetheless, although the finding of this function has been a subject of study ever since the dawn of quantum mechanics (QM), it is to date an open problem. This is mainly due to the complexity of the hunted function, that causes the problem to be theoretically and computationally intractable. The awareness of this limitation paved the way to the re-formulation of quantum

mechanics that is known as Density Functional Theory (DFT).
We highlighted that this theory is based on the physical discovery that all of the information of the system is encoded in the electronic density (n). Consequently, in principle, any observable can be written as a functional of the density. The purpose in DFT is thus to find these density functionals since their knowledge would yield electronic properties, to be exploited for the most differentiated tasks. However, the vast majority of these functionals is not known to date. As a candidate approach for partially solving the problem, in Sec. 1.1.3 we illustrated why the knowledge of the density functional of the one-body reduced density matrix (1-RDM) $\hat{\gamma}$ would yield many other density functionals for free, such as the kinetic energy. From this consideration we highlighted the importance of finding the functional $\hat{\gamma}[n]$. Furthermore, due to the possibility to associate any 1-RDM to an image, as described in Sec. 1.2, we seeked for analytical insight on the functional in the spectrum of the machine learning manifestations. This concept will be resumed in the next section. It is to be remarked that we *did not* employ the ML tools to blindly reconstruct the 1-RDM from the density. What we did was to utilize them to increase our analytical knowledge.
The applicability of the work done is expected to be twofold:

1. The results can be directly applied. Indeed, suppose that there exists a real system for which our 1D model gives an acceptable description. In this case the results obtained could be directly employed. This might be the case for the experimental realization of the Hubbard Dimer, maybe for the hydrogen molecule and maybe for more complex problems, using the concept of auxiliary system.

2. The methodology proposed can be repeated for other problems. As a matter of fact, this work provides an example of analysis in which the models have been derived working side by side with the machine in the learning process. We used machine learning as an "extension of the arm" of the model maker in his/her efforts, and the approach used could be repeated for other auxiliary systems.

Overall, the purpose was to investigate the applicability of machine learning in designing models and two major attitudes can be identified in the process: firstly we considered how the machine can *directly* help the human; secondly we inverted the roles and we questioned how the human can inform the machine. In the following the main results will be travelled over again, distinguishing the two approaches.

8.1.1 Using machine learning for human learning

The way the machine can help to construct models is primarily by employing its capability of learning constraints. We did this by analyzing the way the machine structures the data to create new analytical models.
Remarkably, the diagonal of the 1-RDM is the density. Hence, DFT guarantees that there exist functional constraints between the entries of any considered 1-RDM. This is to say that, since to any density must correspond one and only one 1-RDM, any change in the diagonal will propagate to the off-diagonals, changing them.

We argued that this information allows to treat the 1-RDM as a picture (see Sec. 1.2). In fact, as well as not all the pictures are pictures of a flower, not all the functions of two variables are 1-RDMs. Moreover, as well as different flowers have different names, different 1-RDMs will be associated to different densities. The point of contact between these two concepts is the existence

of constraints between the features, that identify the abstract class of objects by specifying the constraints their pixels are subjected to.

We first discussed the nature of the constraints, proposing a distinction into three classes: the *validity constraints*, the *universal constraints* and the *characterization constraints*. The first ones are those that determine the acceptability of a matrix as belonging to the 1-RDM class, including the normalization of the diagonal and the symmetry. Moving to the *universal constraints*, these are the general functional relations guaranteed by DFT. Finally, the *characterization constraints* are strictly related to the class of problems considered, accounting for the nature of the potential, the number of electrons, the inter-atomic distance etcetera. An example is the vanishing of the entries of the matrix associated to the boundaries in any confining potential. Of these three classes, only the symmetry of the matrix, the normalization of the density and the vanishing associated to the borders are known and in Sec. 2.1 we have shown that they are linear constraints. By contrast, all of the remaining ones are merged together in a potentially strongly non-linear way. We used PCA to identify the linear constraints. This study allowed us to verify the existence of many more linear constraints than what expected from the simple ones. After having motivated their origin as coming from the nature of the potential, we then focused on how to use this information to build the desired density functional.
Due to the nature of the diagonal of the 1-RDM, any change of the density has a direct counterpart in the entries of the 1-RDM. We showed that PCA is able to detect this information and we discussed the existence of a one-to-one mapping between the first principal components obtained from the PCA performed on the density and the PCA performed on the 1-RDM. More specifically, we focused on the principal components obtained from the 1-RDM data-set. We showed that extracting from them the entries associated to the density and renormalizing them it is possible to obtain the corresponding components obtainable from the density. Therefore, we renormalized the principal components of the 1-RDM data-set to match the ones of the density data-set. Thanks to the presence of constraints these components carry also off-diagonal information. Consequently, we showed that the reconstruction of the density using these newly generated components yields an estimate of the full 1-RDM. We named this estimation the PCA-functional. Moreover, we showed that this mapping contains the vast majority of the information content.
One last way we showed that ML can be used in model designing was for improving the accuracy of models. We showed that a neural network architecture named denoising autoencoder can add the non-linearity by treating its absence as noise.
Summarizing, with the creation of the PCA-functional we were able to highlight the importance of constraints in the definition of a 1-RDM. Moreover, we showed how the capability of ML techniques to learn patterns can be creatively used by the human for building density functionals. Finally, we discovered an unexpected dominance of linearity in the characterization of the systems. This linearity was at the basis of the effectiveness of the PCA-functional.

8.1.2 Using human learning for machine learning

When switching the roles of the human and the machine in the learning process there are two major reasons why it ought to be desirable to teach a model to the machine:

- Specifically considering neural networks, they can be implemented in hardware. Suppose that the theoretical model for computing an observable in an auxiliary system is found. If we were able to teach this model to the machine and we were able to minimize the complexity of the architecture, we would straightforwardly dispose of a piece of hardware

optimized for computing the observable in that auxiliary system. Since auxiliary systems can be used as the building blocks for estimating observables in real systems, we would dispose of specialized hardware for computing the associated quantities, potentially leading to a speed-up in the involved calculations;

- More subtly, the teaching process leads to an increased pragmatism. The need for finding the most informative features that the machine can learn and considering its structural constraints allows to address the problem in a more systematic way and, consequently, allows to reach a deeper insight on the theoretical structure of the systems at hand.

We started from the Hubbard Dimer since it is the simplest possible system having a non-trivial 1-RDM. Interestingly it is possible to: diagonalize it exactly under specific conditions; know the desired density functional in two limiting cases; experimentally create it by using two trapped ultracold ^6Li atoms [57]. As a starting point we diagonalized the Hamiltonian in some useful cases and we derived the desired density functional for non-interacting and strongly-interacting electrons following the prescription present in literature [25]. We then focused on teaching the model to a neural network. Using an approach named *feature engineering* we showed how the maximization of the information, obtained from the analytical result, can be exploited to inform the machine. The result of this procedure is the minimization of the architecture complexity, now reduced to the simplest possible NN architecture with pre-processed inputs, denoted as *logarithmic perceptron*. This method could be implemented in order to have dedicated hardware encoding the limiting cases of the HD.
We then went further, finding the functional of the 1-RDM at intermediate values of the interaction. This was done by designing an approximation called the χ-model, obtained from the exact diagonalization of the Hamiltonian of the symmetric Hubbard Dimer ($v_1 = v_2$) and from the intuition gained while teaching the model to the machine. Finally, the small corrections were machine learned using an appropriately optimized MLP. Two additional studies were performed to complete the characterization of the model. The first one was the determination of the density functional of the state vector in the two limiting cases while the second was the designing of the functional connecting the non-interacting 1-RDM to the interacting one, with a ML-aided map. As pointed out, these last results where considered relevant for our purpose because they allowed to increase the usefulness of the HD as an auxiliary system. This is because the deeper is our understanding of an auxiliary system, the more we might be able to use it for connecting it to real systems.
We then focused on how to use this model as an auxiliary system for 1D lattices having a number of grid-points higher than two. This was useful for the consequent determination of a new functional for the 1-RDM, as an alternative to the PCA-functional. First the three grid-points system was considered and an empirical functional was deduced. The resulting accuracy was a good sign in favor of the bottom-up approach we were proposing. Then, moving to the continuum limit, the applicability of the HD to determine the functional for the $N_g = 20$ system was analyzed. This resulted in a quite accurate estimation for certain elements of the diagonal while others were dramatically overestimated. In order to recover the correct 1-RDM, the same DAE used for the PCA-functional was shown to be highly effective, determining with a good accuracy the entries to be modified. This observation should be deepened and, reasonably, it may be possible to add further analytical insight on the model, consequently making even simpler to the machine the task of recovering the exact 1-RDM.
This final result further shows that combining analytical work on simple models with numerical tools based on machine learning is a very efficient way to progress our knowledge on the

construction of density functionals for the observables of interest. Many of the result obtained in this context were included in the paper "Insights into one-body density matrices using deep learning" [24].

8.2 Fitting spectra

In the last chapter we shifted our focus to how it is possible to use machine learning (ML) to reduce the number of measurements needed in Inelastic X-ray Scattering (IXS) experiments.
Despite the apparent discrepancy in the content, this topic was extremely related to the previous analysis. In fact, at the heart of this study there was the wish of employing the capability of the machine to learn patterns in the data. We wanted to exploit the way the machine encodes the constraints existing among the features of the data-points for our own purposes.
First of all we introduced the observable to be measured, namely the spectrum of an irradiated material. The spectrum is a two variable function $S(q,\omega)$ counting the number of photons out-coming from the material with a certain momentum transfer q and with a certain energy loss ω. We argued that the accurate experimental measurement of this function requires extremely long times to be performed. However, thanks to the additive nature of the observable, the result of an accurate long time experiment can be equally obtained by averaging many short time ones. Therefore, any short time experiment can be thought of as a noisy version of the high resolution experiment. Hence, we argued that if the way the low resolution spectrum deviates from the infinitely accuracy measurement contains some physics, there may exist a machine learning tool capable of extracting this information.
We described Gaussian Process Regression (GPR) as a ML method specifically designed for fitting a scalar function with an intrinsic randomness. The way it performs this fitting is by learning correlations of the function at different values of the independent variables. This seemed in accordance with the characteristics of our observable. Therefore, using the only data we had at hand we performed two preliminary tests of the potential applicability of the GPR as a fitting approach. We showed how, using the GPR, it could be possible to reduce the number of samplings in energy from 221 to 32 without loosing much information. Then, considering the 2D data, we divided the experimental measurements into two groups. One group was used for fitting the GPR model while the other one was used to investigate the accuracy of the prediction. Indeed, we verified the capability of the GPR to correctly predict the spectrum at values of the momentum transfer never used before. Among different GPR models we chose the one that seemed to yield the best results. The findings of this analysis were considered sufficient to legitimate the choice of the ML tool for future studies.
Once we will dispose of many low resolution measurements we will have the possibility to investigate whether it is possible to reduce the time needed to perform an high resolution experiment. If the result will be positive, we will then study the nature of the information learned by the machine and, hopefully, we might increase our theoretical knowledge on the properties of these observables.

Appendix A

Intermediate steps for the known relations

A.1 Minimization of the double occupancy

In chapter 3 it was argued that, an essential step for finding the desired functional in the strongly interacting and in the non-interacting limits could be done by minimizing

$$\omega_1 = \langle \Psi | \hat{n}_{1\uparrow} \hat{n}_{1\downarrow} | \Psi \rangle = |a_1|^2$$

This corresponds to solve the nonlinear set of equations for $|a_1|^2$.

$$\begin{cases} |a_2|^2 = \gamma_{1,1} - 2\omega_1 \\ |a_3|^2 = (2 - \gamma_{1,1} - |a_2|^2)/2 = 1 - \gamma_{1,1} + \omega_1 \\ \omega_1 = \left(\frac{\gamma_{2,1}}{\sqrt{2}a_2} - a_3\right)^2 \end{cases} \tag{A.1}$$

Substituting $|a_2|^2(\omega_1)$ and $|a_3|^2(\omega_1)$ in the third equation, and performing the square, one obtains an equation for ω_1

$$\frac{\gamma_{2,1}^2}{2(\gamma_{1,1} - 2\omega_1)} + 1 - \gamma_{1,1} - \sqrt{2}\gamma_{2,1} \frac{\sqrt{1 - \gamma_{1,1} + \omega_1}}{\sqrt{\gamma_{1,1} - 2\omega_1}} = 0 \tag{A.2}$$

$$\begin{gathered} \gamma_{2,1}^2 + (1 - \gamma_{1,1})(2(\gamma_{1,1} - 2\omega_1)) - 2\sqrt{2} \cdot \gamma_{2,1} \sqrt{1 - \gamma_{1,1} + \omega_1} \sqrt{\gamma_{1,1} - 2\omega_1} = 0 \\ [\gamma_{2,1}^2 + (1 - \gamma_{1,1}) 2(\gamma_{1,1} - 2\omega_1)]^2 - 8\gamma_{2,1}^2 (1 - \gamma_{1,1} + \omega_1)(\gamma_{1,1} - 2\omega_1) = 0 \\ \gamma_{2,1}^4 + 4(1 - \gamma_{1,1})^2 (\gamma_{1,1} - 2\omega_1)^2 + 4\gamma_{2,1}^2 (1 - \gamma_{1,1})(\gamma_{1,1} - 2\omega_1) - 8\gamma_{2,1}^2 (1 - \gamma_{1,1} + \omega_1)(\gamma_{1,1} - 2\omega_1) = 0 \\ \gamma_{2,1}^4 + 4(1 - \gamma_{1,1})^2 (\gamma_{1,1} - 2\omega_1)^2 + 4\gamma_{2,1}^2 (1 - \gamma_{1,1})(\gamma_{1,1} - 2\omega_1) + \\ - [2 \cdot 4\gamma_{2,1}^2 (1 - \gamma_{1,1}) - 4\gamma_{2,1}^2 2\omega_1](\gamma_{1,1} - 2\omega_1) = 0 \\ \gamma_{2,1}^4 + 4(1 - \gamma_{1,1})^2 (\gamma_{1,1} - 2\omega_1)^2 - 4\gamma_{2,1}^2 (1 - \gamma_{1,1})(\gamma_{1,1} - 2\omega_1) - 4\gamma_{2,1}^2 2\omega_1 (\gamma_{1,1} - 2\omega_1) = 0 \end{gathered}$$

By forcing the unknown to appear only in the form $\xi = \gamma_{1,1} - 2\omega_1$, the only term to be modified is the last one

$$\begin{aligned} 4\gamma_{2,1}^2 2\omega_1(\gamma_{1,1} - 2\alpha_1^2) &= 4\gamma_{2,1}^2(2\omega_1 - \gamma_{1,1} + \gamma_{1,1})(\gamma_{1,1} - 2\omega_1) \\ &= 4\gamma_{2,1}^2(\gamma_{1,1} - \xi)\xi \\ &= 4\gamma_{2,1}^2\gamma_{1,1}\xi - 4\gamma_{2,1}^2\xi^2 \end{aligned}$$

A further simplification comes from using the parameter $D \doteq 1 - \gamma_{1,1}$ Thanks to which, the equation to be solved becomes

$$\begin{aligned} \gamma_{2,1}^4 + 4D^2\xi^2 - 4\gamma_{2,1}^2 D\xi &= 4\gamma_{2,1}^2(\gamma_{1,1} - 1 + 1)\xi - 4\gamma_{2,1}^2\xi^2 \\ \gamma_{2,1}^4 + 4D^2\xi^2 - 4\gamma_{2,1}^2 D\xi &= -4\gamma_{2,1}^2 D\xi + 4\gamma_{2,1}^2\xi - 4\gamma_{2,1}^2\xi^2 \\ \gamma_{2,1}^4 + 4D^2\xi^2 &= 4\gamma_{2,1}^2\xi - 4\gamma_{2,1}^2\xi^2 \\ 4(\gamma_{2,1}^2 + D^2)\xi^2 - 4\gamma_{2,1}^2\xi + \gamma_{2,1}^4 &= 0 \end{aligned}$$

The roots of this equation are:

$$\begin{aligned} \xi_\pm &= \frac{2\gamma_{2,1}^2 \pm \sqrt{4\gamma_{2,1}^4 - 4\gamma_{2,1}^4(\gamma_{2,1}^2 + D^2)}}{4(\gamma_{2,1}^2 + D^2)} = \\ &= \frac{\gamma_{2,1}^2}{2}\frac{1 \pm \sqrt{1 - \gamma_{2,1}^2 - D^2}}{\gamma_{2,1}^2 + D^2} = \\ &= \frac{\gamma_{2,1}^2}{2}\frac{1 \pm \sqrt{1 - \gamma_{2,1}^2 - (\gamma_{1,1}^2 + 1 - 2\gamma_{1,1})}}{\gamma_{2,1}^2 + (\gamma_{1,1} - 1)^2} = \\ &= \frac{\gamma_{2,1}^2}{2}\frac{1 \pm \sqrt{\gamma_{1,1}(2 - \gamma_{1,1}) - \gamma_{2,1}^2}}{\gamma_{2,1}^2 + (1 - \gamma_{1,1})^2} = \end{aligned}$$

These are the two values of ξ admitted according to the imposed variational constraints. Remembering that

$$\omega_1 \doteq \frac{\gamma_{1,1}}{2} - \frac{\xi}{2}$$

and that the purpose is to obtain the minimum ω_1, the root to be chosen is ξ_+, yielding.

$$\omega_1^* = min\{\omega_1\} = \frac{\gamma_{1,1}}{2} - \frac{\gamma_{2,1}^2}{4}\frac{1+\sqrt{\gamma_{1,1}(2-\gamma_{1,1})-\gamma_{2,1}^2}}{\gamma_{2,1}^2+(1-\gamma_{1,1})^2}\left(\frac{1-\sqrt{\gamma_{1,1}(2-\gamma_{1,1})-\gamma_{2,1}^2}}{1-\sqrt{\gamma_{1,1}(2-\gamma_{1,1})-\gamma_{2,1}^2}}\right) =$$
$$= \frac{\gamma_{1,1}}{2} - \frac{\gamma_{2,1}^2/4}{1-\sqrt{\gamma_{1,1}(2-\gamma_{1,1})-\gamma_{2,1}^2}}\frac{\gamma_{1,1}^2-2\gamma_{1,1}+1+\gamma_{2,1}^2}{\gamma_{2,1}^2+(1-\gamma_{1,1})^2} =$$
$$= \frac{\gamma_{1,1}}{2} - \frac{\gamma_{2,1}^2/4}{1-\sqrt{\gamma_{1,1}(2-\gamma_{1,1})-\gamma_{2,1}^2}}$$

That allows to say that

$$\omega_1 = \frac{\gamma_{1,1}}{2} - \frac{\gamma_{2,1}^2/4}{1-\sqrt{\gamma_{1,1}(2-\gamma_{1,1})-\gamma_{2,1}^2}} \tag{A.3}$$

A.2 Functionals in two limiting cases

In this appendix the functional forms in the strongly interacting case and in the non-interacting case will be explicitly derived.

non-interacting case Let us find the condition of existence for the previously derived equation. The domain correspond to the intersection of three ensembles:

$$\mathscr{D} = \mathscr{I}_1 \cap \mathscr{I}_2 \cap \mathscr{I}_3$$

where

$$\mathscr{I}_1 = \{\gamma_{2,1} \text{ s.t. } \gamma_{1,1}(2-\gamma_{1,1}) - \gamma_{2,1}^2 \geq 0\}$$
$$= \left[-\sqrt{\gamma_{1,1}(2-\gamma_{1,1})}, \sqrt{\gamma_{1,1}(2-\gamma_{1,1})}\right]$$

$$\mathscr{I}_2 = \{\gamma_{2,1} \geq 0\}$$

and

$$\mathscr{I}_3 = \left\{\gamma_{2,1} \neq \pm\sqrt{\gamma_{1,1}(2-\gamma_{1,1})-1}\right\}$$

So

$$\mathscr{D} = \left[0, \sqrt{\gamma_{1,1}(2-\gamma_{1,1})}\right] \cap \mathscr{I}_3$$

Giving a second derivation of the 2-point non-interacting density matrix:

$$\gamma_{2,1}^0 = \sqrt{\gamma_{1,1}(2-\gamma_{1,1})} = \sqrt{n(x_1)n(x_2)} \tag{A.4}$$

Strongly interacting case Let us now explicitely perform the derivative of eq.A.3, that can be now rewritten as

$$\omega_1 = \frac{\gamma_{1,1}}{2} - \frac{\gamma_{2,1}^2/4}{1-\sqrt{(\gamma_{2,1}^o)^2-\gamma_{2,1}^2}} \tag{A.5}$$

and impose it to be zero. Before to perform the differentiation it is worth working on the variables for simplifying the task. One therefore defines

$$\eta \doteq \sqrt{(\gamma_{2,1}^o)^2-\gamma_{2,1}^2} \tag{A.6}$$

and imposes

$$\frac{d\omega_1}{d\eta}\frac{d\eta}{d\gamma_{2,1}} \stackrel{\downarrow}{=} 0$$

the zero induced by the second term is given by the equation

$$\frac{d\eta}{d\gamma_{2,1}} = \frac{-\gamma_{2,1}}{\sqrt{(\gamma_{2,1}^o)^2-\gamma_{2,1}^2}} = 0$$

and correspond to the extrema at $\gamma_{2,1}=0$ that we have previously understood being irrelevant. Therefore, the real condition to be imposed is

$$\frac{d\omega_1}{d\eta} \stackrel{\downarrow}{=} 0$$

At this point, the easiest quantity to be extremized and yielding the same extrema is

$$\begin{aligned}
f(\eta) &= \frac{-\gamma_{2,1}^2}{\sqrt{(\gamma_{2,1}^o)^2-\gamma_{2,1}^2}-1} \\
&= \frac{-(\gamma_{2,1}^o)^2+(\gamma_{2,1}^o)^2-\gamma_{2,1}^2}{\sqrt{(\gamma_{2,1}^o)^2-\gamma_{2,1}^2}-1} \\
&= \frac{\eta^2-1+1}{\eta-1} - \frac{(\gamma_{2,1}^o)^2}{\eta-1} \\
&= \frac{(\eta-1)(\eta+1)}{\eta-1} + \frac{1-(\gamma_{2,1}^o)^2}{\eta-1} \\
&= \eta+1+\frac{1-2\gamma_{1,1}+\gamma_{1,1}^2}{\eta-1} \\
&= \eta+1+\frac{(\gamma_{1,1}-1)^2}{\eta-1}
\end{aligned}$$

This leads to the condition

$$\frac{df}{d\eta} = 1 - \frac{(\gamma_{1,1}-1)^2}{(\eta-1)^2} \overset{\downarrow}{=} 0$$

that corresponds to

$$|\gamma_{1,1}-1| = |\eta-1| \tag{A.7}$$

While the first one depends on the value of $\gamma_{1,1}$, the second is always

$$|\eta-1| = 1-\eta$$

since

$$\begin{aligned}\eta = \sqrt{\gamma_{1,1}(2-\gamma_{1,1}) - \gamma_{2,1}^2} &\overset{?}{<} 1\\ \gamma_{1,1}(2-\gamma_{1,1}) - \gamma_{2,1}^2 &\overset{?}{<} 1\\ -(\gamma_{1,1}-1)^2 &\overset{?}{<} \gamma_{2,1}^2\end{aligned}$$

That is always true.
Therefore, when $\gamma_{1,1} \geq 1$

$$\begin{aligned}\gamma_{1,1}-1 &= 1 - \sqrt{\gamma_{1,1}(2-\gamma_{1,1}) - \gamma_{2,1}^2}\\ (2-\gamma_{1,1})^2 &= \gamma_{1,1}(2-\gamma_{1,1}) - \gamma_{2,1}^2\\ \gamma_{2,1}^2 &= (2-\gamma_{1,1})(\gamma_{1,1}-(2-\gamma_{1,1}))\\ \gamma_{2,1} &= \sqrt{2(2-\gamma_{1,1})(\gamma_{1,1}-1)}\end{aligned}$$

on the other hand, when $\gamma_{1,1} < 1$

$$\begin{aligned}1-\gamma_{1,1} &= 1 - \sqrt{\gamma_{1,1}(2-\gamma_{1,1}) - \gamma_{2,1}^2}\\ \gamma_{1,1}^2 &= \gamma_{1,1}(2-\gamma_{1,1}) - \gamma_{2,1}^2\\ \gamma_{2,1}^2 &= 2\gamma_{1,1}(1-\gamma_{1,1})\\ \gamma_{2,1} &= \sqrt{2\gamma_{1,1}(1-\gamma_{1,1})}\end{aligned}$$

Summing up, one obtains the functional of the off-diagonal term of the density matrix in the strongly interacting limit

$$\gamma_{2,1}^{\infty} = \begin{cases}\sqrt{2(\gamma_{1,1}-1)(2-\gamma_{11})} & \text{if } \gamma_{1,1} \geq 1\\ \sqrt{2\gamma_{1,1}(1-\gamma_{11})} & \text{if } \gamma_{1,1} < 1,\end{cases}$$

that can also be rewritten as

$$\boxed{\gamma_{2,1}^{\infty} = \sqrt{2|\gamma_{1,1}-1| \cdot min\{\gamma_{1,1}, 2-\gamma_{1,1}\}}} \tag{A.8}$$

Appendix B

Additional information on the Hubbard Dimer

The potential of the Hubbard Dimer is extremely high. It is extremely likely that a theory can be constructrd in which the system can be locally approximated with Hubbard Dimers, resulting in a 1-RDM linked to the one of the dimer. Due to its potential, in the following some additional details will be considered. In particular:

- The connection in between the interacting and the non-interacting case will be machine learned
- The state vector will be explicitly parametrized in terms of the density using a synthetic data-set.

The purpose of this section is to generate mappings in between different interaction and, hopefully, to be able to consider the non-interacting data-set as a noisy version of the interacting one.

B.0.1 From the non-interacting case to the interacting: Finding the functional $\gamma[\gamma_o]$

The original purpose of this subsection was to study the mapping in between the non-interacting 1-RDM and the interacting one with the same potential. This is interesting considering the higher easiness in the solution of the non-interacting case. The original idea was to train a Denoising Autoencoder for the task but the presence of a sharp transition in the mapping made the purpose extremely difficult. In the following it will be presented the way this has ben overcome and the prescription for building the corresponding functional.
At this point the functional dependency of the off-diagonal is known in both the kinds of interaction. Therefore, the real mapping to be done is the one in between the densities of the two cases. In Fig.B.1 it is reported the map of the $\gamma_{1,1}$ term from the non-interacting to the interacting.

If $\gamma^o_{1,1} = 0$ or $\gamma^o_{1,1} = 2$ then the minimum must be extremely advantageous, much deeper than the value of the potential at the other site. For this reason both the interacting and the non-interacting $\gamma_{1,1}$ will be the same since the two electrons populate the minimum independently on the interaction. However, as soon as the minimum on the opposite site starts to be more accessible, the interacting electrons will instantly try to occupy the opposite site, and $\gamma^{int}_{1,1}$ jumps

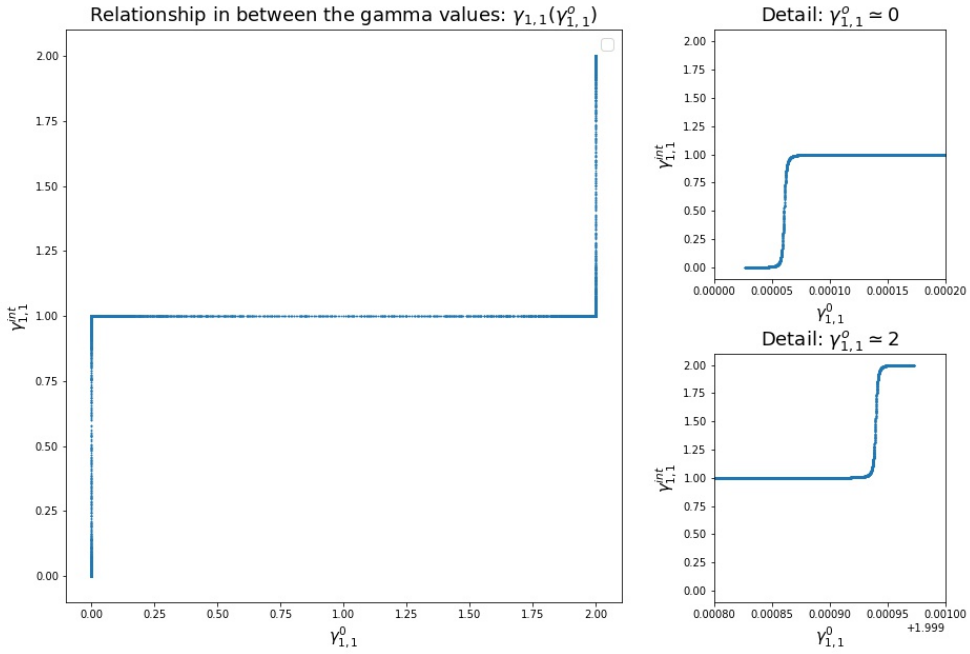

Figure B.1: Relationship in between the gammas

to 1 for remaining such for a very broad range of values of the two potentials($\gamma^o_{1,1}$), up to the moment in which the minimum at the other site becomes again much more advantageous. The mapping in between the densities should be independent on the off-diagonal terms

$$n_o \leftrightarrow V \leftrightarrow n$$

So the autoencoder should take as an input $\gamma^o_{1,1}$ and $\gamma^o_{2,2}$, learn something related to the potential, which may be $\gamma^o_{1,1}$ itself due to all of the information this variable contains, and extract from it the the very steep mapping for small and big values of $\gamma^o_{1,1}$ while constant in the broad interval in the middle. In the meanwhile the autoencoder has also to handle the off-diagonal term that depends only on $\gamma_{1,1}$. Due to these considerations, the optimal encoder should learn how to extract $\gamma_{1,1}$ from the non-interacting density matrix, i.e. from the non-interacting density. Then, starting from it, it should extract the functional of the interacting density matrix in terms of $\gamma_{1,1}$. So differently from the common problem of denoising autoencoders the minimal admissible dimension of the latent space is known to be $N_g - 1$. It is also known what is a good candidate for this latent space, which are the first $N_g - 1$ elements of the interacting density. All in all, the best way to do this is by training an encoder to extract the interacting density from the non-interacting one. Then to train a decoder to restore the off-diagonal terms. In the following this will be done manually.
The first thing to be done is to write the problem in terms of easier variables. With this purpose in mind, as common, let us write everything in terms of γ_m. Then, in order to dilute the growing, the problem is redefined in terms of the following variables:

$$\iota_o \doteq A - \frac{1e-4}{\gamma^o_m} \qquad \iota \doteq 2\gamma_m - 1$$

$\gamma_m^o \in [0,1]$, where the real lower bound is set at $1e-4$ so $1/\gamma_m^o \in [1, \sim 1e4]$. A is the value of $1e4/\gamma_m^o$ at which $\gamma_{1,1} = 0.5$ and

so now $\iota \in [-1,1]$ and $\iota_o \in [-3,3]$ approximately. In this way the function has been mapped to a sigmoid-like function, as it can be observed in Fig.B.2. At this point, with a sigmoid to be approximated, a neural network model is used. A direct hyperbolic tangent does not fit, so one needs to introduce some non-linearity in its arguments. The result of its fitting with a MLP (1,10,15,10,1) with stochastic gradient descent, mean square error, batch size set to 32 and for 20 epochs can be observed in Fig.B.2.

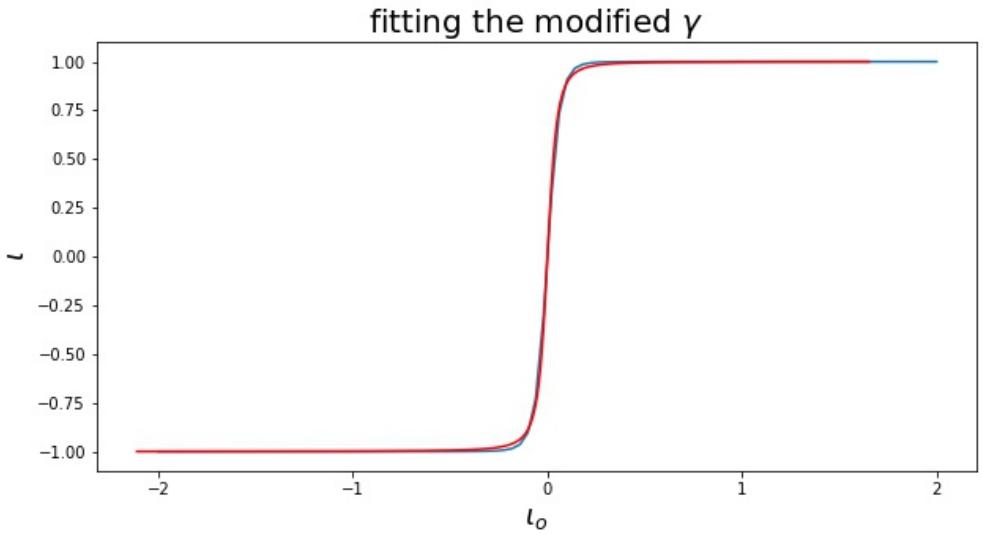

Figure B.2: Relationship in between the modified gammas

one then knows how to estimate $\iota = MLP(\iota_o)$. Moreover, $\gamma_m = (\iota+1)/2$ so

$$\gamma_m = \frac{1}{2}\left[1 + MLP\left(A - \frac{1e-4}{\gamma_m^o}\right)\right]$$

. The fit for γ_m can be observed in Fig.B.3

Thanks to this model it is now possible to obtain the interacting density matrix from the non-interacting one:

$$\gamma[\gamma^o] = \begin{bmatrix} \gamma_{1,1} & \gamma_{2,1}(\gamma_{1,1}) \\ \gamma_{2,1}(\gamma_{1,1}) & \gamma_{2,2} \end{bmatrix} = \begin{bmatrix} \gamma_{1,1}(\gamma^o_{1,1}) & \gamma_{2,1}(\gamma_{1,1}(\gamma^o_{1,1})) \\ \gamma_{2,1}(\gamma_{1,1}(\gamma^o_{1,1})) & 2-\gamma_{1,1}(\gamma^o_{1,1}) \end{bmatrix} \tag{B.1}$$

B.0.2 Parametrizing the Ground State vector in terms of the density

So far the Hubbard model has been used after the observation of the fact that the two-points system led exactly to the theoretical 1-RDM functional. This model has been used for trying to describe the data generated by the `iDEA` code. In this section a different approach will be followed and the data will be generated synthetically.
Starting from the Hamiltonian of the N_g-points system

$$\hat{H}^{(N_g)} = -t\sum_{\langle i,j\rangle}\sum_{\sigma}\hat{c}^{\dagger}_{i,\sigma}\hat{c}_{j,\sigma} + U\sum_i \hat{n}_{i,\uparrow}\hat{n}_{i,\downarrow} + \sum_i V_i\hat{n}_i$$

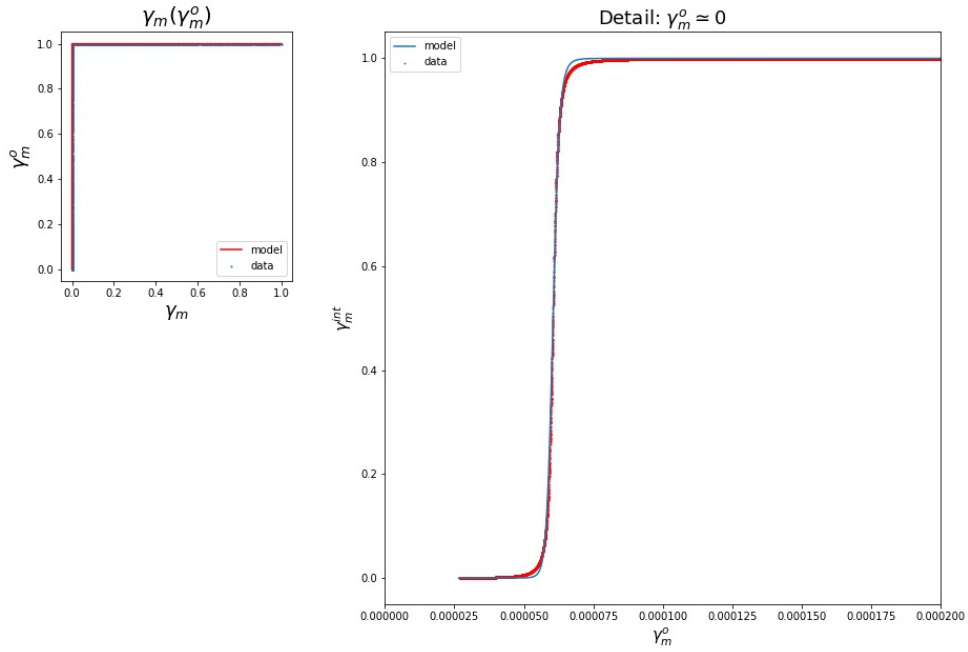

Figure B.3: Fit of the gammas

it must be made dimensionless, coherently with the energy units introduced before

$$\hat{\mathscr{H}}^{(N_g)} = -\frac{1}{4}\sum_{\langle i,j\rangle}\sum_{\sigma}\hat{c}^{\dagger}_{i,\sigma}\hat{c}_{j,\sigma} + u\sum_i \hat{n}_{i,\uparrow}\hat{n}_{i,\downarrow} + \sum_i v_i\hat{n}_i$$

where $x_i := X_i/(4t)$.
The dimensionless Hamiltonian is thus

$$\hat{\mathscr{H}}^{(2)} = -\frac{1}{4}\sum_{\langle i,j\rangle}^{2}\sum_{\sigma}\hat{c}^{\dagger}_{i,\sigma}\hat{c}_{j,\sigma} + u\sum_i^2 \hat{n}_{i,\uparrow}\hat{n}_{i,\downarrow} + \sum_i^2 v_i\hat{n}_i$$

Once introduced the singlet basis

$$\mathscr{B} = \begin{cases} |\varphi_1\rangle = |1\uparrow 1\downarrow\rangle = [1,0,0]^T \\ |\varphi_2\rangle = \frac{1}{\sqrt{2}}(|1\uparrow 2\downarrow\rangle - |1\downarrow 2\uparrow\rangle) = [0,1,0]^T \\ |\varphi_3\rangle = |2\uparrow 2\downarrow\rangle = [0,0,1]^T \end{cases}$$

It is possible to write the Hamiltonian

$$\mathbf{H} = \begin{bmatrix} u+2v_1 & -\sqrt{2}/4 & 0 \\ -\sqrt{2}/4 & v_1+v_2 & -\sqrt{2}/4 \\ 0 & -\sqrt{2}/4 & u+2v_2 \end{bmatrix}$$

The state under analysis is a stable state so the values of the potential must be negative. A synthetic dataset of potential landscapes has been generated considering the full 2-dimensional

plane of potentials defined by

$$(v_1, v_2) \in [-20,0] \times [-20,0]$$

The grid is formed by 500 points, for a total of 250000-potential landscapes. The numerical diagonalization of each matrix is performed exactly and, starting from the density matrix definition, it is possible to obtain the expressions of the 1-RDM terms as a function of the coefficients $a_{s[i]}$, accordingly to the formulas presented in chapter 3. The usual functional behavior can be observed in figure B.4.

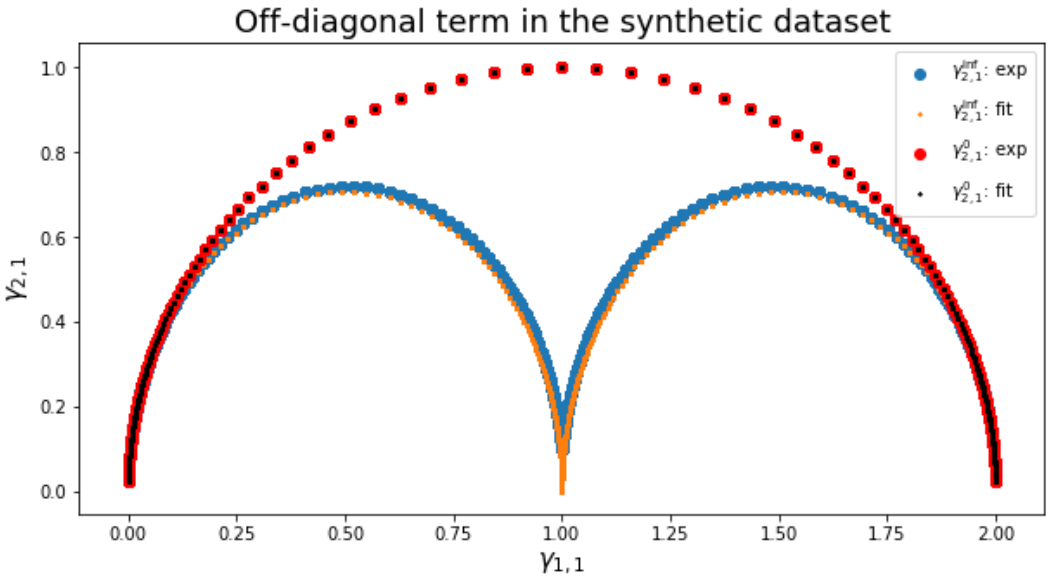

Figure B.4: Synthetic off-diagonal term: For the non-interacting case the interaction strength has been set to $u = 0$ while, for the strongly interacting case $u = 10$

Non-Interacting case

Let us start from the non-interacting data-set. In Fig.B.5 it is possible to observe the behavior of the three coefficients together with their fit.

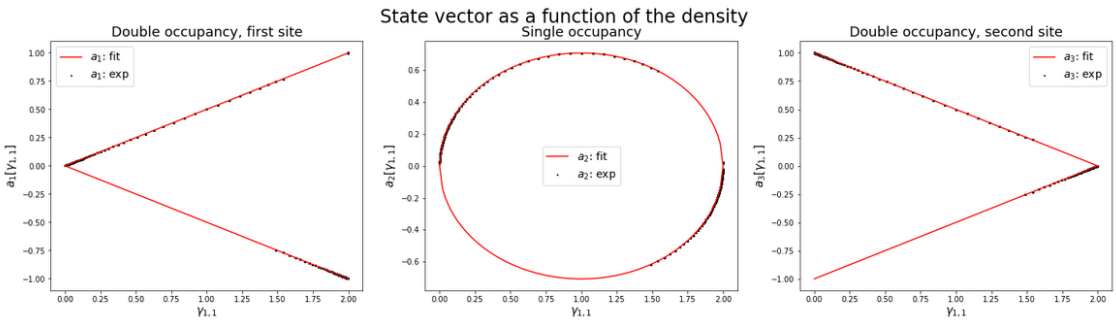

Figure B.5: Non interacting coefficients of the ground state vector.

Looking at the double occupancy of the first site, the modulus of the coefficient can be fitted

with the linear function

$$|a_1[\gamma_{1,1}]| = \frac{\gamma_{1,1}}{2}$$

For what concerns the trend, as expected the double occupancy of the first site is small when the density of the first site is small while it reaches its maximum when $\gamma_{2,2} = 2$, corresponding to the cases in which $v_1 << v_2$ and all of the charge is conveyed into x_1. What is interesting is that, for the non-interacting case, this relationship is linear. Symmetric observations can be done on the double occupancy of the second site

$$|a_3[\gamma_{1,1}]| = 1 - \frac{\gamma_{1,1}}{2}$$

Finally the a_2 term is interesting per-se. It is a rescaled version of the off-diagonal term $\gamma_{2,1}$

$$|a_2[\gamma_{1,1}, \gamma_{2,2}]| = \sqrt{\gamma_{1,1}\gamma_{2,2}/2} = \gamma^o_{2,1}/\sqrt{2}$$

An arbitrary 180-degrees rotation appears in the coefficient inducing a variation in the phase θ. However, this does not influence the 1-RDM since the products $a_1 a_2$ and $a_3 a_2$ are always positive.

So finally

$$|\Psi[n]\rangle = e^{i\theta}\left[\frac{\gamma_{1,1}}{2}|\varphi_1\rangle + \sqrt{\frac{\gamma_{1,1}\gamma_{2,2}}{2}}|\varphi_2\rangle + \frac{\gamma_{2,2}}{2}|\varphi_3\rangle\right] \tag{B.2}$$

Strongly-Interacting case

Moving to the interacting one, in Fig.B.6 it is possible to observe the behavior of the three coefficients together with their fit.

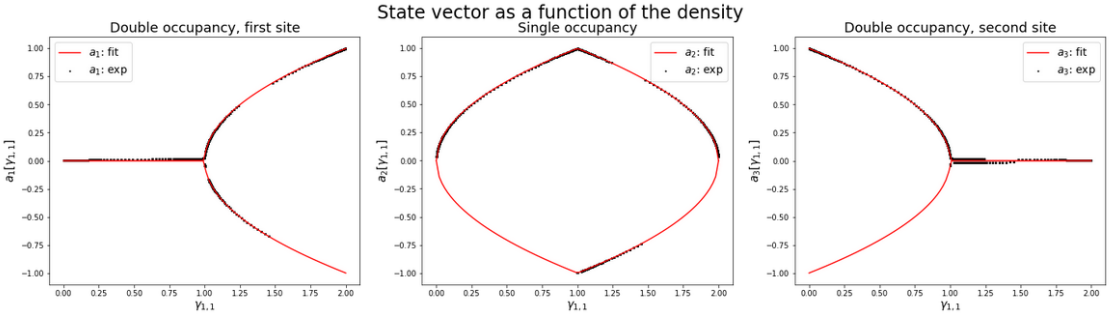

Figure B.6: Strongly interacting coefficients of the ground state vector.

Looking at the double occupancy of the first site, the modulus of the coefficient can be fitted with a piecewise defined function

$$|a_1[\gamma_{1,1}]| = \begin{cases} 0 & \text{if } \gamma_{1,1} \in [0,1) \\ \sqrt{\gamma_{1,1} - 1} & \text{if } \gamma_{1,1} \in [1,2] \end{cases}$$

Again, the double occupancy of the first site is small when the density of the first site is small while it reaches its maximum when $\gamma_{2,2} = 2$. The difference here is that, for the strongly interacting case, if the density in x_1 is smaller than one the probability of double occupancy is

zero since or the particles are both in x_1 or one is in one site and the other in the other. Symmetric observations can be done on the double occupancy of the second site

$$|a_3[\gamma_{1,1}]| = \begin{cases} \sqrt{1-\gamma_{1,1}} & \text{if } \gamma_{1,1} \in [0,1) \\ 0 & \text{if } \gamma_{1,1} \in [1,2] \end{cases}$$

Finally the a_2 term is:

$$|a_2[\gamma_{1,1},\gamma_{2,2}]| = \sqrt{min\{\gamma_{1,1},\gamma_{2,2}\}}$$

Again is not completely clear to me the meaning of the 180-degrees rotation of the phase $\theta[n]$. The important thing is that the products $a_1 * a_2$ and $a_3 * a_2$ are always positive.

So finally

$$|\Psi[n]\rangle = \begin{cases} e^{i\theta[n]}\left[(1-\gamma_{1,1})|\varphi_3\rangle + \sqrt{\gamma_{1,1}}|\varphi_2\rangle\right] & \text{if } \gamma_{1,1} \in [0,1] \\ e^{i\theta[n]}\left[(\gamma_{1,1}-1)|\varphi_1\rangle + \sqrt{\gamma_{2,2}}|\varphi_2\rangle\right] & \text{if } \gamma_{1,1} \in (1,2] \end{cases} \tag{B.3}$$

Appendix C

Constructing the one-dimensional Hamiltonian

Let us build the Hamiltonian used so far. For the aim of clarity the main step proposed in the book [69] will be here reported. Let us start by defining the generic N_e-body Hamiltonian

$$\hat{H} = \sum_{a=1}^{N_e} \left(\frac{\hat{p}_a^2}{2m} + V(r_a) \right) + \sum_{1 \leq a < b \leq N_e} V_{e,e}(|r_a - r_b|) \tag{C.1}$$

where $V(r_a)$ is the local potential acting on the electron and $V_{e,e}(|r_a - r_b|)$ is the many-body interaction, that in the `iDEA` code corresponds to the softened coulomb interaction

$$V_{e,e}(|r_a - r_b|) = \frac{1}{|r_a - r_b| + \beta} \tag{C.2}$$

where β is an arbitrarily small parameter.
After having chosen a number of grid-points N_g it is possible to indicate the corresponding positions with capital letters, so that the whole lattice is defined by the set of positions $\{R_j\}_{j=1}^{N_g}$, just as there was an ion per each site. This having been done, it is possible to introduce a Wannier basis, in which to each lattice site it is associated an orbital centered at the corresponding position $\mathscr{B}_W = \{\phi_j(r)\}_{j=1}^{N_g} = \{\phi(r - R_j)\}_{j=1}^{N_g}$. Thanks to the fact that we are considering few electrons systems there is no need to introduce more than one band and the associated field operator becomes

$$\hat{\psi}_\sigma^\dagger(r) = \sum_{j=1}^{N_g} \phi_j^*(r) \hat{c}_{j,\sigma}^\dagger \tag{C.3}$$

Finally, the second quantization Hamiltonian becomes

$$\hat{H} = \sum_{j,k=1}^{N_g} \sum_{\sigma=\uparrow,\downarrow} t_{j,k} \hat{c}_{j,\sigma}^\dagger \hat{c}_{k,\sigma} + \frac{1}{2} \sum_{j,k,l,m} \sum_{\sigma,\sigma'} U_{j,k,l,m} \hat{c}_{j,\sigma}^\dagger \hat{c}_{k,\sigma'}^\dagger \hat{c}_{l,\sigma} \hat{c}_{m,\sigma'} + \sum_{j=1}^{N_g} v_j \hat{n}_j \tag{C.4}$$

where the hopping term is defined as

$$t_{j,k} = \int dr \phi_j^*(r) \left(-\frac{1}{2} \nabla \right) \phi_k^*(r) \tag{C.5}$$

the local potential term is

$$v_j = \int dr \phi_j^*(r) V(r) \phi_k^*(r) \tag{C.6}$$

and the interaction term reads

$$U_{j,k,l,m} = \int dr dr' \; \phi_j^*(r) \phi_k^*(r') V_{e,e}(|r-r'|) \phi_l(r) \phi_m(r') \tag{C.7}$$

This finally yields the full Hamiltonian for the 1D system

$$\hat{H} = \sum_{j,k=1}^{N_g} \sum_{\sigma=\uparrow,\downarrow} t_{j,k} \hat{c}_{j,\sigma}^\dagger \hat{c}_{k,\sigma} + \frac{1}{2} \sum_{j,k,l,m} \sum_{\sigma,\sigma'} U_{j,k,l,m} \hat{c}_{j,\sigma}^\dagger \hat{c}_{k,\sigma'}^\dagger \hat{c}_{l,\sigma} \hat{c}_{m,\sigma'} + \sum_{j=1}^{N_g} v_j \hat{n}_j. \tag{C.8}$$

Bibliography

[1] Giuseppe Carleo et al. "Machine learning and the physical sciences". In: *Rev. Mod. Phys.* 91 (4 2019), p. 045002. DOI: 10.1103/RevModPhys.91.045002. URL: https://link.aps.org/doi/10.1103/RevModPhys.91.045002.

[2] Jörg Behler and Michele Parrinello. "Generalized neural-network representation of high-dimensional potential-energy surfaces". In: *Physical review letters* 98.14 (2007), p. 146401.

[3] Albert P Bartók, Mike C Payne, Risi Kondor, and Gábor Csányi. "Gaussian approximation potentials: The accuracy of quantum mechanics, without the electrons". In: *Physical review letters* 104.13 (2010), p. 136403.

[4] Matthias Rupp, Alexandre Tkatchenko, Klaus-Robert Müller, and O Anatole Von Lilienfeld. "Fast and accurate modeling of molecular atomization energies with machine learning". In: *Physical review letters* 108.5 (2012), p. 058301.

[5] Jörg Behler. "Perspective: Machine learning potentials for atomistic simulations". In: *The Journal of chemical physics* 145.17 (2016), p. 170901.

[6] Justin S Smith, Olexandr Isayev, and Adrian E Roitberg. "ANI-1: an extensible neural network potential with DFT accuracy at force field computational cost". In: *Chemical science* 8.4 (2017), pp. 3192–3203.

[7] Linfeng Zhang et al. "Deep potential molecular dynamics: a scalable model with the accuracy of quantum mechanics". In: *Physical review letters* 120.14 (2018), p. 143001.

[8] Nicholas Lubbers, Justin S Smith, and Kipton Barros. "Hierarchical modeling of molecular energies using a deep neural network". In: *The Journal of chemical physics* 148.24 (2018), p. 241715.

[9] Albert P Bartók, Risi Kondor, and Gábor Csányi. "On representing chemical environments". In: *Physical Review B* 87.18 (2013), p. 184115.

[10] Stefan Chmiela, Huziel E Sauceda, Klaus-Robert Müller, and Alexandre Tkatchenko. "Towards exact molecular dynamics simulations with machine-learned force fields". In: *Nature communications* 9.1 (2018), pp. 1–10.

[11] Kristof T Schütt et al. "SchNet–A deep learning architecture for molecules and materials". In: *The Journal of Chemical Physics* 148.24 (2018), p. 241722.

[12] Andrew E Sifain et al. "Discovering a transferable charge assignment model using machine learning". In: *The journal of physical chemistry letters* 9.16 (2018), pp. 4495–4501.

[13] Elia Schneider et al. "Stochastic neural network approach for learning high-dimensional free energy surfaces". In: *Physical review letters* 119.15 (2017), p. 150601.

[14] Hythem Sidky and Jonathan K Whitmer. “Learning free energy landscapes using artificial neural networks”. In: *The Journal of chemical physics* 148.10 (2018), p. 104111.

[15] Christoph Wehmeyer and Frank Noé. “Time-lagged autoencoders: Deep learning of slow collective variables for molecular kinetics”. In: *The Journal of chemical physics* 148.24 (2018), p. 241703.

[16] Andreas Mardt, Luca Pasquali, Hao Wu, and Frank Noé. “VAMPnets for deep learning of molecular kinetics”. In: *Nature communications* 9.1 (2018), pp. 1–11.

[17] Frank Noé, Simon Olsson, Jonas Köhler, and Hao Wu. “Boltzmann generators: Sampling equilibrium states of many-body systems with deep learning”. In: *Science* 365.6457 (2019), eaaw1147.

[18] Walter Kohn. “Nobel Lecture: Electronic structure of matter—wave functions and density functionals”. In: *Reviews of Modern Physics* 71.5 (1999), p. 1253.

[19] John C Snyder et al. “Finding density functionals with machine learning”. In: *Physical review letters* 108.25 (2012), p. 253002.

[20] Ryo Nagai, Ryosuke Akashi, Shu Sasaki, and Shinji Tsuneyuki. “Neural-network Kohn-Sham exchange-correlation potential and its out-of-training transferability”. In: *The Journal of chemical physics* 148.24 (2018), p. 241737.

[21] Felix Brockherde et al. “Bypassing the Kohn-Sham equations with machine learning”. In: *Nature communications* 8.1 (2017), pp. 1–10.

[22] Michael Eickenberg et al. “Solid harmonic wavelet scattering for predictions of molecule properties”. In: *The Journal of chemical physics* 148.24 (2018), p. 241732.

[23] Eric Schmidt, Andrew T Fowler, James A Elliott, and Paul D Bristowe. “Learning models for electron densities with Bayesian regression”. In: *Computational Materials Science* 149 (2018), pp. 250–258.

[24] Jack Wetherell, Andrea Costamagna, Matteo Gatti, and Lucia Reining. “Insights into one-body density matrices using deep learning”. In: *Faraday Discussions* (2020).

[25] W Töws and GM Pastor. “Lattice density functional theory of the single-impurity Anderson model: Development and applications”. In: *Physical Review B* 83.23 (2011), p. 235101.

[26] Max Born and Robert Oppenheimer. “On the quantum theory of molecules”. In: *Quantum Chemistry: Classic Scientific Papers*. World Scientific, 2000, pp. 1–24.

[27] Jan Philip Solovej. “Many body quantum mechanics”. In: *Lecture Notes. Summer* (2007).

[28] Jun John Sakurai, Jim Napolitano, et al. *Modern quantum mechanics*. Vol. 185. Pearson Harlow, 2014.

[29] Sami H Altoum. “Derivation of Schrödinger equation from a variational principle”. In: *Pure and Applied Mathematics Journal* 2.4 (2014), p. 146.

[30] Pierre Hohenberg and Walter Kohn. “Inhomogeneous electron gas”. In: *Physical review* 136.3B (1964), B864.

[31] Walter Kohn and Lu Jeu Sham. “Self-consistent equations including exchange and correlation effects”. In: *Physical review* 140.4A (1965), A1133.

[32] Stefan Kurth and John P Perdew. “Role of the exchange–correlation energy: Nature’s glue”. In: *International Journal of Quantum Chemistry* 77.5 (2000), pp. 814–818.

[33] Weitao Yang, Yingkai Zhang, and Paul W Ayers. “Degenerate ground states and a fractional number of electrons in density and reduced density matrix functional theory”. In: *Physical Review Letters* 84.22 (2000), p. 5172.

[34] NN Lathiotakis and Miguel AL Marques. “Benchmark calculations for reduced density-matrix functional theory”. In: *The Journal of chemical physics* 128.18 (2008), p. 184103.

[35] W Töws, M Saubanère, and GM Pastor. “Density-matrix functional theory of strongly correlated fermions on lattice models and minimal-basis Hamiltonians”. In: *Theoretical Chemistry Accounts* 133.1 (2014), p. 1422.

[36] Stefano Di Sabatino, Jan A Berger, Lucia Reining, and Pina Romaniello. “Reduced density-matrix functional theory: Correlation and spectroscopy”. In: *The Journal of chemical physics* 143.2 (2015), p. 024108.

[37] Guido Van Rossum and Fred L Drake Jr. *Python reference manual*. Centrum voor Wiskunde en Informatica Amsterdam, 1995.

[38] François Chollet et al. *Keras*. `https://keras.io`. 2015.

[39] F. Pedregosa et al. “Scikit-learn: Machine Learning in Python”. In: *Journal of Machine Learning Research* 12 (2011), pp. 2825–2830.

[40] Alexander LeNail. “Nn-svg: Publication-ready neural network architecture schematics”. In: *Journal of Open Source Software* 4.33 (2019), p. 747.

[41] Karl Pearson. “LIII. On lines and planes of closest fit to systems of points in space”. In: *The London, Edinburgh, and Dublin Philosophical Magazine and Journal of Science* 2.11 (1901), pp. 559–572.

[42] Jake VanderPlas. *Python data science handbook: Essential tools for working with data*. " O’Reilly Media, Inc.", 2016.

[43] Nev Acar. *Eigenfaces: Recovering Humans from Ghosts*. 2018. URL: `https://towardsdatascience.com/eigenfaces-recovering-humans-from-ghosts-17606c328184`.

[44] David E Rumelhart, Geoffrey E Hinton, and Ronald J Williams. “Learning representations by back-propagating errors”. In: *nature* 323.6088 (1986), pp. 533–536.

[45] Balázs Csanád Csáji et al. “Approximation with artificial neural networks”. In: *Faculty of Sciences, Etvs Lornd University, Hungary* 24.48 (2001), p. 7.

[46] Seong-Whan Lee. “Multilayer cluster neural network for totally unconstrained handwritten numeral recognition”. In: *Neural Networks* 8.5 (1995), pp. 783–792.

[47] Matthew JP Hodgson et al. “Exact time-dependent density-functional potentials for strongly correlated tunneling electrons”. In: *Physical Review B* 88.24 (2013), p. 241102.

[48] Jack Wetherell. “Electron correlation and screening in model nanostructures”. PhD thesis. University of York, 2018.

[49] Jack Wetherell, Matthew James Paul Hodgson, Leopold Talirz, and Rex William Godby. “Advantageous nearsightedness of many-body perturbation theory contrasted with Kohn-Sham density functional theory”. In: *Physical Review B* 99.4 (2019), p. 045129.

[50] MJP Hodgson, JD Ramsden, TR Durrant, and RW Godby. “Role of electron localization in density functionals”. In: *Physical Review B* 90.24 (2014), p. 241107.

[51] Jack Wetherell, MJP Hodgson, and RW Godby. "G W self-screening error and its correction using a local density functional". In: *Physical Review B* 97.12 (2018), p. 121102.

[52] Matthew JP Hodgson, Eli Kraisler, Axel Schild, and Eberhard KU Gross. "How interatomic steps in the exact Kohn–Sham potential relate to derivative discontinuities of the energy". In: *The journal of physical chemistry letters* 8.24 (2017), pp. 5974–5980.

[53] AH Skelt, RW Godby, and I D'Amico. "Measuring adiabaticity in nonequilibrium quantum systems". In: *Physical Review A* 98.1 (2018), p. 012104.

[54] Ian Goodfellow, Yoshua Bengio, and Aaron Courville. *Deep Learning*. `http://www.deeplearningbook.org`. MIT Press, 2016.

[55] John Hubbard. "Electron correlations in narrow energy bands". In: *Proceedings of the Royal Society of London. Series A. Mathematical and Physical Sciences* 276.1365 (1963), pp. 238–257.

[56] Matthieu Saubanère, Marie Bernadette Lepetit, and GM Pastor. "Interaction-energy functional of the Hubbard model: Local formulation and application to low-dimensional lattices". In: *Physical Review B* 94.4 (2016), p. 045102.

[57] Simon Murmann et al. "Two fermions in a double well: Exploring a fundamental building block of the Hubbard model". In: *Physical review letters* 114.8 (2015), p. 080402.

[58] B Alvarez-Fernández and JA Blanco. "The Hubbard model for the hydrogen molecule". In: *European journal of physics* 23.1 (2001), p. 11.

[59] K Capelle and LN Oliveira. "Dimensional scaling estimate of the energy of a large system from that of its building blocks: Hubbard model and Fermi liquid". In: *Physical Review B* 73.11 (2006), p. 113111.

[60] AL Kholodenko. "From a Hubbard dimer to a Hubbard model in d dimensions: a path integral solution". In: *Journal of Physics: Condensed Matter* 1.1 (1989), p. 93.

[61] DJ Carrascal, Jaime Ferrer, Justin C Smith, and Kieron Burke. "The Hubbard dimer: a density functional case study of a many-body problem". In: *Journal of Physics: Condensed Matter* 27.39 (2015), p. 393001.

[62] HA Brown. "A Simple Derivation of the Spin-Exchange Operator". In: *American Journal of Physics* 40.11 (1972), pp. 1696–1697.

[63] Matthieu Saubanere and GM Pastor. "Density-matrix functional study of the Hubbard model on one-and two-dimensional bipartite lattices". In: *Physical Review B* 84.3 (2011), p. 035111.

[64] Marvin Minsky and Seymour A Papert. *Perceptrons: An introduction to computational geometry*. MIT press, 2017.

[65] Kurt Hornik. "Approximation capabilities of multilayer feedforward networks". In: *Neural networks* 4.2 (1991), pp. 251–257.

[66] J Wesley Hines. "A logarithmic neural network architecture for a PRA approximation". In: *Proceedings of the 1996 American Nuclear Society, International Topical Meeting on Nuclear Plant Instrumentation, Control and Human-Machine Interface Technologies*. Vol. 1. Citeseer. 1996, pp. 235–241.

[67] Marco Vanzini et al. "Recycling knowledge to explore materials: a connector theory approach". In: *arXiv preprint arXiv:1903.07930* (2019).

[68] Carl Edward Rasmussen. “Gaussian processes in machine learning”. In: *Summer School on Machine Learning*. Springer. 2003, pp. 63–71.

[69] Fabian HL Essler et al. *The one-dimensional Hubbard model*. Cambridge University Press, 2005.